

Fabrication of an enzyme responsive biomaterial for the treatment of  
recurrent corneal erosion

by

Susmita Bose

A thesis

presented to the University of Waterloo

in fulfillment of the

thesis requirement for the degree of

Doctor of Philosophy

in

Vision Science

Waterloo, Ontario, Canada, 2022

© Susmita Bose 2022

## Examining Committee Membership

The following served on the Examining Committee for this thesis. The decision of the Examining Committee is by majority vote.

External Examiner	Debarun Dutta Lecturer, Aston University
Supervisors	Lyndon Jones Professor
Internal Members	Paul J. Murphy Professor
	Evelyn Yim Associate Professor
	David J. McCanna Research Assistant Professor
Internal-external Member	Maud Gorbet Associate Professor

## **Author's Declaration**

I hereby declare that I am the sole author of this thesis. This is a true copy of the thesis, including any required final revisions, as accepted by my examiners.

I understand that my thesis may be made electronically available to the public.

## Abstract

**Purpose:** Recurrent corneal erosion (RCE) arising from the loss of superficial corneal epithelial cells causes tremendous ocular pain affecting one's productivity and quality of life. RCE was traditionally treated with eye lubricants and patching (to stop blinking). Soft bandage contact lenses (BCLs), which enable the use of vision during the healing process, have become more widely used in recent years. Because BCLs do not yet contain the therapeutic components necessary for ocular surface repair, they do not outperform ocular lubricants in terms of effectiveness or recovery time. This is a problem. Multiple studies have shown elevated levels of matrix metalloproteinase (MMP) enzymes, particularly MMP-9 and MMP-2, in RCE. The purpose of this thesis was to develop an enzyme-triggered therapeutic release platform using a unique gelatin methacrylate formulation (GelMA+) and bovine-lactoferrin (BLF), a potential corneal wound healing therapeutic.

**Method:** Two different formulations of GelMA+ gels were synthesized: 20% w/v and 30% w/v GelMA+ gels. To determine the effect of polymer concentration on the physical characteristics and cytotoxicity of the gels, physical characterization, including mechanical strength, swelling behaviour, pore size, optical clarity, degradation profile in the enzyme MMP-9 and MMP-8, were evaluated. To evaluate whether GelMA+ is suitable to be a biomaterial, cytotoxicity assays (alamarBlue and live/dead assay) were performed on both the GelMA+ formulations. These physical and biological characterization of GelMA+ gels helped to choose the specific GelMA+ formulation for studying the in vitro release profile of BLF from the GelMA+ matrix. To assess the efficacy and therapeutic window of BLF for corneal epithelial cells wound healing, a scratch induced assay model was used.

### Results:

GelMA showed a tunable profile suitable for the diffusion- and enzyme-mediated controlled release of therapeutics above the molecular weight region of 70 kDa. Owing to the high polymer concentration as opposed to 20% w/v GelMA+, the 30% w/v GelMA+ had a higher crosslinking density, tensile strength, smaller pore size, and lower swelling ratio than the 20% w/v GelMA+ ( $p < 0.05$ ). The degradation rate of the 20% w/v gel was much faster ( $p < 0.001$ ), degrading almost completely after 48 hours at 300  $\mu\text{g/mL}$  of MMP-9 whereas 30% w/v GelMA+ gels took almost 6 days to achieve around 95% degradation in the same MMP-9 concentration. After 5 days, no cytotoxicity was detected in the

live/dead staining for either formulation, but the 30% w/v GelMA+ showed significantly higher cell viability ( $p < 0.05$ ). In the BLF release study, no burst release of BLF was observed for the 30% w/v gel, and the therapeutic release was sustained over 5 days. The rate of release from the gel significantly increased with increasing concentrations of MMP-9 ( $p < 0.001$ ) and correlated to the rate of degradation of the gels. BLF at 10 mg/mL induced complete wound closure in four days, and 7.5 mg/mL completely closed the wound in six days, suggesting that BLF might be an excellent therapeutic option for corneal abnormalities brought on by mechanical injury. A concentration of 7.5 mg/mL or 10 mg/mL BLF would be an appropriate therapeutic window to be released from 30% w/v GelMA+ for treating RCE within a week.

**Conclusion:** The results showed that the degradation of GelMA+ can be tuned by modifying the cross-linking density or exposure to different concentrations of MMP-9. The release of BLF from 30% w/v GelMA+ is driven by a combination of diffusion and degradation of the material by MMP-9 enzymes. Hence the therapeutic releasing enzyme responsive GelMA+ as a BCL can be potential future treatment for RCE. Future work will focus on optimizing the materials to deliver other therapeutic agents at physiologically relevant concentrations of MMP enzymes found in the tear fluid.

## **Acknowledgements**

I would like to express my sincere gratitude to my supervisor Dr. Lyndon Jones for his continuous support and guidance throughout my PhD study. I am grateful for his endless support and encouragement throughout my PhD program.

I am also indebted to my lab members and colleagues at CORE for their support and contribution and for helping me complete my experiments efficiently. Special sincere gratitude and heartfelt thanks to Dr. Chau Minh Phan for his guidance at every step of my PhD life.

Last but not the least, I would like to thank my parents and friends back in India for providing me with the emotional support to sail throughout this PhD journey.

## **Dedication**

Thanks to my Ma and Baba, who have made endless sacrifices and given up their dreams so that I can achieve mine.

# Table of Contents

Examining Committee Membership .....	ii
Author’s Declaration .....	iii
Abstract.....	iv
Acknowledgments .....	vi
Dedication .....	vii
List of Figures .....	xvi
List of Tables .....	xx
List of Symbols .....	xxi
List of Abbreviations .....	xxi
Chapter 1 : Introduction.....	1
1.1 Anatomy of the eye .....	2
1.1.1 Cornea.....	3
1.1.1.1 Corneal epithelium .....	5
1.2 Recurrent Corneal Erosion .....	6
1.2.1 Treatments for RCE.....	7
1.3 Bandage Contact Lenses .....	9
1.4 Therapeutic contact lenses for drug delivery.....	11



1.4.1 Methodology to design therapeutic contact lenses .....	12
1.5 Gelatin Methacrylate (GelMA) hydrogel.....	19
1.5.1 Synthesis of GelMA hydrogels .....	20
1.5.2 Biomedical applications of GelMA.....	21
1.5.2.1 Tissue Engineering.....	21
1.5.2.2 Drug delivery .....	25
1.5.2.3 Biosensor .....	26
1.5.3 GelMA+ .....	26
1.6 Bovine lactoferrin– a potential corneal wound healing therapeutic .....	27
1.7 Role of MMP-9 in corneal epithelial wound healing.....	30
1.8 Stages of corneal epithelial wound healing .....	35
1.9 Conclusion.....	37
Chapter 2 : Rationale and Objectives .....	38
2.1 Rationale and Objectives.....	38

Chapter 3 : Preparation and Characterization of GelMA+ gels .....	41
3.1 Introduction .....	41
3.2 Materials and Methods .....	43
3.2.1 Gelatin methacrylate synthesis .....	43
3.2.2 Preparation of GelMA+ hydrogel.....	43
3.2.3 Physical Characterization.....	44
3.2.3.1 Scanning Electron Microscopy .....	44
3.2.3.2 Enzymatic Degradation of GelMA+ hydrogel .....	45
3.2.3.3 Swelling Percentage and Water Content of GelMA+ hydrogel .....	46
3.2.3.4 Mechanical Properties of GelMA+ hydrogel (Tensile test) .....	46
3.2.3.5 Optical transmittance of GelMA+ hydrogel.....	47
3.3 Statistical Analysis.....	48
3.4 Results .....	49
3.4.1 Physical Characterization.....	49

3.4.1.1 Scanning electron microscopy (SEM) images .....	49
3.4.1.2 Enzymatic Degradation of GelMA+ hydrogel .....	51
3.4.1.3 Swelling profile and Water Content.....	56
3.4.1.4 Tensile test.....	57
3.4.1.5 Optical transmittance.....	59
3.5 Discussion.....	60
Chapter 4 : Cytotoxicity of GelMA+ .....	64
4.1 Introduction .....	64
4.2 Materials and Methods .....	67
4.2.1 Materials .....	67
4.2.2 Biological Characterizations .....	67
4.2.2.1 Cell Culture.....	67
4.2.2.2 Cell Culture in the presence of GelMA+ hydrogels .....	67
4.2.2.3 Cell Viability Assay .....	68

4.2.2.4 Live/Dead Assay .....	69
4.3 Statistical Analysis.....	70
4.4 Results .....	71
4.4.1 Cell Growth with GelMA+ gels .....	71
4.4.2 Cell Viability Assay.....	71
4.4.3 Live/Dead assay .....	73
4.5 Discussion.....	75
Chapter 5 : In vitro release profile of bovine lactoferrin from GelMA+ gels .....	78
5.1 Introduction .....	78
5.2 Materials and Methods.....	80
5.2.1 Materials .....	80
5.2.2 Gelatin methacrylate synthesis.....	80
5.2.3 Preparation of BLF or FITC-dextran loaded GelMA+ hydrogel .....	80

5.2.4 In vitro release study of FITC-dextran and BLF at room temperature (23 °C – 25 °C)	81
5.2.5 In vitro release study of BLF at 37 °C	82
5.2.6 Optical Transmittance of BLF loaded GelMA+ gels	83
5.3 Statistical analysis	83
5.4 Results	84
5.4.1 In vitro release kinetics of FITC-dextran and BLF at room temperature (23 °C – 25 °C)	84
5.4.2 In vitro release study of BLF at 37 °C	91
5.4.3 Optical transmittance of BLF loaded GelMA+	92
5.5 Discussion	94
Chapter 6 : Bovine Lactoferrin-induced corneal epithelial wound healing	98
6.1 Introduction:	98
6.2 Materials and Methods	99
6.2.1 Materials	99

6.2.2 Cell Culture .....	99
6.2.3 Making a scratch induced wound on HCEC monolayer .....	100
6.2.4 Effect of BLF on HCEC Wound Healing of Scratch-Induced Wound Model .....	100
6.3 Statistical Analysis.....	101
6.4 Results .....	102
6.4.1 Effect of BLF on HCEC Wound Healing of Scratch-Induced Wound Model for 6 days.....	102
6.4.2 Effect of BLF on HCEC Wound Healing of Scratch-Induced Wound Model for 4 days (96 hours).....	105
6.5 Discussion.....	108
Chapter 7 : Conclusions and Recommendations.....	112
7.1 Conclusions: .....	112
7.2 Recommendations:.....	116
7.2.1 Studying the effect of lipids and protein deposition on GelMA+ lens.....	116

7.2.2 Degradation of GelMA+ gels in a physiologically relevant MMP-9 concentration .....	116
7.2.3 Incorporation of GelMA+ into the commercial contact lenses .....	117
7.2.4 Incorporation of GelMA+ as lid implant .....	117
7.2.5 Testing the enzyme responsive drug delivery system in vivo .....	118
References.....	119
Appendix A- Copyright permission .....	146
Figure 1-1: Anatomy of the eye.....	146
Figure1-2: Structure of the cornea.....	147
Figure 1-3: Cross-sectional view of corneal epithelial layer.....	148
Figure 1-5: Synthesis of GelMA .....	148
Figure 1-6: Structure of biferric BLF .....	150

## List of Figures

Figure 1-1: Anatomy of the eye (Figure courtesy of the National Eye Institute, National Institute of Health NEI/NIH <sup>19</sup> ).....	2
Figure 1-2: Structure of the cornea <sup>24</sup> .....	4
Figure 1-3: Cross-sectional view of corneal epithelial layer <sup>23</sup> .....	5
Figure 1-4: Schematic representation of a drug laden contact lens placed over the cornea .....	12
Figure 1-5: Synthesis of GelMA. (A) Primary amine groups of gelatin react with MA to add methacrylated groups. (B) Formation of hydrogel network of GelMA <sup>132</sup> .....	21
Figure 1-6: Structure of biferric BLF <sup>203</sup> .....	28
Figure 3-1: Schematic representation of the preparation of GelMA+ gels.....	44
Figure 3-2: Experimental setup for tensile test. The gels are clamped on both ends with the help of Kimwipes.....	47
Figure 3-3: SEM images (n=3) of (A) pre-polymerized GelMA at 100 X magnification (B) 20% w/v GelMA+ hydrogel at 436 X magnification, (C) 30% w/v GelMA+ hydrogel at 18k X magnification. All three images show the surface morphology and depict the pore size of the GelMA+.....	50
Figure 3-4: Degradation profile (n=4) of (A) 20% w/v GelMA+ in varying MMP-9 concentrations, (B) 30% w/v GelMA+ in varying MMP-9 concentrations, (C) 20% w/v GelMA+ in varying MMP-8 concentrations, (D) 30% w/v GelMA+ in varying MMP-8	



concentrations, (E) 20% w/v GelMA+ in varying MMP-8+ MMP-9 concentrations, (F) 30% w/v GelMA+ in varying MMP-8+ MMP-9 concentrations; The shape of (G) 20% w/v GelMA+ in PBS (0 µg/mL of MMP-9) after 48 hours, (H) 20% w/v GelMA+ in 100 µg/mL of MMP-9 after 48 hours, (I) the shape of 30% w/v GelMA+ in PBS (0 µg/mL of MMP-9) after 144 hours, (J) the shape of 30% w/v GelMA+ in 100 µg/mL of MMP-9 after 144 hours, (K) the shape of 30% w/v GelMA+ in 300 µg/mL of MMP-9 after 144 hours .....55

Figure 3-5: The swelling ratio (n=4) of 20% w/v and 30% w/v GelMA+ hydrogels after immersion in 1X PBS for 24 hours .....56

Figure 3-6: (A) Tensile stress-strain curves (n=3) of 20% w/v GelMA+, (B) Tensile stress-strain curves of 30% w/v GelMA+ .....58

Figure 3-7: Optical transmittance of both the formulations of GelMA+ (n=5) measured at wavelength range of 450 nm to 700 nm. ....59

Figure 4-1: (A) Growth of immortalized HCEC cells in the presence of 20% w/v GelMA+ gels, (B) Growth of immortalized HCEC cells in the presence of 30% w/v GelMA+ gels.....71

Figure 4-2: Percentage of HCEC cell viability in the presence of different formulations of GelMA+ in comparison to control (HCECs were not exposed to GelMA+ gels) (n=4) .....73

Figure 4-3: Live/Dead cells distribution on (A) Control (No GelMA+), (B) 20% w/v GelMA+, (C) 30% w/v GelMA+. The green fluorescence (calcein AM) denotes the

presence of live cells, and the red fluorescence (EthD-1) denotes the presence of dead cells. A negative control with all dead HCEC cells was not studied. ....74

Figure 5-1: Schematic representation of the BLF / FITC-dextran loaded GelMA+ gels .....81

Figure 5-2: Release of FITC-dextran from 10% w/v GelMA+ formulation in varying concentrations of MMP-9 over 24 hours.....85

Figure 5-3: Release of FITC-dextran from 20% w/v GelMA+ formulation in varying concentrations of MMP-9 over 24 hours (n=3) .....86

Figure 5-4: Release of FITC-dextran from 30% w/v GelMA+ formulation in varying concentrations of MMP-9 over 24 hours (n=3) .....87

Figure 5-5: Release of FITC-dextran from 10%, 20% and 30% w/v GelMA+ in varying concentrations of MMP-9 at 24 hours (n=3) .....88

Figure 5-6: Release of BLF from 30% w/v GelMA+ at 23 °C – 25 ° in varying concentrations of MMP-9 over 24 hours (n=4) .....90

Figure 5-7: In vitro release of BLF from 30% w/v GelMA+ at 37 °C in the presence of varying MMP-9 concentrations (n=4).....92

Figure 6-1: Percent closure of scratch induced HCEC wounds in response to treatment with BLF (0, 5, 7.5, 10 mg/mL) (n=4) .....103

Figure 6-2: Images of wound closure of scratch induced HCEC wounds in response to treatment with BLF (0, 5, 7.5, 10 mg/mL) with Day 0 showing the original wound size (n=4) .....104

Figure 6-3: Percent closure of scratch induced HCEC wounds in response to treatment with BLF (0, 5, 7.5, 10 mg/mL) (n=4) ..... 106

Figure 6-4: Images of wound closure of scratch induced HCEC wounds in response to treatment with BLF (0, 5, 7.5, 10 mg/mL) with Day 0 showing the original wound size (n=4) ..... 107

## List of Tables

Table 1-1: Lists several FDA-approved soft BCLs <sup>16, 58</sup> .....	10
Table 1-2: An overview of methods for the fabrication of therapeutic contact lenses ..	17
Table 1-3: GelMA with different modifiers for tissue engineering applications .....	24
Table 1-4: Role of MMP-9 in various clinical conditions.....	33
Table 3-1: Water Content of GelMA+ (n=4).....	57
Table 3-2: Tabular data of tensile strength and Young's modulus of both the GelMA+ formulations (n=3) .....	57
Table 4-1:Percentage of cell viability of 20% and 30% w/v GelMA+ when compared to control (n=4) .....	72
Table 5-1: The amount of FITC-dextran ( $\mu\text{g}$ ) released during the wash period (24 hours) from different formulations of GelMA+ gels in phosphate buffered saline (n=3) .....	89
Table 5-2: Pro MMP-9 levels in ocular diseases .....	96
Table 5-3: MMP-9 levels in ocular diseases.....	97

## List of Symbols

%	percentage
°	degree
°C	degrees centigrade
g	gram
h	hrs
L	litre
M	molar
mg	milligram
mL	millilitre
mm	millimeter
min	minutes
nm	nanometre
pH	negative logarithm hydronium ion concentration
µg	microgram
µL	microliter
µm	micrometre
kDa	kilodalton
mbar	millibar
kv	kilovolt
w/v	weight/volume
v/v	volume/volume
mw/cm <sup>2</sup>	milliwatt/centimetre <sup>2</sup>
MPa	megapascal

## List of Abbreviations

RCE	recurrent corneal erosion
BCL	bandage contact lenses

NSAIDs	non-steroidal anti-inflammatory drugs
MMPs	matrix metalloproteinases
HCECs	human corneal epithelial cells
GelMA	gelatin methacrylate
PBS	phosphate buffer saline
HEMA	hydroxyethyl methacrylate
SH	silicone hydrogel
Dex	dexamethasone
RGD	arginine-glycine-aspartic acid
MA	methacrylic anhydride
DS	degree of substitution
PCL	poly- $\epsilon$ -caprolactone
VEGF	vascular endothelial growth factors
TGF	transforming growth factor
BLF	bovine lactoferrin
GRAS	generally regarded as safe
FDA	food and drug administration
TNF	tumour necrosis factor
IL	interleukin
ICAM	intercellular adhesion molecule
NF- $\kappa$ B	nuclear factor kappa
PAF	platelet-activating factor
DNA	deoxyriboneucleic acid
RNA	riboneucleic acid
AP	activator protein
TIMP	tissue inhibitor metalloproteinases
LASIK	laser assisted in situ keratomileusis
DR	diabetic retinopathy
PXE	Pseudoxanthoma elasticum
AMD	age-related macular degeneration
ACI	acute cerebral infarction
PDGF	platelet derived growth factor

UV	ultraviolet
ELISA	enzyme-linked immunosorbent assay
ANOVA	analysis of variance
CORE	centre for ocular research & education
FITC	fluorescein isothiocyanate
RPM	rotation per minute
ESEM	environmental scanning electron microscopy
DI	deionized
ECM	extracellular matrix
PAA	polyacrylamide
ATS	artificial tear solution

# Chapter 1: Introduction

The primary cause of recurrent corneal erosion (RCE) is mechanical trauma to the corneal epithelium.<sup>1</sup> It is estimated that ocular trauma accounts for up to 5% of blinding conditions.<sup>2</sup> An estimated 1.5 to 2.0 million cases of monocular blindness are caused by ocular trauma annually.<sup>3</sup> An estimated 20,000 traumatic corneal abrasions cases per year come from the province of Quebec alone.<sup>4</sup> Historically, the standard clinical approach for treating RCE and corneal abrasion is using an eye patch, antibiotics, topical non-steroidal anti-inflammatory drugs (NSAIDs), and lubricating ointments.<sup>1, 5-7</sup> However patching disrupts normal vision and several randomized trials have revealed that the patch is not routinely maintained<sup>8-12</sup> and antibiotics do not help in corneal abrasions.<sup>13</sup> Even lubricating ointments given at night resulted in significantly more patients with mild to moderate symptoms of RCE at three months.<sup>14</sup> In more recent times, especially since the release of highly oxygen permeable silicone hydrogel contact lens materials, practitioners often prescribe bandage contact lenses (BCLs) for the management of corneal abrasions.<sup>15-17</sup> However, current BCLs do not outperform the standard treatment in terms of recovery speed.<sup>18</sup>

This thesis aims to develop an enzyme responsive biomaterial that can be used as a therapeutic releasing BCL for the treatment of RCE. These therapeutic-loaded lenses would ideally release the matrix bound wound healing agent on being acted upon by the enzymes present in situ and promote a speedy recovery from the corneal abrasion. The application of therapeutic releasing BCLs serve two purposes: a) protection of the wounded cornea from the frictional force of the eyelid and b) controlled release of corneal wound healing agents over time.

To better understand this area, the following introductory chapter will provide an overview of the cornea and its epithelial layer, RCE, bandage contact lenses, gelatin methacrylate and bovine lactoferrin.



## 1.1 Anatomy of the eye

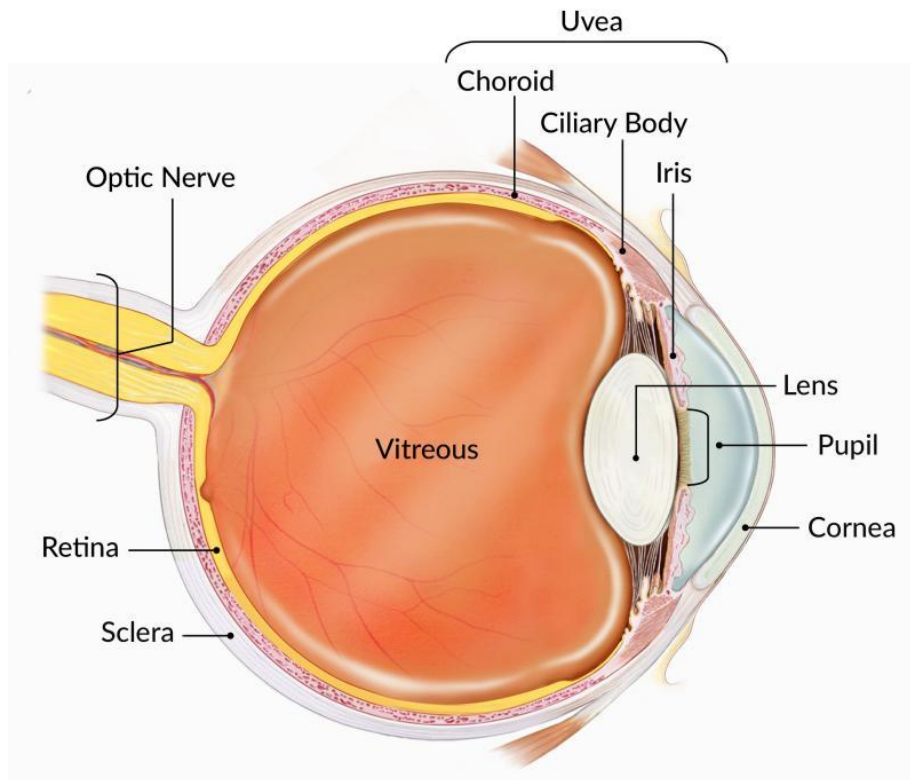


**Figure 1-1:** Anatomy of the eye (Figure courtesy of the National Eye Institute, National Institute of Health NEI/NIH<sup>19</sup>)

The eye is one of the human body's most complex and unique organs. It helps us to connect with the external world through vision. Anatomically, the eye is divided into two parts: the anterior and posterior portions.<sup>20</sup> The main structures of the eye are highlighted in Figure 1-1. Because this thesis focuses on treating RCE, the cornea and its epithelial layer will be discussed.

### **1.1.1 Cornea**

The cornea is a clear, avascular tissue that provides mechanical integrity and acts as an immunological defense shield. Together with the tear film, the cornea provides an anterior refractive surface for the eye. The cornea and crystalline lens refract light that enters the eye. Two-thirds of the eye's overall focusing power comes from the cornea.<sup>21</sup> The horizontal diameter of an adult human cornea ranges from 11.5 to 12.0 mm, with a central thickness of 0.5 mm.<sup>22</sup> The cornea is composed of five distinct layers: the epithelium, Descemet's membrane, Bowman's membrane, stroma, and endothelium. Figure 1-2 shows the structure of the cornea, of which the epithelium is the outermost layer. It provides a smooth refractive surface and acts as an infection barrier. Bowman's membrane is located underneath the epithelium and its basement membrane. The stroma, which comprises interweaving lamellae of collagen fibrils and makes up 90% of the corneal thickness, gives the cornea physical structure. The innermost layers are made up of the endothelium and its basement membrane (Descemet's membrane). The relative corneal dehydration required for corneal clarity is caused by endothelial cells through an active sodium potassium-adenosine triphosphatase pump.<sup>21,23</sup>

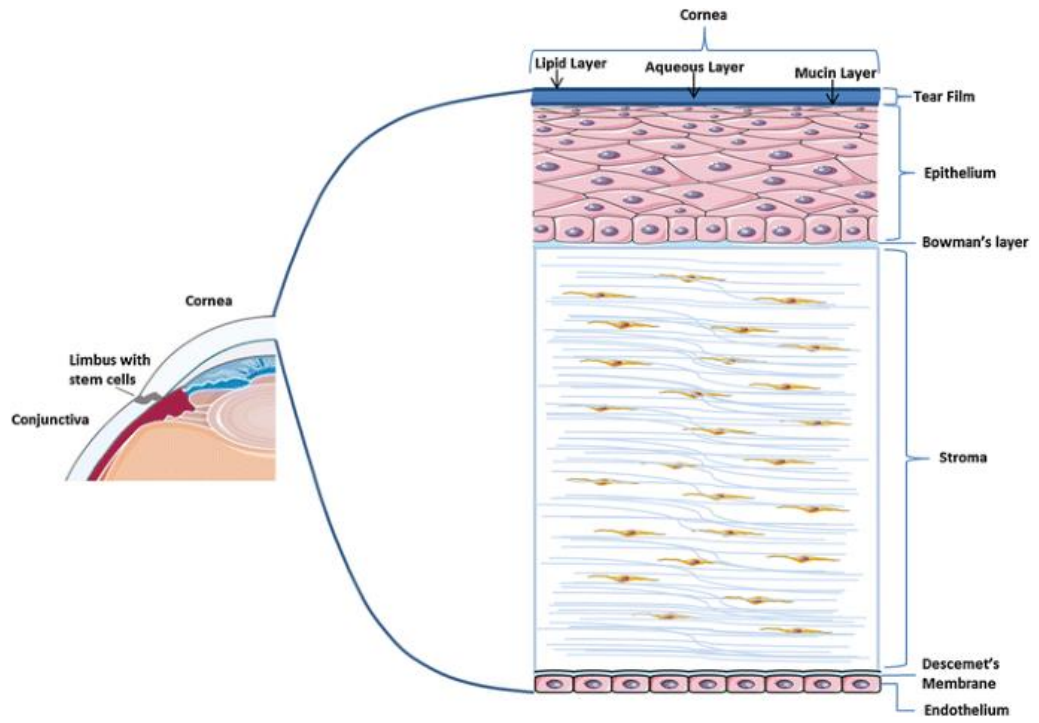


**Figure 1-2:** Structure of the cornea<sup>24</sup>

### 1.1.1.1 Corneal epithelium

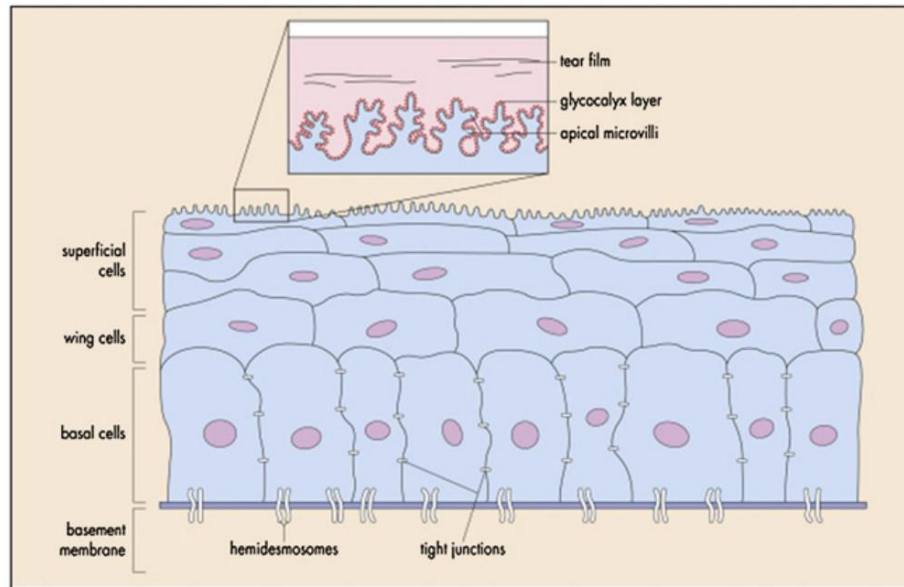


**Figure 1-3:** Cross-sectional view of corneal epithelial layer<sup>23</sup>

The corneal epithelium is the external most layer of the cornea. It is a uniform smooth layer of 40 to 50  $\mu\text{m}$  (4 to 6 cell layers) in thickness composed of non-keratinized, stratified squamous epithelial cells.<sup>25</sup> These cells have many microvilli and microplacae, which enhance their surface area and help sustain the tear film above them. These cells are relatively flat. In order to keep pathogens from adhering to the ocular surface cells, the epithelial glycocalyx aids in holding tears to those cells.<sup>23, 26, 27</sup> The loss of glycocalyx during injury or disease leads to the loss of tear-film stability and subsequent breakdown of the ocular optical system. The tear film serves as the ocular surface's main defense against microbial invasion, chemical, toxic, and foreign-body harm. Additionally, the tear film provides immunological and growth elements that are essential for the survival, growth, and repair of epithelial cells.<sup>28</sup> Desmosomes and tight junctions, mostly made of zonula occludens, are used to connect these surface cells.<sup>23, 26, 27</sup>

Wing cells arranged in two to three layers and connected by adherens junctions and desmosomes make up the second layer of the epithelium. Desmosomes and gap junctions connect them to the surface cells and basal cells, respectively, and allow for direct exchange of chemicals between the individual cells.<sup>23, 26, 27</sup>

The basal cell layer is the last layer of the corneal epithelium, and it is made up of a single layer of columnar cells. Desmosomes and gap junctions, which are involved in mediating and differentiating intercellular communication, are used to bind these cells to one another.<sup>23, 26, 27</sup> A basement membrane that is separated into an anterior lamina lucida and a more posterior lamina densa is secreted by these basal cells.<sup>29</sup> Collagens, laminins, proteoglycans, and nidogens make up the majority of the corneal epithelial basement membrane.<sup>30</sup>

The basement membrane is crucial to cellular processes, particularly those involved in healing. It regulates the binding of growth factors and their local concentrations between cell layers. The anchoring fibrils pass through the hemidesmosomes to Bowman's layer and down into the underlying stroma, where they attach to anchoring plaques of the extracellular matrix, forming an anchoring complex. The basement membrane of the basal cells attaches to the underlying Bowman's layer via hemidesmosomes.<sup>31</sup>

## **1.2 Recurrent Corneal Erosion**

RCE is a clinical syndrome characterized by repeated episodes of corneal de-epithelization specific to the area where epithelium is weakly adhered.<sup>1, 6, 7</sup> These episodes are typically acute and can cause symptoms ranging from minor irritability to severe pain.<sup>1, 17, 32</sup> The first report of RCE was published in 1872.<sup>33</sup> The most common cause of RCE is mechanical trauma (45% to 69%) followed by epithelial basement membrane dystrophy (EBMD) (20% to 30%). An abrasion from a fingernail, piece of paper, or tree branch is a common example of physical trauma, which causes a shallow corneal lesion. Between 5% and 25% of severe corneal abrasion cases are thought to subsequently develop RCE.<sup>1, 7, 32</sup>

Specialized adhesion complexes attach the corneal epithelium to Bowman's layer and basement membrane. Hemidesmosomes and anchoring fibrils make up these complexes. Damage to the adhesion complexes from trauma and corneal dystrophies puts the epithelium at risk for RCE.<sup>1,7</sup> The specific cause of the failure of adhesion complexes is unknown, however, a lack of the basement membrane, or hemidesmosomes are among the theories put forward by researchers.<sup>32</sup> This causes the epithelium to repeatedly rise, resulting in further abnormalities in the basement membrane.<sup>32</sup> Matrix metalloproteinase (MMP -2 and -9) activity is elevated in RCE patients.<sup>34</sup> These enzymes have the potential to harm the anchoring fibrils and basement membrane, leading to defective adhesion complexes.<sup>1,32</sup>

### 1.2.1 Treatments for RCE

Rapid re-epithelialization facilitation and pain relief are the two main therapeutic goals of RCE. The prevention of further erosion is a secondary objective.<sup>32</sup>

**Medical treatment** is chosen as the initial form of treatment to avoid recurrences, but 60% of patients will continue to experience symptoms after receiving care.<sup>35</sup>

**Antibiotics and pain relievers:** To treat discomfort, a topical nonsteroidal anti-inflammatory (NSAID) may be administered, however prolonged usage should be avoided as it may impede epithelial healing.<sup>36</sup> To reduce the risk of microbial keratitis, topical preventive antibiotics are commonly applied.<sup>1</sup> Oral opioids (such as hydrocodone with or without acetaminophen) may be required to offer appropriate pain control for patients with considerable pain or with substantial epithelial defects.<sup>37</sup>

**Combination therapy:** MMP-9 inhibitors, such as doxycycline, enhance resolution and aid in preventing recurrences.<sup>38,39</sup> For lubrication, topical ointments can be applied before bed. To maintain deturgescence of the corneal epithelium and increase adhesion, hypertonic ointments are frequently administered for weeks to months.<sup>40</sup> The salt concentration of these ointments, however, may irritate

certain patients.<sup>1</sup> Antibiotic prophylaxis is offered by erythromycin ointment, which may also lower MMP-9 levels.<sup>1,40</sup>

**Bandage Contact Lenses:** Patients who are unresponsive to lubrication may benefit from extended wear BCL. Patients can restore tight epithelial basement membrane adhesions by consistently wearing a BCL for six to twelve weeks, with the lens changed as necessary.<sup>18,41</sup>

Some patients will continue to experience small and significant RCE occurrences despite therapy for acute episodes. Surgery may be required for refractory situations. Through the stimulation of new and more powerful epithelial adhesion complexes, **surgical intervention** aids in preventing further recurrences.<sup>1,17,35</sup>

**Epithelial debridement:** This creates a smooth basement membrane by mechanically removing nonadherent or loosely attached epithelium, allowing healthy epithelium to reattach.<sup>1,5-7</sup> Under topical anesthetic, this treatment is usually carried out at the slit lamp and is safe and less invasive.<sup>1,5-7</sup>

**Diamond burr polishing:** Polishing may eliminate more abnormal basement membrane in comparison to basic debridement. As a result, the surface will be smoother, and the subsequent epithelial-stromal adhesion will be stronger, which should improve the outcome.<sup>42</sup> A diamond burr is used to lightly buff Bowman's layer until a smooth surface is achieved.<sup>40,42</sup>

**Anterior stromal puncture:** In this procedure, multiple shallow penetrations are made through the epithelium, reaching the anterior stroma. This leads to the forming of scarring attachments which improve epithelial adhesion.

### 1.3 Bandage Contact Lenses

Following Otto Wichterle's invention of hydroxyethyl methacrylate (HEMA), BCLs were first utilized in the 1970s.<sup>43</sup> Typically, they are recommended to treat pain, protect the cornea mechanically, and promote corneal surface healing.<sup>43, 44</sup> A promising treatment for patients who need BCLs has been made available to clinicians with the commercialization in 1999 of highly oxygen permeable silicone hydrogel materials.<sup>44</sup> Today's BCLs offer the same advantages as their predecessors but with better convenience, faster healing, and better corneal health due to improvements in material technology.<sup>43, 45</sup> The materials offer better mechanical protection and safer overnight wear than standard hydrogel lenses due to their increased oxygen transmissibility<sup>46</sup> and increased rigidity.<sup>47</sup>

Wearing a BCL over the injured cornea, ideally, will:

- i. Protect the injured cornea from the shearing forces of the blinking eyelid, thus preventing the dislodgement of the newly formed epithelial cells. Upon waking, as the eyes open, the shearing forces generated from the blinking pull away the newly formed epithelial cells.<sup>16, 48</sup> This is why patients experience pain upon waking in the morning without a BCL in place.<sup>17</sup>
- ii. Maintain the tear film on the ocular surface stable.<sup>16</sup>
- iii. Promote the repair of the corneal wound by acting as a shield from the external environment<sup>49</sup> and enabling the smooth development of adhesion plaques in the presence of extracellular matrix proteins like fibronectin, fibrinogen/fibrin, laminin, and tenascin.<sup>50, 51</sup> Fibrin and fibronectin release plasminogen activator which converts plasminogen to plasmin. Plasmin dissolves cell-to-substrate adhesions and permits the cells to move forward and create new adhesions.<sup>50, 51</sup>

BCLs are most frequently used in North America to treat corneal wounds and surgical problems. 72% of optometrists have recommended soft contacts for therapeutic purposes for some problem.<sup>44</sup> More than 81% of patients receiving BCL treatment also take medications concurrently.<sup>44</sup> Given that BCLs may be used on an extended-wear regimen for several weeks, the use of low oxygen transmissibility traditional hydrogel BCLs for the management of RCE's and abrasions is controversial. Traditional



hydrogel materials do not give enough corneal oxygenation when worn overnight,<sup>52</sup> which increases the risk of microbial keratitis.<sup>53</sup> Numerous studies examining the effectiveness of BCLs have been published. Ahmed and Breslin<sup>54</sup> showed that topical drops alone were more effective than BCLs at relieving pain following laser-assisted in situ keratomileusis, eliminating the need for BCLs. However, Brilakis and Deutsch employed BCLs in combination with topical medications to effectively manage pain following photorefractive keratectomy.<sup>55</sup> According to Simsek et al., using BCLs alone significantly enhanced corneal wound healing in rabbits, with BCLs helping to significantly reduce wound sizes.<sup>56</sup> Four patients with perforated corneal injuries were successfully treated with a BCL and topical medications without requiring surgical intervention.<sup>57</sup>

**Table 1-1:** Lists several FDA-approved soft BCLs <sup>16,58</sup>

<b>Brand</b>	<b>Manufacturer</b>
Acuvue Oasys with Hydraclear Plus	Johnson & Johnson Vision
Air Optix Night & Day Aqua	Alcon
Air Optix Aqua	Alcon
PureVision	Bausch & Lomb
UCL 55%	United Contact Lenses
Biofinity	CooperVision

BCLs are typically prescribed with the concurrent use of additional antibiotic eye drops at least twice daily, despite being effective in increasing patient comfort.<sup>59</sup> Antibiotics do not contribute to the healing process and include no substance that actively contributes to the regeneration of corneal epithelial cells, and the healing process can take months to recover in some cases.<sup>18, 59, 60</sup> To enhance the rate of wound

healing, these BCLs could be manufactured to incorporate therapeutic agents or drugs that speed up the healing process.

## **1.4 Therapeutic contact lenses for drug delivery**

The concept of using contact lenses for ocular drug delivery was proposed in the 1960s.<sup>61, 62</sup> Unfortunately, there were too many challenges with the materials of this era, primarily due to poor oxygen delivery to the cornea. The long-term therapeutic potential of contact lenses was constrained by the hypoxia-related problems that resulted, particularly during overnight wear.<sup>63, 64</sup> This problem was not remedied until oxygen permeable silicone hydrogel (SH) contact lenses were invented in the 1990s, which came about several decades later. These novel lenses rekindled interest in creating contact lenses to deliver medications by overcoming the substantial hypoxic hurdle.<sup>47</sup> Several ocular limitations that prevent effective drug absorption and penetration can be removed by using contact lenses for ocular drug delivery.

The natural tear film is divided into the pre- and post-lens tear compartments when a contact lens is applied to the cornea.<sup>65</sup> There is limited mixing and exchange of tears in the post-lens compartment.<sup>66-68</sup> In contrast to eye drop solutions, which have a residence time of just 1-3 minutes, drug release from therapeutic contact lenses into the pre- and post-lens tear film can be present for more than 30 minutes.<sup>69, 70</sup> Therefore, the drugs released from the contact lens into this compartment will exhibit prolonged contact with the cornea, resulting in greater bioavailability of up to 50%, as opposed to 5% for topical drug administration.<sup>71, 72</sup>

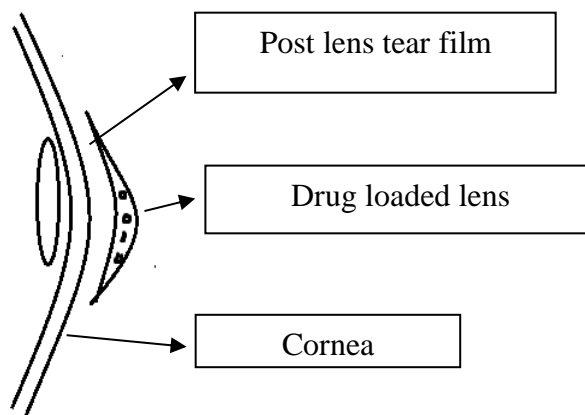


**Figure 1-4:** Schematic representation of a drug laden contact lens placed over the cornea

The goal of creating contact lenses for ocular drug administration has been to prolong the time that pharmaceuticals are released from them. Due to their improved qualities, including the ability for extended wear and a higher bioavailability than eye drop formulation, therapeutic contact lenses have been proposed for controlled and sustained ocular drug delivery.<sup>72-74</sup> Incubating a commercial contact lens in a pharmaceutical preparation is the simplest way for simple drug loading, although this frequently leads to rapid drug release that might not be clinically helpful.<sup>73, 75</sup> As a result, alternative techniques for creating novel contact lens materials have been investigated, such as molecular imprinting,<sup>76</sup> vitamin E coatings,<sup>73, 77</sup> and drug encapsulation utilizing nanoparticles.<sup>78, 79</sup>

### 1.4.1 Methodology to design therapeutic contact lenses

**Soaking Method:** This is the simplest method to load drugs into contact lenses. It involves soaking a preformed contact lens in a drug solution or suspension or emulsion followed by simple drug uptake by the lens and subsequent release onto the ocular surface.<sup>72, 80-82</sup> The drug is absorbed due to the

different concentrations of the active ingredients in the soaking solution and the polymer matrix.<sup>72</sup> The drug uptake by the lens matrix is dependent on the soaking time of the lens in the drug solution, the lens material charge and hydrophobicity and the drug concentration, charge and molecular weight.<sup>72</sup> A comparison study on soaking a contact lens in a solution and microemulsion of bimatoprost showed that drug absorption using a microemulsion was twice that found with the solution alone.<sup>83</sup> Several studies have explored the use of therapeutic contact lenses following this soaking method to release drugs, including timolol,<sup>84</sup> pilocarpine,<sup>85</sup> dexamethasone<sup>86</sup> and brimonidine tartrate.<sup>87</sup> Ionic contact lenses with negatively charged surfaces (balafilcon A and etafilcon A) showed improvement in drug uptake release of ketotifen fumarate.<sup>88</sup> Schultz et al. studied timolol maleate and brimonidine tartrate uptake and release from soaking solution using contact lenses.<sup>87</sup> Clinical studies in glaucoma patients (30 minutes wear per day for two weeks) revealed a reduction in IOP, which was equal to eye drop treatment with a 10-times lower dose.<sup>87</sup> By manipulating the composition of the hydrogel monomer and creating microstructural alterations with water during the fabrication process, Eva Garcia et al. increased the drug-loading capacity of triamcinolone acetonide and modulated release profile from soft contact lenses.<sup>89</sup>

Though the soaking method is simple and cost-effective, the soaked therapeutic contact lenses have two major limitations.<sup>90-93</sup> A high initial burst release, in conjunction with a high concentration of ophthalmic medications impregnated on the contact lens outer surface rather than deep within the polymeric matrix. In many instances, the contact lenses released 90–95% of the drug loaded following the soaking method in just a few hours.<sup>90-94</sup> Hyaluronic acid and other high molecular weight substances do not pass thorough the aqueous channels of contact lenses and instead stay on the surface, demonstrating the ineffectiveness of continuous medication administration for the treatment of dry eye.<sup>95</sup> Most ophthalmic medications, including timolol maleate,<sup>93</sup> olopatadine hydrochloride, brimonidine tartrate, etc.,<sup>87</sup> have a low affinity for contact lenses. Low affinity causes the drug to be poorly retained by the contact lenses, release quickly (burst release), and then decrease steeply, never achieving relevant therapeutic levels for any extended period of time within the therapeutic window.<sup>96</sup>

**Drug-loaded therapeutic contact lenses:** Incorporating drug or drug-loaded structures such as nanomaterials, liposomes, and micelles into the contact lens matrix prolongs the release of ophthalmic drugs.<sup>97,98</sup> A drug's half-life and retention period can be extended by encasing it, and it also allows for targeted delivery to a particular region or portion of the eye. These tiny polymer particles can be tailored for targeted administration or to facilitate the carrier's passage across some hydrophobic regions of the tear film. Drug or formulated drug-loaded structures are dispersed into the contact lens matrix to fabricate therapeutic contact lenses.<sup>99,100</sup> Drug-loaded nanoparticles provide further resistance to drug release and stop drugs from interacting with the polymerization mixture.<sup>97</sup> Thus, contact lenses with nanoparticles can deliver medications for a long time at a controlled rate.<sup>97</sup> Jung et al. created therapeutic contact lenses by dispersing timolol-loaded propoxylated glyceryl triacylate nanoparticles in contact lens matrix. The drug was released at a sustained rate for one month and reduction in intraocular pressure was confirmed.<sup>97</sup> To decrease natamycin's dosage and dosing frequency, Chandasana et al. developed corneal targeted nanoparticle-loaded contact lenses. Gulsen et al. incorporated dimyristoyl phosphatidylcholine liposomes that were loaded with lidocaine in the contact lens material, which released lidocaine for around eight days.<sup>101</sup> In another study by Danion et al., two layers of liposomes in hydrogel contact lenses demonstrated drug release for up to 30 hours, whereas ten layers showed drug release for up to 120 hours.<sup>102</sup>

**Molecular imprinting:** Another unique technique used to make therapeutic contact lenses is molecular imprinting.<sup>103,104</sup> During the fabrication process, a cavity in the shape of the desired drug to be delivered is created.<sup>105</sup> As a result, the amount of drug injected into the polymer matrix rises while the drug's burst release into the environment decreases. Because of the interactions between the polymer and the drugs, sustained release of the drug template is generally promoted when imprinted devices are used for drug delivery.<sup>104</sup> Using molecular imprinted lenses, an extended release of hydroxypropyl methylcellulose was achieved for 60 days at rate of 16  $\mu\text{g}/\text{day}$  for dry eye treatment.<sup>106</sup> Using molecular imprinted technology, hyaluronic acid was delivered for 24 hours at a 6  $\mu\text{g}/\text{hour}$  release rate.<sup>107</sup>

This method showed potential for delivering a single drug, but it is not scalable for other purposes and involves a complex production process that is difficult to incorporate into already available commercial products.<sup>105</sup> One of the main limitations of this technology is the highly cross-linked structure of

hydrogels, which impacts the lens material's optical and physical performance.<sup>108</sup> In this technology, template molecules and functional monomers limit how much drug can be loaded into them, and contact lens deformation (change in dimension) after the drug has been released has also been observed.<sup>109</sup> Molecular imprinted contact lenses cannot be worn for an extended period of time due to the decreased ion and oxygen permeability caused by the decrease in water content (reduction in swelling).<sup>110</sup>

**Loading Vitamin E into therapeutic lenses:** Incorporating Vitamin E into lenses is another promising approach for sustaining drug release, especially for hydrophilic compounds.<sup>73, 74, 77, 111, 112</sup> It was observed that vitamin E loading slowed down the drug release rate.<sup>65, 73</sup> Vitamin E loadings of 10 and 40% extend timolol's release duration by a factor of around 5 and 400, respectively. However, this approach impacted the oxygen and ion permeability.<sup>73</sup> In another study, dexamethasone contact lenses were developed and modified using vitamin E loading. Dexamethasone release duration was 16 times higher compared to release from contact lenses without vitamin E loading.<sup>77</sup> Using vitamin E as a barrier, Peng et al. developed contact lenses containing cyclosporine for chronic dry eye treatment. Due to the high partition coefficient of the drug in the gel, the release profile from silicone hydrogel contact lenses demonstrated sustained drug release for almost a month, as compared to the hydrogel ACUVUE® lens (etafilcon A), which demonstrated release for only 24 hours (due to its hydrophilic nature).<sup>113</sup>

Vitamin E is a powerful antioxidant. It protects the cornea from harmful ultraviolet radiation and even prevents the oxidation of susceptible drugs.<sup>114</sup> Although loading vitamin E was explored to be a promising approach that delays the release of many hydrophilic drugs, it has limitations, including protein adsorption due to vitamin E's hydrophobic nature, reduction in ion permeability,<sup>73</sup> oxygen permeability<sup>73</sup> and change in mechanical properties,<sup>73,77</sup> which may restrict its use for the development of therapeutic contact lenses.

**Supercritical fluid technology:** Yañez et al. developed a novel supercritical fluid-assisted molecular imprinting approach to overcome the primary drawbacks of using the traditional soaking and molecular imprinting.<sup>115</sup> It is one of the most efficient ways to load or impregnate both hydrophilic and

hydrophobic drugs in contact lenses using a supercritical solvent like carbon dioxide. The impregnation process involves the drug being dissolved in a supercritical solvent, such as carbon dioxide (at subcritical or supercritical conditions), and then subsequent interaction with hydrogel contact lenses. The drug loading and release kinetics can be controlled by controlling pressure, temperature, processing time, and depressurization rate.<sup>116, 117</sup> The supercritical fluid approach does not change the essential functional characteristics of contact lenses and demonstrated enhanced drug loading and extended release.<sup>115, 118</sup> Yokozaki et al. demonstrated that changing the temperature or pressure increased the amount of salicylic acid loaded into contact lenses.<sup>119</sup> However, in the same study, it was observed that less salicylic acid was impregnated by accelerating the depressurization process, which induced the contact lens material microstructure to collapse.<sup>119</sup> In another study with the supercritical impregnation of cefuroxime sodium into contact lenses, the drug release was significantly extended up to several days. However, in certain conditions, a foaming phenomenon was observed due to supercritical carbon dioxide.<sup>120</sup> Because it jeopardizes one of the contact lenses' most crucial functional characteristics, their optical transparency, polymer foaming must be avoided when it comes to the development of contact lenses.

All of the drug loading and release methods described above have their own benefits, and while each technique is viable, they are not very scalable, and remain quite challenging to implement into existing commercial products or demand for complicated manufacturing processes.

**Table 1-2:** An overview of methods for the fabrication of therapeutic contact lenses

<b>Fabrication technique</b>	<b>Drug</b>	<b>Clinical condition</b>	<b>Result</b>	<b>References</b>
Molecular imprinting	Brimonidine tartrate	Glaucoma	Improved drug loading and controlled release profile	Omranipour et.al. <sup>121</sup>
Molecular imprinting	Bimatoprost	Glaucoma	Improved drug uptake and sustained release kinetics compared to soaking method	Yan et.al. <sup>122</sup>
Molecular imprinting	Olopatadine	Allergic conjunctivitis	Sustained drug release with good ocular biocompatibility	Gonzalez-Chomon et.al. <sup>123</sup>
Copolymerization and casting method	Olopatadine	Allergic conjunctivitis	Sustained release up to 120 hours and without changing optical and swelling properties of lens	Xue et.al. <sup>124</sup>
Copolymerization	Timolol maleate	Glaucoma	Sustained drug release for 2-4 weeks	Jung et.al. <sup>125</sup>
Copolymerization	Betaxolol hydrochloride	Glaucoma	Extended drug release for 10 days	Zhu et.al. <sup>126</sup>



<b>Fabrication technique</b>	<b>Drug</b>	<b>Clinical condition</b>	<b>Result</b>	<b>References</b>
Copolymerization	Loteprednol etabonate	Inflammation	Extended drug release up to 12 days	Nasr et.al. <sup>79</sup>
Soaking	Timolol	Glaucoma	Prolonged reduction in intraocular pressure for 96 hours	Wei et.al. <sup>127</sup>
Soaking	Pirfenidone	Corneal scarring due to chemical burns	Improved drug concentration and retention in the cornea and tear fluid	Yang et.al. <sup>128</sup>
Soaking	Latanoprost	Glaucoma	Silicone hydrogel lenses provided an ideal platform for the rapid loading and sustained delivery of a hydrophobic drug, latanoprost	Home et.al. <sup>129</sup>
Casting polymer film on the periphery of methafilcon	Dexamethasone (Dex)	Retinal vascular leakage	Achieved 200 times increased in retinal drug concentration compared to Dex eye drops	Ross et.al. <sup>130</sup>

## 1.5 Gelatin Methacrylate (GelMA) hydrogel

The soft lens material chosen for a therapeutic BCL must be transparent and able to adjust to the shape of the eye without irritating the cornea as the ocular drug delivery system comes into contact with it. One potential option is a hydrogel material called GelMA because of its odourless, transparent, biocompatible, and adjustable characteristics.<sup>131, 132</sup>

Hydrogels comprise three-dimensional hydrophilic polymer networks.<sup>133</sup> Their physicochemical characteristics can be altered by varying their co-monomer combinations, crosslink densities, and synthetic circumstances (such as reaction time, temperature, and types and dosage of solvent).<sup>134</sup> Hydrogels play a significant role in biomedical disciplines, such as tissue engineering, regenerative medicine, drug delivery, and others.<sup>134-137</sup> Hydrogels are quite similar to the extracellular matrix found in the human body,<sup>137</sup> which makes them a good mimic for in vitro cell culture. Hydrogels are categorized into natural and synthetic hydrogels.<sup>138</sup> Natural hydrogels are more biocompatible than synthetic hydrogels, and this significantly influences cellular survival, proliferation, differentiation, and migration.<sup>139</sup>

Gelatin is a natural hydrophilic polymer formed by the hydrolysis and denaturation of collagen at an elevated temperature.<sup>140</sup> It is a biocompatible and degradable polymer.<sup>140</sup> Owing to its biocompatibility, gelatin is used in tissue engineering applications.<sup>141, 142</sup> Gelatin contains the arginine-glycine-aspartic acid (RGD) peptide sequence, which supports specific cell behaviours (such as adhesion, proliferation, and differentiation), and an MMP degradation sequence, which encourages enzymatic degradation.<sup>143, 144</sup> However, gelatin has low thermostability (gelatin will dissolve at temperatures over 37 °C due to the cleavage of hydrogen bonds), and chemical crosslinking may impair gelatin's biocompatibility because some crosslinking agents are hazardous. The poor thermostability limits the application of gelatin as a result. Fortunately, gelatin has numerous large active groups in its side chains, including -OH, -COOH, -NH<sub>2</sub>, -SH, and others. As a result, the disadvantages of gelatin can be relatively easily overcome using a variety of approaches.<sup>138, 140</sup>

Van Den Bulcke et al. introduced GelMA in 2000,<sup>143</sup> which is formed by combining gelatin and methacrylic anhydride (MA). Methacryloyl groups of MA replace many of the amino groups found on the side chains of gelatin, resulting in modified gelatin.<sup>143</sup> Covalently crosslinked hydrogels are created when GelMA, with the help of a photo-initiator undergoes photoinitiated radical polymerization on exposure to ultraviolet light.<sup>138</sup> Since GelMA is a gelatin derivative, it retains most of the RGD sequences and MMP sensitive degradation sites.<sup>131</sup> Hence GelMA is an excellent biocompatible material<sup>131, 138, 145-147</sup> (which is tolerated by the host body with low degree of inflammatory reaction<sup>148</sup>) with the potential for being broken down by collagenase enzymes, particularly MMP-9.<sup>149, 150</sup> This allows for enzyme responsive controlled release delivery by adjusting methacrylation degree, polymer concentration, and ultraviolet exposure.<sup>131, 151</sup> GelMA possesses excellent thermostability<sup>131, 152</sup> and tunable properties.<sup>131, 153</sup>

### 1.5.1 Synthesis of GelMA hydrogels

GelMA is synthesized by substituting lysine and hydroxyl lysine with MA in an alkaline buffer solution such as phosphate-buffered saline (PBS) (pH 7.4)<sup>131, 154</sup> and carbonate-bicarbonate buffer.<sup>155</sup> MA is added dropwise into the vigorously stirred gelatin/buffer solution to produce the reaction. A 5-day dialysis procedure is used to remove any remaining MA and any accompanying methacrylic acids. The resultant mixture is freeze dried, generating foam-like GelMA.<sup>131, 156</sup> Due to the introduction of photo-crosslinkable functional groups and the gelatin backbone, GelMA has both reversible and irreversible solidification processes.<sup>131, 156</sup> Reversible solidification takes place in a temperature dependent solid-liquid transition. Non-reversible solidification occurs in the presence of a photoinitiator (e.g., Irgacure 2959 or Lithium phenyl-2,4,6-trimethylbenzoylphosphinate) and ultraviolet light.<sup>131, 156</sup> The percentage of carbon double bonds that have been substituted with MA in a single GelMA molecule, also known as the degree of substitution (DS), is a critical factor in determining GelMA's mechanical properties, water retention, and degradability.<sup>131, 156</sup> Young's modulus, degradation time, and swelling ratio are all higher in GelMA with a higher DS.<sup>157, 158</sup> GelMA has numerous applications in the biomedical sector due to its straightforward one-step production and controllable properties.<sup>131, 138, 146, 147, 159, 160</sup>

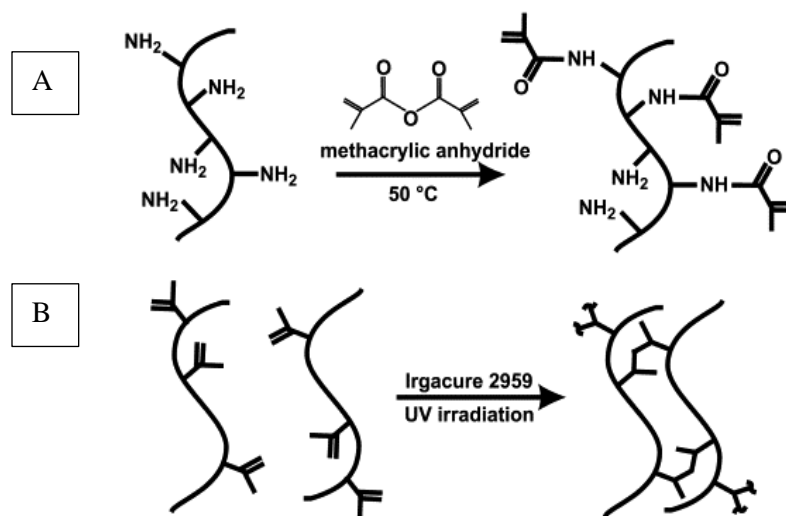


**Figure 1-5:** Synthesis of GelMA. (A) Primary amine groups of gelatin react with MA to add methacrylated groups. (B) Formation of hydrogel network of GelMA<sup>132</sup>

## 1.5.2 Biomedical applications of GelMA

### 1.5.2.1 Tissue Engineering

**Skin regeneration:** GelMA hydrogels can be used as a primary component of wound dressings because they resemble the natural dermal extracellular matrix and their controllable mechanical and degrading properties.<sup>161, 162</sup> Zhao et al. demonstrated that GelMA scaffolds could facilitate the formation of the multi-layered epidermis and the development of keratinocytes into tissue that function like the multi-layered epidermis. They used GelMA hydrogels to build a 3D cellularized extracellular matrix mimetic scaffold to promote wound healing.<sup>163</sup> GelMA-based intelligent, responsive wound dressing vesicle systems were developed by Zhou et al. to kill or inhibit bacteria like methicillin-resistant *S. aureus* and *P. aeruginosa* with a visible infection alert.<sup>164</sup> GelMA scaffolds with Ag nanoparticles embedded, as

demonstrated by Jahan et al., can hasten the healing of wounds, particularly deep skin wounds.<sup>165</sup> These scaffolds encouraged fibroblast migration and reduce microbial infections when used as a wound dressing.<sup>165</sup>

**Tendon regeneration:** Tendons form a link between muscle and bones, allowing the former to move the latter with ease. Tendons are vulnerable to rupture and laceration because of their load-bearing nature.<sup>166</sup> Using dual electrospinning, Yang et al. created a GelMA/poly- $\epsilon$ -caprolactone (PCL) composite scaffold.<sup>167</sup> The cells encased within these scaffolds remained receptive to topographical cues and exogenous tenogenic factors, and these multilayer constructs mimic the natural structure of tendon tissue.<sup>167</sup> With the aid of 3D printing, Visser et al. proposed a highly structured and highly porous GelMA composite microfibre network to enhance mechanical and biological properties.<sup>168</sup> This composite scaffold's rigidity and elasticity were comparable to the native tissue.<sup>168</sup> In a recent study, Rinoldi et al. created a scaffold that mimics the form and structure of real tendon tissues using GelMA and alginate as bioinks.<sup>169</sup> This scaffold offered mechanical stretching and orientation alignment that mimics the natural tendon.<sup>169</sup>

**Bone regeneration:** GelMA can be combined with various growth factors, and the hydrogel's combination of polymer and organic components can make it a viable option for bone tissue engineering. GelMA/bioglass nanoparticles developed by Kwon et al., demonstrated the value of the bioglass-infused GelMA cryogels for bone repair.<sup>170</sup> These cryogels exhibit great mechanical strength and can stimulate osteogenic differentiation in human turbinate mesenchymal stromal cells.<sup>170</sup> Liu et al. developed biomimetic GelMA composite nanofibers by electrospinning that encouraged angiogenesis and osteogenesis.<sup>170</sup> This structure showed excellent cytocompatibility, favourable biocompatibility, and good mechanical qualities. Additionally, they discovered that this composite encouraged osteogenic differentiation of MC3T3-E1 murine osteoblast cells and angiogenesis of human umbilical vein endothelial cells.<sup>170</sup>

**Cartilage regeneration:** Because of its tunable mechanical qualities, which can simulate the structure of native cartilage, GelMA hydrogels have also been widely used for cartilage regeneration.

GelMA/PCL microfibrinous networks were created by Visser et al. using melt electrospinning to improve the mechanical properties of GelMA.<sup>170</sup> The stiffness of these networks demonstrated similar stiffness and elasticity to cartilage tissue.<sup>170</sup> Han et al. developed a GelMA/polyacrylamide biohybrid hydrogel for the construction of composite structures.<sup>171</sup> This hydrogel showed improvements in compression strength, elasticity, degradation rate, and growth factor release. This biohybrid hydrogel was tested both *in vitro* and *in vivo*, and the results demonstrated that it could preserve the phenotype of chondrocytes while repairing cartilage defects.<sup>171</sup> A GelMA-based poly (ethylene glycol), gelatin, and heparin multi-composite scaffold was developed by Chen et al. to preserve the cartilaginous phenotype.<sup>172</sup> They showed that these hydrogels could regenerate cartilaginous interfacial tissues *in situ*.<sup>172</sup>

**Vascular regeneration:** GelMA has a wide range of applications for building a 3D vascular network. GelMA hydrogels were shown by Chen et al. to facilitate the development of vascular networks from human progenitor cells.<sup>173</sup> The extent of methacrylation modulates the degree of vascular development and affected the physical properties of GelMA. GelMA's lower degree of methacrylation exhibited softer properties and promoted favourable vascular formation.<sup>173</sup> In another study, sustained release of desferrioxamine from a GelMA hydrogel for diabetic skin regeneration was fabricated by Chen et al.<sup>174</sup> This hydrogel network created an environment conducive to cell proliferation and increased the expression of hypoxia-inducible factor 1 $\alpha$ , which is essential for blood vessel creation and skin reconstruction.<sup>174</sup> Jia et al. 3D-printed biologically relevant, highly structured, and porous vessels with substantial promise for engineering large-scale vascularized tissue structures using GelMA, sodium alginate, and poly (ethylene glycol)-tetra-acrylate as the bioink.<sup>175</sup> PCL/GelMA coaxial electrospun fibres were created by Coimbra et al. to offer good mechanical and biocompatibility qualities.<sup>176</sup> When interacting with blood, this type of shear structure reduced hemolysis and thrombosis while boosting the biological performance of the materials.<sup>176</sup>

Below (Table 1-3) is the list of applications of GelMA in tissue engineering.

**Table 1-3:** GelMA with different modifiers for tissue engineering applications

<b>Modifier</b>	<b>GelMA concentration</b>	<b>Application of hydrogel</b>	<b>References</b>
Vascular endothelial growth factors (VEGF)	9% w/v	Skin wound healing in porcine model	Nutilla et.al. <sup>177</sup>
VEGF-mimicked peptide	5% w/v	In vitro microvascularization of endothelial cells	Parthiban et.al. <sup>178</sup>
Transforming growth factor (TGF)- $\beta$ 3	10% w/v	Cartilage regeneration in rat model	Cao et.al. <sup>179</sup>
TGF- $\beta$ 1-affinity peptide	20% w/v	Cartilage regeneration	Ju et.al. <sup>180</sup>
Platelet lysates	15% w/v	Skin tissue engineering	Daikuara et.al. <sup>181</sup>
Hyaluronic acid	15% w/v	Skin wound healing	Guan et.al. <sup>182</sup>
Hyaluronic acid	7% w/v	Cartilage regeneration	Lee et.al. <sup>183</sup>
Chitosan	15% w/v	Bone osteogenesis and angiogenesis	Zhang et.al. <sup>184</sup>
Chitosan	5% w/v	Peripheral nerve tissue regeneration	Chen et.al. <sup>185</sup>
Alginate	1% w/v	Wound healing and soft tissue regeneration	Ansari et.al. <sup>186</sup>

<b>Modifier</b>	<b>GelMA concentration</b>	<b>Application of hydrogel</b>	<b>References</b>
Alginate	10% w/v	Bioprinting tunable small diameter blood vessels	Zhou et.al. <sup>187</sup>
Silk fibroin	10% w/v	Wound healing in mouse	Naderi et.al. <sup>188</sup>
Silk fibroin	10% w/v	Bioink	Na et.al. <sup>189</sup>
Silk fibroin	10% w/v	Corneal regeneration	Farasatkia et.al. <sup>190</sup>
Carbon nanotubes	7% w/v	Cardiac tissue engineering	Lee et.al. <sup>191</sup>
Nanosilver	15% w/v	Antibacterial activity for infected bone defects	Ou et.al. <sup>192</sup>
Dopamine	6.25% w/v	Promoting neural degeneration	Zhou et.al. <sup>193</sup>

### **1.5.2.2 Drug delivery**

GelMA has been utilized as a drug delivery vehicle in different forms. Chen et al. employed GelMA hydrogels with chitosan microspheres to treat osteoarthritis. A promising treatment method for osteoarthritis involved delivering the sinomenium encapsulated by chitosan and GelMA hydrogel intra-articularly to activate autophagy and effectively ameliorate cartilage matrix degradation.<sup>194</sup> GelMA can be used as a microparticle drug delivery system. Using microfluidics technology, Li et al. created a novel, sustained GelMA/poly (lactic-co-glycolic acid) microparticle drug delivery system. With the degradation of the biopolymer layer, these microparticles deferred the burst release of the loaded drugs and extended the release.<sup>195</sup> Luo et al. developed a controlled GelMA-based microneedle to deliver



doxorubicin. The loaded doxorubicin in the GelMA-based microneedle patch was released gradually, particularly at greater crosslinking intensities.<sup>196</sup>

### **1.5.2.3 Biosensor**

An analytical tool called a biosensor is used to find a specific chemical or biological component. A low-cost, disposable cell-based paper biosensor for the milk allergy casein was created by Jiang et al. GelMA, carbon nanofiber, and graphene, consisting of high conductivity, stability, and practical qualities, were used in this study to modify the biosensor.<sup>197</sup> Topkaya created a new DNA hybridization indicator with improved sensitivity to detect minute concentrations of oligonucleotides by altering the pencil graphite electrode with GelMA.<sup>198</sup> Li et al. used micro-structured GelMA as the primary dielectric layer to create a wearable touch sensor. The resulting sensor was highly sensitive, transparent, and biocompatible. Compared to existing hydrogel-based sensors, the GelMA tactile sensor performed at a higher pressure sensitivity of 0.19 kPa and a lower detection limit of 0.1 Pa because of its excellent mechanical and electrical capabilities.<sup>198</sup>

### **1.5.3 GelMA+**

It is interesting to note that in some studies, enzymatically cross-linked gelatin hydrogels with pre-formed physical networks reported lower mechanical strength at an elevated temperatures around 37 °C.<sup>199, 200</sup> In a previous study undertaken within Dr. Evelyn Yim's lab (Department of Chemical Engineering, University of Waterloo), a sequential hybrid crosslinking involving both physical and chemical crosslinking was executed on the conventional GelMA hydrogel to address the weak mechanical properties of GelMA, to form an improved GelMA material, termed as “GelMA+”.<sup>201</sup>

To synthesize hybrid crosslinked GelMA+ hydrogel, the prepolymer mixture of GelMA goes through an additional incubation at 4 °C for 1 hour before being irradiated with ultraviolet radiation to form a permanent gel.<sup>201</sup> Compared to the standard GelMA, the production of a physical gel at 4 °C before ultraviolet crosslinking develops triple helix and physical networks, which boosts covalent crosslinking

density and provides for a more homogenous microstructure. The combined impacts enhances the GelMA+ hydrogels' mechanical properties like compressive and dynamic modulus.<sup>201</sup>

According to Bode et al. study on enzymatically crosslinked gelatin hydrogels, it was observed that at higher temperatures around 37 °C, physical crosslinks of gelatin hydrogels demonstrated weaker physical strength and came apart.<sup>199</sup> However, Rizwan et al. showed that the mechanical rigidity of GelMA+ hydrogels did not significantly deteriorate when the temperature rose from 10 °C to 40 °C and was thermally stable.<sup>201</sup> The reason being that physical cross linkages might instead prevent the enzyme from accessing crosslinking sites. Since the mechanical properties remained constant up to 40 °C and no melting transitions were noticed, it appeared that the covalent crosslinks created by ultraviolet exposure stabilize the physical crosslinks.<sup>201</sup>

Rizwan et al. study on bioactive hydrogel showed that the GelMA+ hydrogels at a given enzymatic concentration degraded more slowly than the GelMA hydrogels.<sup>201</sup> The prepolymer concentration and degree of crosslinking were generally correlated with the rate of biodegradation. Thus, the slower breakdown rates of GelMA+ revealed a larger crosslinking density of GelMA+ than GelMA.<sup>201</sup> The degradation-mediated sustained and slow release of therapeutics from the matrix over an extended period of time may also be successfully accomplished using the slowly degrading GelMA+ hydrogels.

Since, in this project, the release of potential corneal wound therapeutic agent bovine lactoferrin in the presence of MMP-9 was undertaken at 37 °C and the aim was to obtain a sustained release profile of bovine lactoferrin for 5 days, GelMA+ was the choice of biomaterial for this project.

## **1.6 Bovine lactoferrin– a potential corneal wound healing therapeutic**

Lactoferrin is an iron binding glycoprotein belonging to the transferrin protein family alongside serum transferrin, ovotransferrin, melanotransferrin, and carbonic anhydrase inhibitor.<sup>202-204</sup> Initially found in bovine milk,<sup>205</sup> mucosal epithelial cells and neutrophils naturally produce and secrete it in various

mammalian species,<sup>206</sup> including humans. Particularly present in bodily fluids including saliva,<sup>207</sup> milk,<sup>208</sup> and tears,<sup>209</sup> lactoferrin is also expressed in several organs, including the mammary gland,<sup>210</sup> uterus,<sup>210</sup> kidney,<sup>211</sup> and brain.<sup>212</sup>

Bovine lactoferrin (BLF) is a 78 kDa glycoprotein.<sup>213</sup> Lactoferrin from bovine milk is termed as BLF, the main lactoferrin used in human medicine because of its easy availability.<sup>214</sup> Like human lactoferrin (HLF), it is a simple polypeptide chain folded into two symmetrical lobes (N and C lobes).<sup>203, 213</sup> Each lobe contains two domains, referred to as N1 and N2, or C1 and C2, which enclose a deep cleft where the iron-binding site is located.<sup>215</sup> The polypeptide chain of BLF consists of 689 residues while HLF consists of 691 residues. BLF and HLF both have nearly identical polypeptide chain conformations. Additionally, compared to HLF, BLF has an extra disulfide bond.<sup>215</sup> BLF plays important biological functions, including being a wound healing agent,<sup>213, 216-219</sup> antioxidant,<sup>220</sup> and having anticancer,<sup>221</sup> anti-inflammatory,<sup>222</sup> anti-fungal<sup>223</sup> and antimicrobial properties.<sup>224</sup>

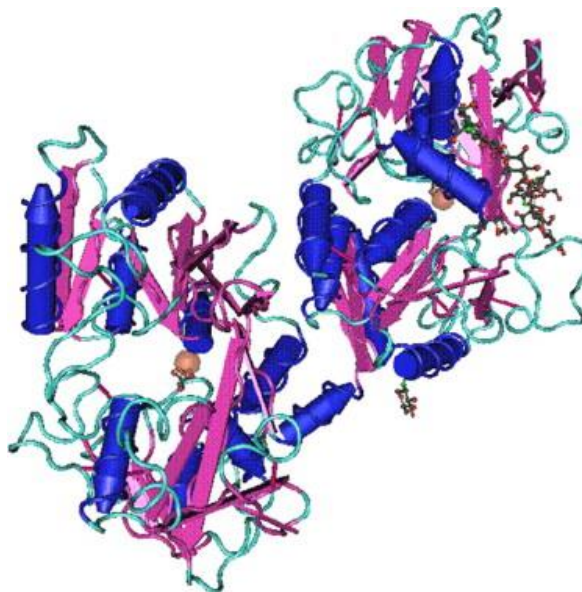


**Figure 1-6:** Structure of biferric BLF<sup>203</sup>

The finding that BLF encourages fibroblast-mediated collagen gel contraction led to the proposal of a role for lactoferrin in enhancing skin wound healing.<sup>225</sup> A crucial step in the healing process is when fibroblasts produce enough mechanical force to constrict the wound, which reduces the wound borders and allows for re-epithelialization.<sup>226</sup> Both bovine and human lactoferrins function in a dose-dependent manner to encourage collagen gel contraction by WI-38 human fibroblasts.<sup>219, 225, 227</sup> Compared to native BLF or its N-lobe (amino acids 1–284), the C-lobe of BLF (amino acids 341-689) has a more pronounced impact on collagen gel contractile activity.<sup>228</sup>

BLF has been demonstrated to minimize irradiation-induced corneal epithelium damage in mouse models<sup>216</sup> and to speed up corneal wound healing following an alkali-burn injury when applied topically.<sup>229</sup> Ashby et al. showed that the C lobe of BLF is the active part responsible for inducing corneal epithelial wound healing in an alkali wound model.<sup>213</sup> BLF controls the expression of proinflammatory and anti-inflammatory cytokines during the healing of corneal wounds, causing a small rise in the expression of Interleukins (IL)-1 $\beta$  and tumour necrosis factor (TNF)- $\alpha$ . TNF- $\alpha$  deficiency causes a delay in corneal wound closure, whereas IL-1 $\beta$  is crucial in the initial stages of alkaline corneal wound repair.<sup>229</sup> Polymorphonuclear neutrophils are attracted to the site of ocular damage and inflammation by BLF therapy, which also reduces the generation of IL-8, a potent chemotaxis factor for neutrophils.<sup>217</sup>

The molecule lactoferrin comprises 25% of the proteins found in human tears and is mostly secreted by the lacrimal gland.<sup>230</sup> Studies have shown a significant correlation between low tear lactoferrin levels and development of dry eye.<sup>231, 232</sup> Markers of inflammation and oxidative stress are present in dry eye.<sup>233</sup> Due to increased tear evaporation, decreased tear volume, and altered qualitative content of the tear film, a hyperosmolar environment is created, which sets off inflammatory and oxidative cascades and impairs epithelial proliferation and differentiation.<sup>233</sup> The potential use of BLF in the management of dry eye disease is justified by its ability to combat the underlying inflammation and oxidative stress. BLF, in particular, provides oxygen free radical and hydroxyl scavenging capabilities because of its capacity to chelate iron, which inhibits reactive oxygen species' pro-inflammatory and tissue-damaging

actions.<sup>234</sup> The inflammatory mediators TNF- $\alpha$ , (ILs)-1, -6, and -8, the intercellular adhesion molecule (ICAM)-1, and CD14 are downregulated by lactoferrin by inhibiting complement activation.<sup>235</sup> Patients who took oral lactoferrin (obtained from bovine milk) supplements demonstrated improved tear film stability and improvement in dry eye symptoms.<sup>236</sup> In a rabbit model of dry eye, locally applied BLF was able to restore corneal epithelial integrity, pointing to the possible use of lactoferrin eye drops for treating dry eye disease.<sup>237</sup>

GelMA is porous in structure (around 200 microns dimension)<sup>238</sup>; hence, a high molecular weight corneal wound healing agent would be appropriate for a sustained release profile of the therapeutic. Owing to the large molecular size (78 kDa) and wound healing properties of BLF, it was chosen as the corneal wound healing therapeutic for this project.

## **1.7 Role of MMP-9 in corneal epithelial wound healing**

MMPs are a collection of 25 zinc-dependent proteinases which break down at least one element of the extracellular matrix, and control numerous physiological and pathological processes.<sup>239</sup> They are essential for the development of organs, subsequent tissue remodeling, inflammation, and damage.<sup>239</sup> According to their preference for particular substrates, MMPs can be roughly classified into four groups: membrane-type MMPs, collagenases, gelatinases, and stromelysins. Connective tissue cells, granulocytes, and monocyte macrophages produce the majority of MMPs.<sup>240</sup> MMPs are linked to the pathophysiology of numerous diseases affecting the ocular surface.<sup>241</sup> These molecules affect the structure of collagenous filaments, cellular adhesion, and basement membrane permeability to induce changes in the ocular surface in response to an external insult.<sup>241</sup> They interact with numerous pro inflammatory cytokines, signal transduction molecules, and transcription factors.<sup>241</sup> These cellular alterations impact vascular proliferation, epithelial migration, and tissue remodeling.<sup>242, 243</sup> Although these enzymes are essential for wound healing, they are frequently overexpressed in ocular surface disease, making them useful for diagnosing these conditions.<sup>244</sup> MMP-9 is secreted as a stable, inactive zymogen (pro-MMP-9).<sup>245</sup> It is activated by the conversion of its latent or inactive form (pro-MMP-9) to active form (active MMP-9 or MMP-9) by propeptide processing.<sup>246</sup> When MMPs are activated, their

natural inhibitors, known as tissue inhibitors of matrix metalloproteinases (TIMPs), counterbalance their proteolytic activity.<sup>246</sup>

Although various MMPs have been implicated in many systemic diseases, only the role of MMP-9 in ocular surface injury will be discussed here. MMP-9 is the enzyme of focus in this project, and the responsiveness of GelMA+ toward different MMP-9 concentrations was explored. Table 1-4 lists the role and observations related to the expression of MMP-9 in various clinical conditions.

The complex signaling pathway that triggers the production of MMP-9 in cells includes a wide range of molecular interactions. A nuclear transcription factor known as nuclear factor kappa (NF- $\kappa$ B) has been shown to bind to MMP-9 DNA promoter sites and increase the amount of MMP-9 mRNA.<sup>247</sup> NF- $\kappa$ B attaches to nucleus DNA (deoxy ribonucleic acid) where it gets activated under stimulated conditions such as inflammation.<sup>248</sup> Activated NF- $\kappa$ B increase cytokine IL-1 $\beta$  productions which in turn promotes MMPs expressions.<sup>249</sup> Similarly, following surface inflammation or injury, NF- $\kappa$ B suppression has been demonstrated to reduce MMP-9 transcriptional activity and limbal epithelial cell proliferation.<sup>250, 251</sup> IL-1 $\beta$  and/or TNF- $\alpha$  upregulate MMP-9 promoter activity and stimulate the migration of corneal epithelial cells in both the presence and absence of mechanical and chemical stress.<sup>252, 253</sup> A hormone-like peptide TGF- $\beta$ , released by corneal epithelial cells and ocular surface fibroblasts, induces MMP-9 expression.<sup>254</sup> Following an alkali burn and corneal ulceration, higher quantities of platelet-activating factor (PAF), was discovered in corneal epithelial cells.<sup>255</sup> In vitro studies of human corneal epithelial cell cultures using reporter-gene transfection studies and electrophoretic mobility shift assays demonstrated that PAF increases the MMP-9 promoter binding activity of NF- $\kappa$ B and activator protein 1 (AP 1).<sup>255</sup> Inflammatory situations also result in an upregulation of tissue inhibitor metalloproteinases (TIMPs), which limit the conversion of pro-MMP-9 (inactive zymogen) to active MMP-9 and are frequently detected as MMP-9/TIMP complexes.<sup>256, 257</sup> The degree of MMP-9 induction is up to 100 times greater from 1 hour to up to 16 hours after corneal injury, while TIMP expression starts to rise at 16 hours, highlighting the significance of the balance between these two proteins in the presence of inflammation and wound healing.<sup>256-258</sup>

Corneal epithelial barriers can be broken down by MMP-9, promoting epithelial migration and wound healing.<sup>259</sup> MMP-9 expression following corneal wounding using mechanical epithelial debridement, anterior keratectomy, and lamellar keratectomy wounds was studied in both in vitro and in vivo animal models, and results showed significantly elevated tear fluid MMP-9 levels.<sup>243, 260, 261</sup> In animal models of peripheral ulcerative keratopathy, ulcerative keratitis, and in post-LASIK (laser assisted in situ keratomileusis) human corneal epithelial cells, elevated MMP-9 has also been reported in corneal epithelial and superficial stromal cells.<sup>262, 263</sup> At three months after LASIK, MMP-9 levels and chondroitin sulphate levels were high and were associated with clinical signs of continued wound healing.<sup>264</sup>

MMP-9 plays a crucial role in corneal wound healing, as shown by the upregulation of MMP-9 following ocular surface trauma, its continued overexpression along with clinical signs of ongoing wound healing, as well as the reduction in MMP-9 levels following effective medical management of an ocular surface disease. In wound healing process, when a wound repairs, corneal epithelial cells first temporarily adhere to the basement membrane before tearing it down and migrating.<sup>265</sup> MMP-9 is one of the primary gelatinase enzymes responsible for extracellular matrix degradation. Thus, during the migration phase, high activation or over expression of MMP-9 can slow down the migration process by degrading extracellular matrix and damaging basement membrane components which can lead to delayed wound healing.<sup>266</sup> This over-expressed MMP-9 during corneal injury can be utilized for degrading therapeutic loaded GelMA+ material to be used as a BCL and the degraded GelMA+ in turn will release entrapped therapeutic (Bovine Lactoferrin). The released BLF can aid in the corneal wound healing following a mechanical injury.

**Table 1-4:** Role of MMP-9 in various clinical conditions

<b>Clinical conditions</b>	<b>Role of MMP-9</b>	<b>References</b>
Diabetic retinopathy (DR)	A diabetic environment stimulates the secretion of MMP-9, and increased levels are found in the retina and vitreous. In the early stage of DR, MMP-9 facilitates retinal capillary cells apoptosis, while in the later stage of DR, MMP-9 facilitates neovascularization.	Kowluru et.al. <sup>267</sup>
Vernal keratoconjunctivitis	In this condition, there is an increased level of activity of MMP-9. Higher levels of MMP-9 tend to imply tissue remodeling.	Leonardi et.al. <sup>268</sup>
Retinal degeneration	In this condition, there is an upregulation of MMP-9. Inhibition of MMP-9 promotes neuron survival.	George et.al. <sup>269</sup>
Pseudoxanthoma elasticum (PXE)	An upregulation of MMP-9 is observed. Plays a crucial role in extracellular matrix remodeling.	Diekmann et.al. <sup>270</sup>
Dry eye	In response to dry eye condition, increased MMP-9 activity on the ocular surface impairs the corneal epithelial barrier function.	Pflugfelder et.al. <sup>271</sup>
Age-related macular degeneration (AMD)	MMP-9 may aid in the development of AMD, and targeted inhibition of MMP-9 effectively inhibits subretinal angiogenesis.	Lambert et.al. <sup>272</sup>
Dilated cardiomyopathy	Upregulation of MMP-9 and down-regulation of TIMP-1 results in the loss of cardiac contractility leading to the end stage of heart failure.	Rouet-Benzineb et.al. <sup>273</sup>



<b>Clinical conditions</b>	<b>Role of MMP-9</b>	<b>References</b>
Allergic rhinitis	A high MMP-9 to TIMP-1 ratio contributes to the inflammatory cell migration in the nasal mucosa suggesting an active role of MMP-9 in the pathomechanism of allergic rhinitis.	Mori et.al. <sup>274</sup>
Asthma	An imbalance of MMP-9 and TIMP-1 results in airway inflammation in asthma.	Erlewyn-Lajeunesse et.al. <sup>275</sup>
Lung cancer	Upregulation of MMP-9 by 4.5-fold in patients with lung tumor. Induction of MMP-9 by primary tumor increases the chance of metastasis.	Hiratsuka et.al. <sup>276</sup>
Pancreatic cancer	MMP-9 is a crucial regulator of angiogenesis. Upregulation of MMP-9 activity leads to an increase in angiogenesis inducers like VEGF.	Bergers et.al. <sup>277</sup>
Oral squamous cell carcinoma	High MMP-9 activity in tumor is associated with shorter disease-free survival.	Yoriyoka et.al. <sup>278</sup>
Acute cerebral infarction (ACI)	An increase in MMP-9 level during the first 12 hours after ACI is observed. ACI-induced cerebral edema is linked to elevated blood serum MMP-9 levels and a higher MMP-9/TIMP-1 ratio.	Li et.al. <sup>279</sup>
Chouronic pressure ulcers	A clinically worse wound is associated with increased levels of MMP-9. A high ratio of MMP-9/TIMP-1 slows down wound healing.	Ladwig et.al. <sup>280,</sup> 281
Spinal cord injury (SCI)	Increased MMP-9 contributes to the early failure of motor relearning after SCI. A robust locomotor flexibility and enhanced recovery are made possible by MMP-9 deletion, which also decreases the inflammatory signature in the lumbar cord.	Hansen et.al. <sup>282</sup>

## 1.8 Stages of corneal epithelial wound healing

Corneal epithelial wound healing consists of latent or lag phase, migration, proliferation and epithelial reattachment.<sup>283</sup>

**Latent or lag phase:** The first stage of corneal wound healing is characterized by cellular remodeling and tear composition adjustments to facilitate healing.<sup>283</sup> During this stage, more enzymes, such as MMP-9, are produced, breaking down the injured epithelial basement membrane.<sup>284</sup> MMPs have a crucial role in the breakdown and remodeling of extracellular matrix maintenance, and reducing cellular adherence and promoting cellular motility. However, high quantities of these enzymes can obstruct the healing process.<sup>285</sup>

The latent phase consists of multiple distinct stages that happen over the course of several hours. The first step is the apoptosis of injured epithelial cells. Adherens junctions and gap junctions in cells close to the defect's border are destroyed, and basal cells' connections to the basement membrane close to the borders of the wound are damaged. These basal cells undergo a morphological change and shed their microvilli before developing cellular extensions known as filopodia and lamellipodia.<sup>284, 286</sup> During the lag period, integrins separate from the desmosomes and hemidesmosomes and disperse evenly across the cellular surface. This subsequently acts as adherens molecules to the nearby extracellular matrix.<sup>287</sup> Additionally, these surface glycoproteins are thought to be in charge of the cytoskeleton and extracellular matrix's reciprocal bidirectional communication.<sup>288</sup> The deposition of fibronectin along the basement membrane of wound sites serves as a temporary matrix to encourage the assembly of integrins, such as  $\alpha 5\beta 1$ , to aid corneal epithelial cell migration and adhesion.<sup>289</sup> Fibronectin is then deposited onto the epithelial defect, providing a base for the neighbouring epithelial cells to migrate.<sup>283, 290</sup> Fibronectin causes the actin cytoskeleton to reorganize in conjunction with the extension of lamellopodia for migration by inducing the tyrosine phosphorylation of  $\beta$ -pix in epithelial cells in contact with the basement membrane.<sup>291</sup>

**Migration:** After the lag phase remodeling of the epithelial cells is finished, cells near the incision start migrating to restore the integrity of the ocular surface epithelium. It has been postulated that the basal and wing cells play a role in the development of the leading edge.<sup>292</sup> Cells close to the wound edge flatten and spread during the second stage. These cells then send out filopodia and lamellipodia that temporarily connect to the basal lamina, and contractile components then pull the cell in the direction of the defect.<sup>284</sup> Adjacent cells slide across the denuded area while still being connected by desmosomes and maintaining their position in relation to one another. The aforementioned temporary attachments are then severed, and the filopodia and lamellipodia are once more propelled forward to complete the process. This cycle repeats again until a single layer of cells entirely covers the defect. Depending on the size and location of the fault, the process normally takes 24 to 36 hours.<sup>27, 283, 293</sup>

**Proliferation:** After the migration is accomplished, the monolayer of cells covering the defect multiplies to increase the epithelium's normal thickness and fill in the defect. The wound region then begins to repopulate as a result of cell proliferation. The limbal and peripheral epithelial responses to migration and proliferation are divided. The proliferative rate of cells increases after injury, but cells at the leading margin of migrating epithelium do not.<sup>294</sup> The temporary amplifying basal cells divide by mitosis, and the resultant cells travel upward and inward to fill the deficiency.<sup>27, 283, 286</sup> An increase in the proliferation of epithelial cells away from the border of the wound and in the limbal region, which raises the local "density" of cells to "push" epithelial cells forward and aids in wound healing.<sup>295</sup> Daughter cells are displaced inward and upward towards the more superficial layers as the region of proliferation moves toward the center, where they differentiate into wing and then squamous cells to re-stratify the epithelium.<sup>284, 296</sup> The zonula occludens, which emerge behind the wound's leading edge and restore the epithelial barrier function even before migration is finished, are the first junctions to reform.<sup>297, 298</sup> The moved epithelium remodels the basement membrane and secretes laminin, which can bind to integrin v6 on the cell membrane, within 24 hours.<sup>289, 298</sup> Immediately above, adherens junctions, gap junctions, and desmosomes are reassembled at the same time.<sup>298</sup> As a result, the period of proliferation begins, with cells outside the region of the wound increasing their mitotic activity and the daughter cells starting to differentiate as they repopulate the epithelium.<sup>298</sup>

**Epithelial reattachment:** The epithelial layer's strong adhesion to the underlying substrate is restored during the attachment period. Basal epithelial cells firmly adhere to the stroma and basement membrane because of hemidesmosomes.<sup>299, 300</sup> The epithelial layer is firmly attached to the substrate during the final phase when hemidesmosomes reconstruct and anchoring fibrils reassociate with anchoring plaques in the stroma. Hemidesmosomes reform over existing anchoring fibrils in incisions where the basement membrane is still intact [109].<sup>300</sup> The anchoring fibrils and the hemidesmosomes are concurrently re-synthesized moving from beneath the wound margin towards the central cornea when the basement membrane and stroma have been damaged or removed.<sup>301</sup> This process takes place in a couple of days as long as the basement membrane was not damaged; however, if damage was sustained, the final development of attachments and the re-anchoring of cells may take months or longer.<sup>302</sup>

## 1.9 Conclusion

The usual approach for the treatment of RCE involves conservative or medical approaches. However, these approaches are prone to patient noncompliance and RCE can take several months to fully heal. Wear of a BCL allows the patient to use their normal vision, provides pain relief, and aid in wound healing simultaneously. However, due to the lack of corneal wound healing agents, this BCL-assisted process can take 2-3 months to heal a large or recurrent RCE. To speed up the healing process and provide relief to the patient, the BCL can be loaded with corneal wound healing agents to deliver at the site of the injured corneal epithelium. As mentioned in the previous section of role of MMP-9, there is an over expression of MMP-9 during injury or inflammation. Excessive MMPs presence can slow down the wound healing progress.

Using the novel approach of enzyme responsive GelMA+ hydrogel as the polymer for BCL will enable the lens to degrade in situ in the presence of over expression MMPs at the wounded site, and simultaneously slowly releasing the matrix bound therapeutic. The released therapeutic can increase the wound healing rate and heal the wounded cornea in a week ideally. The successful development of an enzyme responsive drug delivery system for RCE will be valuable for the ocular drug delivery field.

## Chapter 2: Rationale and Objectives

### 2.1 Rationale and Objectives

The corneal epithelium is a unique transparent biological barrier that functions to focus vision while also protecting the inner layers of the eye.<sup>303</sup> When this corneal epithelium undergoes repeated detachment from the underlying epithelial basement membrane, it leads to recurrent corneal erosion (RCE).<sup>1, 17</sup> The primary cause of RCE is corneal abrasions inflicted by physical trauma (45-64% of cases).<sup>5, 7</sup> Other causes, including epithelial basement membrane dystrophies such as lattice degeneration, can also lead to RCE.<sup>3</sup>

The standard treatment for RCE is ocular lubricants and eye patches. Most of the time, a cycloplegic agent such as cyclopentolate, topical antibiotic ointment, patching, and prophylactic administration of gels during the day and ointment at night to stop additional erosion are used to treat acute episodes.<sup>7, 17</sup> Both the patient and the doctor may find the condition to be frustrating. Using an eye patch disrupts the patient's vision, leading to visual dissatisfaction. Furthermore, if the eye patch is not worn correctly, it can lead to delays in recovery. It is also cumbersome for clinicians to assess the wound healing progress without removing the eyepatch.<sup>1, 109, 304</sup> These treatments take months to cure RCE.<sup>1</sup> These approaches fall short of being ideal and may require alternative treatment techniques. Recently, therapeutic contact lenses or bandage contact lenses (BCLs) have increasingly been prescribed to manage corneal abrasions.<sup>15-17</sup>

In cases of ocular damage, contact lenses have been used as bandage lenses to manage pain and encourage re-epithelialization.<sup>15, 44, 305, 306</sup> Antibiotics and anti-inflammatory medications are given simultaneously during lens insertion to prevent microbial infections.<sup>44, 307</sup> Clinicians can also easily visually track the wound healing progression without removing the lens.<sup>109, 304, 308-310</sup> Unfortunately, current BCLs alone do not outperform ocular lubricants in terms of efficacy or speed of recovery, as they lack the ocular surface factors or therapeutic efficacy essential to aid ocular surface repair. Continuous BCL wear for an extended period (around three months) with replacing the BCLs every

two weeks<sup>18</sup> is required to permit tight epithelial basement membrane adhesions to be restored.<sup>18</sup> Therefore, it would be beneficial if BCLs could also deliver topical therapeutic agents concurrently to the surface of the eye to achieve a more speedy recovery.<sup>311</sup>

Several studies have been undertaken on delivering therapeutic agents using contact lenses.<sup>65, 74, 116, 312-314</sup> There are two advantages of delivering drugs using contact lenses. The first is the separation of the tear film into pre- and a post-lens (between the lens and the cornea) compartments. The contact lens acts as a barrier, limits tear mixing and exchange in the post-lens tear film<sup>66, 67</sup> and shields the corneal epithelium from the detrimental blinking reflex. The second advantage relates to the contact lens materials. The hydrogels used for making contact lenses serve as drug reservoirs, releasing drugs in a controlled<sup>98, 315, 316</sup> and sustained manner.<sup>317</sup> However, past studies have shown that commercial contact lens materials typically are unable to maintain sustained drug release, and the vast majority of the drugs are released within the first few hours, which is not desirable.<sup>75, 77, 78, 116, 307, 318, 319</sup> Hence, modifications to current materials are needed to improve the release kinetics of currently available BCLs.

In summary, to advance the speed of recovery of RCE using the novel therapeutic-releasing BCL drug delivery technology, it is important to develop a new material that is responsive to external stimuli, such as MMPs enzymes (present at the wounded site) and can release the drug in situ within a week and achieve corneal epithelial wound closure. Choosing the appropriate therapeutic for achieving a complete corneal epithelial wound closure is also essential.

This leads to the hypothesis:

“Therapeutic loaded enzyme sensitive hydrogel (GelMA+) used as a drug delivering BCL can provide sustained release of corneal wound healing therapeutic in the presence of MMP-9 for the treatment of RCE.”

For these reasons, there are two main aims of this thesis:

- a) The first objective was to prepare and characterize an enzyme-responsive hydrogel (Gelatin Methacrylate) GelMA+ and study the in vitro release kinetics of a corneal epithelial wound healing agent, bovine lactoferrin in the presence of MMP-9 enzyme (which is over expressed during RCE). Tuning the concentration of GelMA+ and the MMP-9 enzyme concentration will allow for a controlled and steady release of the wound healing agent. To this end, chapter 3 sets the foundation for subsequent experiments. It focused on the preparation and characterization of two formulations of GelMA+ and the behaviour of GelMA+ in the presence of varying enzymatic concentrations. To study the biocompatibility of GelMA+, chapter 4 details the cytotoxicity assays of both GelMA+ formulations on immortalized human corneal epithelial cells. In chapter 5, after selecting the appropriate GelMA+ formulation from the previous two chapters, the release kinetics of a model compound (FITC-Dextran) and wound agent (bovine lactoferrin) were tested.
- b) The second objective focused on the influence of wound healing therapeutic bovine lactoferrin on scratch-induced corneal wounds. Chapter 6 outlines the study of bovine lactoferrin promoting corneal epithelial wound healing using the scratch wound assay model.

The four aims of the thesis are:

- I Preparation and characterization of GelMA+ gels
- II Cytotoxicity assay of GelMA+
- III Characterization of in vitro release profile of bovine lactoferrin from GelMA+ gels
- IV Bovine Lactoferrin-induced corneal epithelial wound healing

## Chapter 3: Preparation and Characterization of GelMA+ gels

### 3.1 Introduction

Recurrent corneal erosion (RCE) is a syndrome characterized by repeated episodes of corneal epithelial detachment from the underlying epithelial basement membrane.<sup>1,17</sup> Patients with a history of physical trauma to the corneal epithelium, epithelial basement membrane dystrophies, corneal dystrophies such as lattice degeneration, or exposure to prior ocular surgeries are more prone to develop RCE, with physical trauma being the primary cause.<sup>1</sup> Patients suffer from sharp acute pain upon waking and have blurred vision and photophobia.<sup>1,7</sup> These conditions severely affect the quality of life for those affected.

The conventional treatment for RCE involves using an ocular patch or administering ocular lubricants and pain-relieving drugs.<sup>1, 6, 7, 305</sup> However, topical eye drops suffer from poor efficiency and low bioavailability.<sup>320</sup> Eye patches, on the other hand, restrict the patient's vision. The use of bandage contact lenses overcomes the disadvantages of the approaches mentioned earlier. Bandage contact lenses (BCLs) are worn to protect the cornea, reduce pain, and enhance the corneal epithelium's capacity to heal after an illness, accident, or surgery.<sup>45</sup> It acts as a shield for the cornea from the friction generated by blinking.<sup>18</sup> The BCL also enables the patient to use their vision normally and the clinician to track the healing process. Additionally, it is also possible to incorporate therapeutic agents into the lens to help facilitate the wound healing process.<sup>285</sup> Studies have shown that contact lens drug delivery is more effective than an eye drop, and can also be designed to provide sustained drug release.<sup>65, 74, 312</sup> However, past studies have shown that commercial contact lens materials typically are unable to maintain sustained drug release, and the vast majority of the drugs are released within the first few hours, which is not desirable.<sup>75, 77, 78, 116, 307, 318, 319</sup> Further modifications to current materials are needed to improve the release kinetics from the BCLs.

The use of naturally occurring hydrogels is gaining significant attention in biomedical applications. Among the various types of natural hydrogels available, gelatin is one of the most common polymers used in biomedical applications.<sup>131, 321</sup> However, due to its low melting point, unmodified gelatin suffers



from thermal degradation. The weak mechanical properties of gelatin-based hydrogels can be overcome by chemical modifications or by integrating it with other monomers or polymers.<sup>131, 322, 323</sup> Gelatin methacrylate (GelMA), a gelatin-derived hydrogel, is produced by substitution of the free amine groups of gelatin by crosslinking with methacrylate anhydride.<sup>131</sup>

One unique feature of GelMA-based hydrogels is the presence of matrix metalloproteinase sensitive sites on the polymer, which enables its biodegradation by matrix metalloproteinase enzymes (MMPs).<sup>324-326</sup> MMPs have an essential role in wound healing by regulating excessive extracellular matrix (ECM) degradation and deposition, which is essential for wound reepithelization. However, an increase in the expression of MMPs may slow down the wound healing process by disrupting the equilibrium of the ECM components.<sup>327, 328</sup> The presence of a highly upregulated concentration of MMPs during corneal wounds<sup>243, 329-331</sup> could be utilized in this situation as a means to degrade the polymer material.

As mentioned in the introduction, in a previous study undertaken within Dr. Evelyn Yim's lab (Department of Chemical Engineering, University of Waterloo), a sequential hybrid crosslinking involving both physical and chemical crosslinking was executed on the conventional GelMA hydrogel to address the weak mechanical properties of GelMA, to form a material termed "GelMA+."<sup>201</sup>

In this present work, the objective was to fabricate different formulations of GelMA+ hydrogels, characterize their physical properties, and study their rate of enzymatic biodegradation in various concentrations of MMPs. Dr. Evelyn Yim's lab had worked on three different formulations of GelMA which were 10% w/v, 20% w/v and 30% w/v. Hence the three different formulations chosen for this experiment initially were 10% w/v, 20% w/v and 30% w/v GelMA+. However, 10% w/v GelMA+ gels were difficult to handle (fragile and easily broken). Thus, 20% w/v and 30% w/v GelMA+ were chosen as the two formulations to be studied in chapters 3, 4 and 5.

## **3.2 Materials and Methods**

Gelatin Type A, methacrylic anhydride and Irgacure 2959 were obtained from Sigma Aldrich (St. Louis, MO, USA). MMP-9 (92 kDa Type IV Collagenase) and MMP-8 (Collagenase Type II) were obtained from Gibco Thermo Fisher Scientific (Grand Island, NY, USA). The bovine lactoferrin ELISA kit was obtained from Bethyl Laboratories Inc (Montgomery, TX, USA). The Spectrum™ Spectra/Por™ 4 RC Dialysis Membrane Tubing 12,000 to 14,000 Dalton MWCO was purchased from Fisher Scientific (Carlsbad, CA, USA).

### **3.2.1 Gelatin methacrylate synthesis**

5 g of gelatin (type A) was dissolved in 50 mL of phosphate-buffered saline 1X (PBS) (10% w/v) using a glass conical flask with continuous magnetic stirring at 50-60 °C till the gelatin dissolves for at least an hour. 10 mL of methacrylic anhydride (20% v/v) was then added dropwise at 50-60 °C with continuous magnetic stirring. The reaction was continued for 1 hour. The resulting mixture was diluted with ~40 °C 1X PBS (1X dilution) followed by a centrifugation at 5000 rpm for 5 minutes to remove any impurities. The supernatant was then dialyzed in deionized (DI) water for 5 days at 40 °C using 12-14 kDa cut-off dialysis membrane tubes. The DI water was changed every 2 hours in an 8 hour period for the first 2 days followed by replacing the water every day for another (?) 3 days. 40 °C was maintained to prevent the GelMA from physically gelling at room temperature. The GelMA solution was then frozen at -80 °C and lyophilized for a week to remove the water content. The lyophilized GelMA was stored at -20 °C to -80 °C.

### **3.2.2 Preparation of GelMA+ hydrogel**

Irgacure 2959 (photo-initiator) was dissolved in 1X PBS at room temperature (22-24 °C) to form a 0.5% w/v solution. To that photo initiator solution, lyophilized GelMA was mixed to obtain mixtures with 20% w/v and 30% w/v of GelMA. The mixture was incubated at 60 °C for 48 hours for the GelMA to completely solubilize in the Irgacure 2959 solution and then centrifuged for 10 mins at 5000 rpm.

The mixtures were further incubated for 30 minutes at 60 °C before carefully pipetted into an acrylic mold to create circular disks (thickness ~ 0.65 mm, diameter ~ 6 mm). The samples were then incubated at 4 °C for 1 hour, before being exposed to ultraviolet (UV) radiation (360-420 nm) at an intensity of 32 mW/cm<sup>2</sup> and polymerized in Dymax UV Curing Chamber (Torrington, CT, USA) for 5 minutes to create GelMA+ gels.

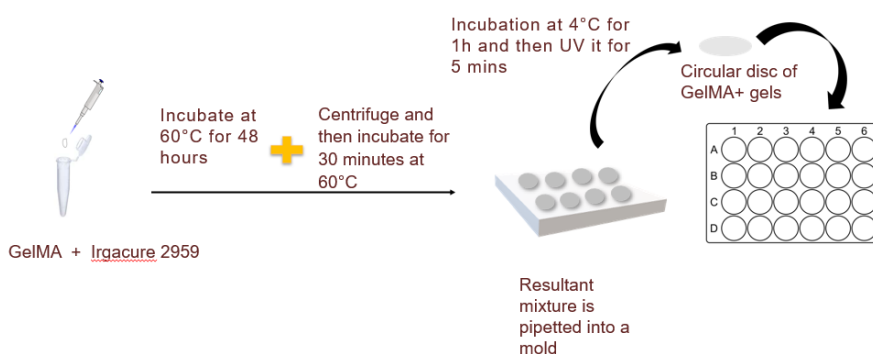


**Figure 3-1:** Schematic representation of the preparation of GelMA+ gels

### 3.2.3 Physical Characterization

#### 3.2.3.1 Scanning Electron Microscopy

The pore size and the surface morphology of lyophilized GelMA, 20% w/v and 30% w/v GelMA+ hydrogels were determined using Environmental Scanning Electron Microscopy (ESEM; QUANTA<sup>TM</sup> FEG 250) manufactured by Field Electron and Ion Company (FEI) (Hillsboro, OR, United States). The Scanning Electron Microscopy was done at the WATlab of the University of Waterloo by Lei Zhang. 20% w/v and 30% w/v GelMA+ gels were prepared following the previous section 3.2.2 using an acrylic mold. The gels were kept in 1X PBS at room temperature (22-24 °C) to ensure complete swelling and obtain a clear picture of the morphology of GelMA+ gels. The samples (GelMA+ gels soaked in 1X PBS) were mounted on a metal holder with clips. The clips are small copper clips which use a small spring force to hold the samples and the samples were directly exposed into the ESEM

chamber. The samples were observed under an accelerating voltage of 20 kV, in a low vacuum mode with a chamber pressure of 0.8 mbar. The electron beam energy was 20 keV. The sample surface was imaged with two detectors simultaneously: large field detector to detect secondary electrons, which is more morphology sensitive, and backscattering electron detector to detect backscattered electrons, which is more concentration sensitive.

### **3.2.3.2 Enzymatic Degradation of GelMA+ hydrogel**

The degradation of the 20% w/v and 30% w/v GelMA+ hydrogels were studied in the presence of varying concentrations of MMP-9. MMP-9 solution was prepared by dissolving MMP-9 in 1X PBS at room temperature (22 °C -24 °C). The MMP-9 concentrations chosen were 0, 10, 50, 100, 300 µg/mL. The circular disk shaped GelMA+ samples were weighed to determine the initial weight of the GelMA+ gels ( $W_0$ ). Then the GelMA+ disc shaped gels were placed in 24 well plate for the degradation study. To it, 2 mL of the chosen MMP-9 concentration solutions were added. The 24 well plate was kept at 37 °C. The GelMA+ gels were then weighed at predetermined time intervals (0 hour, 4 hour, 8 hour, 12 hour, 24 hour, 48 hour, 96 hour, 144 hour) to determine the weight changes over time ( $W_t$ ). Before weighing the sample, the gels were gently blotted using lens paper to remove any excess moisture. The MMP-9 solutions were replaced every day to maintain the enzyme activity. The percent degradation was calculated using equation 1. Similar steps were repeated for conducting the degradation of GelMA+ gels in MMP-8 and a combination of MMP-8 + MMP-9 enzyme solutions respectively. For preparing MMP-8 solution, the enzyme was dissolved in 1X PBS to prepare a varying concentrations of MMP-8 solutions (0, 10, 50, 100, 300 µg/mL). For MMP-8 + MMP-9 solutions, equal amount of MMP-8 and MMP-9 were combined and mixed in 1X PBS to prepare 0, 10, 50, 100, 300 µg/mL concentrations solutions.

$$\text{Equation 1: Percent Degradation} = \frac{W_0 - W_t}{W_0} \times 100\%$$

### 3.2.3.3 Swelling Percentage and Water Content of GelMA+ hydrogel

The swelling property of the 20% w/v and 30% w/v GelMA+ gels were studied using 1X PBS. After the GelMA+ gels were prepared (section 3.2.2), the GelMA+ disc shaped gels samples were incubated in 2 mL of PBS at 37 °C for 24 hours on a 24 well plate. After 24 hours, the samples were blotted dry using a lens paper and weighed ( $W_s$ ). The same samples were then freeze-dried and weighed ( $W_d$ ). The percent swelling was calculated using equation 2. The water content of the gels was measured in a similar way. Water content was calculated using equation 3.

$$\text{Equation 2: Percent Swelling} = \frac{W_s - W_d}{W_d} \times 100\%$$

$$\text{Equation 3: Water Content} = \frac{W_s - W_d}{W_s} \times 100\%$$

### 3.2.3.4 Mechanical Properties of GelMA+ hydrogel (Tensile test)

The modulus of the 20% w/v and 30% w/v GelMA+ hydrogels were assessed using Mandel-Shimadzu (AGS-X) tensile testing unit (Shimadzu Corp, Kyoto, Japan) at room temperature (22 °C to 24 °C). The GelMA+ samples were molded in a rectangular shape of 7 cm by 1 cm by 0.7 cm (length x width x thickness) and then soaked in PBS for 24 hours at room temperature (22 °C to 24 °C). The samples were clamped with two steel clamps at 5 mm distance. Kim wipes tissues were used to hold the edges of the gels to prevent the gels from breaking at the edge of the clamp and to prevent slippage. The rectangular-shaped gels were stretched at a 1 mm/min rate to the breaking point with a load of 500 N. The Young's modulus was calculated from the slope of the linear region of the stress-strain curve.



**Figure 3-2:** Experimental setup for tensile test. The gels are clamped on both ends with the help of Kimwipes

### **3.2.3.5 Optical transmittance of GelMA+ hydrogel**

The optical transmittance of both 20% w/v and 30% w/v GelMA+ hydrogels in 1X PBS was measured using the UV spectrophotometer (Biotek Citation 5 (Winooski, VT, USA)). The GelMA+ disc-shaped gels were placed in 1 mL 1X PBS in a 48 well plate and the measurements were performed at the wavelength range of 450 nm to 700 nm. For the blank measurement, the wavelength of the PBS 1X was measured at the wavelength range of 450 nm to 700 nm. The transmittance values of the 20% w/v and 30% w/v GelMA+ were obtained by subtracting the value GelMA+ gels in 1X PBS with 1X PBS.

### **3.3 Statistical Analysis**

Statistical analysis and graphs were plotted using GraphPad Prism 6 software (GraphPad, La Jolla, CA, USA). An analysis of variance (ANOVA) and a post-hoc Tukey's test was performed when necessary to determine the statistical significance between different conditions.

## **3.4 Results**

### **3.4.1 Physical Characterization**

#### **3.4.1.1 Scanning electron microscopy (SEM) images**

Figure 3-3 (A-C) shows the surface morphology and surface pore size of the 20% w/v and 30% w/v GelMA+ hydrogels (n=3) (from the same day) obtained by Environmental SEM. The SEM gives a display of the porous structure of both the formulations of GelMA+. Figure 3-3A shows the morphology of the pre-polymerized GelMA, in which the surface appears highly porous, with an estimated pore size to be around 150  $\mu\text{m}$  to 300  $\mu\text{m}$ . Figures 3-3B and 3-3C show the porous structure of 20% and 30% w/v GelMA+ hydrogel respectively. The surface for the 20% w/v GelMA+ appears porous in nature, with a pore size ranging from 30  $\mu\text{m}$  to 90  $\mu\text{m}$  in thickness. The surface of 30% w/v GelMA+ appears denser, with pore sizes ranging from 0.078  $\mu\text{m}$  to 0.8  $\mu\text{m}$  in thickness.



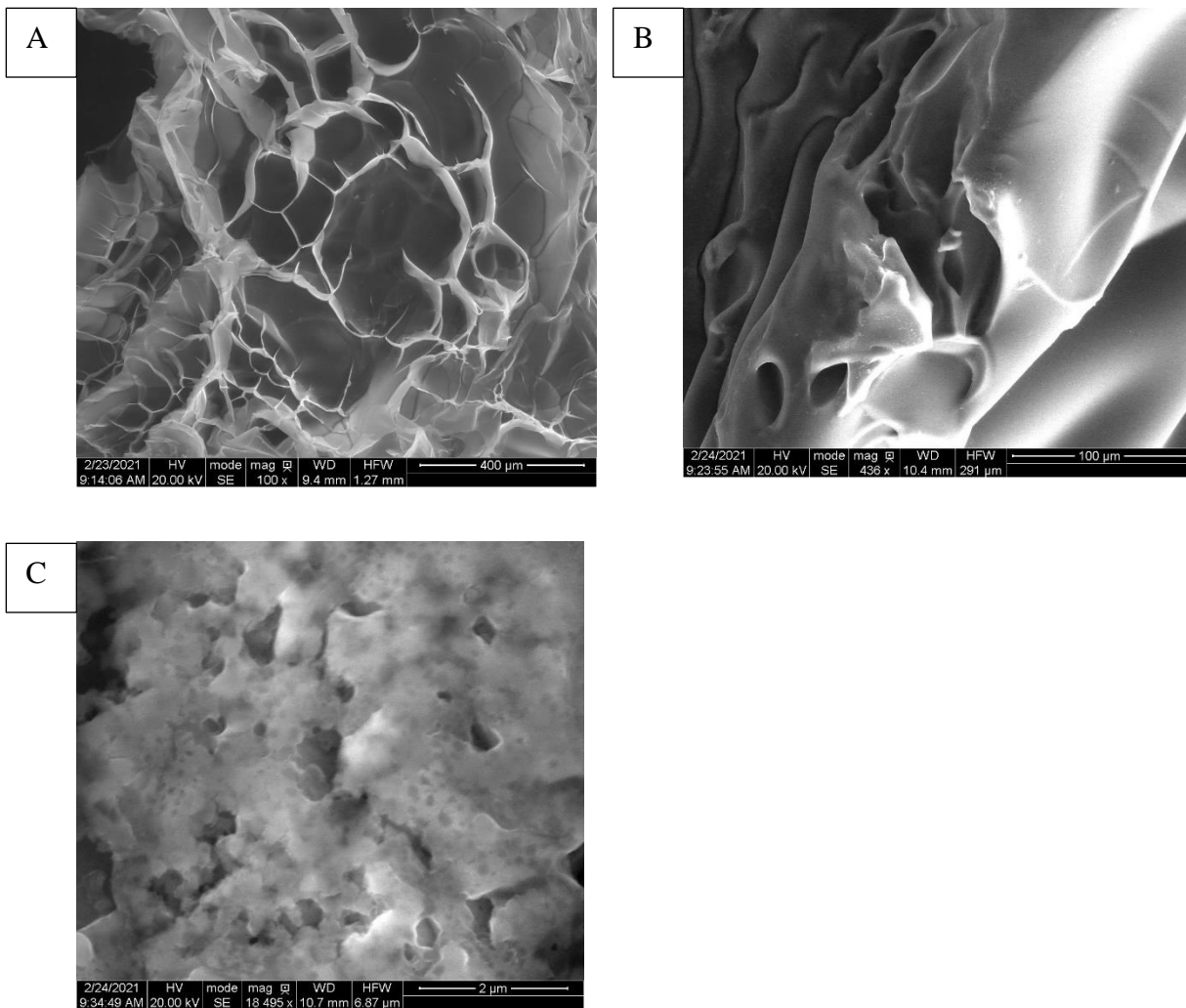


**Figure 3-3:** SEM images (n=3) of (A) pre-polymerized GelMA at 100 X magnification (B) 20% w/v GelMA+ hydrogel at 436 X magnification, (C) 30% w/v GelMA+ hydrogel at 18k X magnification. All three images show the surface morphology and depict the pore size of the GelMA+

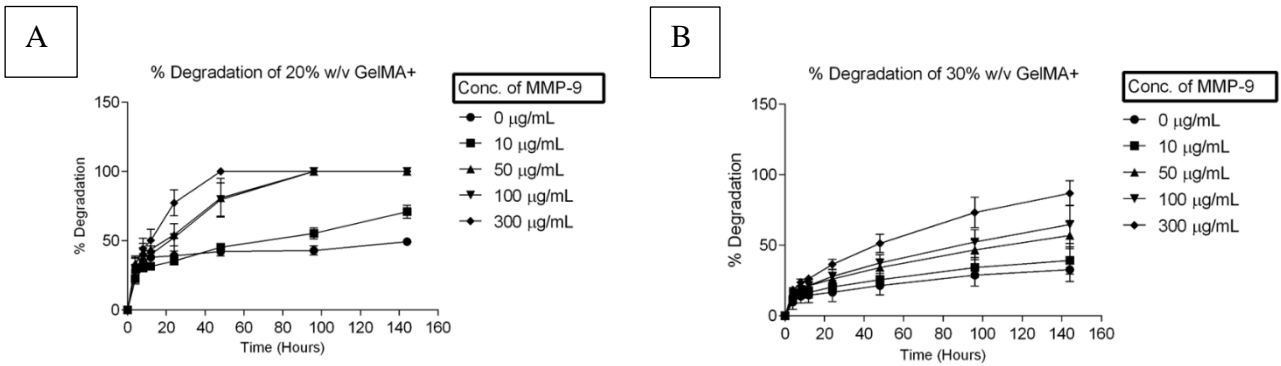
### 3.4.1.2 Enzymatic Degradation of GelMA+ hydrogel

Degradation studies of the 20% w/v and 30% w/v GelMA+ hydrogels (n=4) (experimental data were obtained from different sets of samples at predetermined time points were undertaken in the presence of varying concentrations of MMP-9 for a period of 6 days (144 hours). Figure 3-4A and 3-4B show the degradation profile of GelMA+ in the presence of different MMP-9 concentrations solution. For both the 20% and 30% w/v gels, the degradation increased significantly with time for all the concentrations of MMP-9 ( $p < 0.0001$ ) and the degradation increased significantly with increasing concentrations of MMP-9 ( $p < 0.0001$ ). However, the 20% w/v GelMA+ gels degraded faster than the 30% w/v GelMA+ gels ( $p < 0.0001$ ). On the 2<sup>nd</sup> day (48 hours), the circular shaped 20% w/v GelMA+ gels completely degraded in the presence of 300  $\mu\text{g/mL}$  of MMP-9 with no gel remnants. However, the same size and thickness of 30% w/v GelMA+ gels took almost 6 days (144 hours) to degrade about 95% of the gels, leaving behind only a thin piece from the edge of the circular gel. This suggests that 30% w/v GelMA+ has more cross-linking density, which in turn increases the degradation time for the GelMA+ hydrogels in the presence of matrix metalloproteinase enzymes. Similar degradation patterns were observed for GelMA+ gels degradation in MMP-8 and MMP-8 + MMP-9 respectively where the study was conducted for a period of 5 days (120 hours). From the degradation study of GelMA+ gels in MMP-9, it was observed that the gel degrades by 90% of its weight in the higher MMP-9 concentration solutions of 100 and 300  $\mu\text{g/mL}$  within 5 days (figure 3-4A and 3-4B). Hence, for the degradation profile of GelMA+ gels in MMP-8 and MMP-8 + MMP-9 were conducted for 5 days (120 hours). Figure 3-4C and 3-4D depict the enzymatic degradation of both the GelMA+ formulation in MMP-8. Figure 3-4E and 3-4F show the enzymatic degradation of the GelMA+ formulations in MMP-8 + MMP-9. For both the 20% and 30% w/v gels, the degradation increased significantly with time for all the concentrations of MMP-8 ( $p < 0.0001$ ) and MMP-8 +MMP-9 ( $p < 0.0001$ ). The degradation increased significantly with increasing concentrations of MMP-8 ( $p < 0.0001$ ) and MMP-8 +MMP-9 ( $p < 0.0001$ ). The 20% GelMA+ gels degraded by 100% of their original weight in MMP-8 at 48 hours and the 30% GelMA+ disc shaped gels degraded by  $90.4 \pm 5.8\%$  of their original weight in MMP-8 at 120 hours. The 20% GelMA+ gels degraded by 100% of their original weight in the combination of MMP-8 + MMP-9 at 48 hours and the 30% GelMA+ disc shaped gels degraded by  $92.2 \pm 2.8\%$  of their

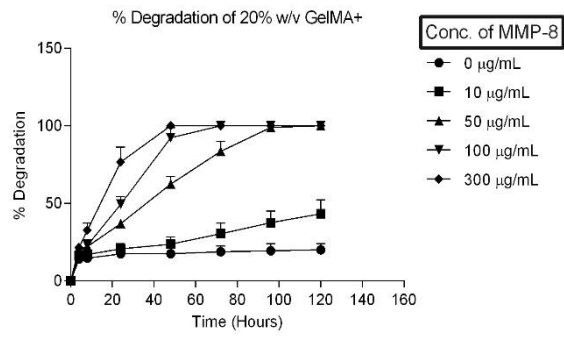
original weight in the combination of MMP-8 + MMP-9 solutions at 120 hours. The degradation of the 30% GelMA+ gels in the control (1X PBS) for MMP-9 study at 144 hours showed  $32.7 \pm 8.5\%$  degradations whereas the same formulation of GelMA+ showed  $10.6 \pm 2.0\%$  degradation and  $10.66 \pm 1.6\%$  in 1X PBS during the MMP-8 and MMP-8 + MMP-9 enzymatic degradation kinetics study respectively. One possible reason for the difference in the degradation rate in the control can be attributed to human factors (preparation of the GelMA mixture, pipetting error, duration of UV exposure of GelMA+) of preparation of the GelMA+ gels. The different set of samples used for studying the degradation profile in varying enzyme solutions were studied and prepared on different days. The 30% GelMA+ gels used for degradation in MMP-9 could have been more porous than the 30% GelMA+ gels used for MMP-8 and MMP-8 + MMP-9 as they were prepared in different batches and studies were conducted on separate days.

In all the varying MMPs, the 20% w/v GelMA+ gels degraded faster as compared to the 30% w/v GelMA+, owing to the lower polymer mass and lower polymer crosslinking density (Figure 3-4A to 3-4F). There was no significant difference in the degradation profile of the two GelMA+ formulations in different MMPs ( $p > 0.05$ ) in  $300 \mu\text{g/mL}$ . In figures 3-4H, 3-4J, 3-4K we can see the edges of the circular gels remained after degradation. The reason is the shape of the mold being used for this study. The mold resulted in the gels having a thicker edge as compared to the centre. The thinner centre degraded sooner compared to the thicker edge. As the 20% GelMA+ had less hydrogel concentration, it degraded faster than 30% GelMA+ in the presence of the highest MMP-9 concentration. Similar GelMA+ degradation profiles were observed with both MMP-8 and MMP-8 + MMP-9. There was no difference ( $p > 0.05$ ) in the degradation profile of GelMA+ gels in the presence of different enzymes studied here.

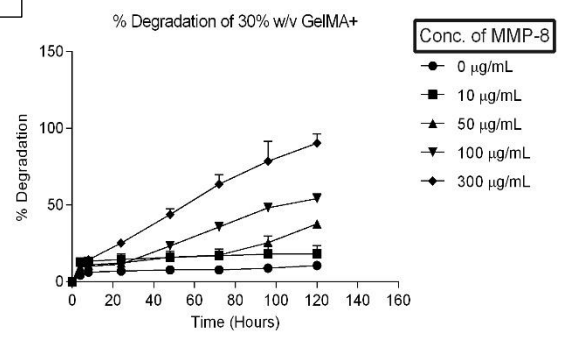
Figures 3-4G to 3-4K show the gels' shape during the degradation stages. All the enzymatic degradation followed a similar pattern, the degradation rate of the polymer is directly proportional to the enzyme concentration. There was no significant difference in the degradation rate in the presence of various enzymes in 300  $\mu\text{g/mL}$  of MMPs ( $p>0.05$ ).



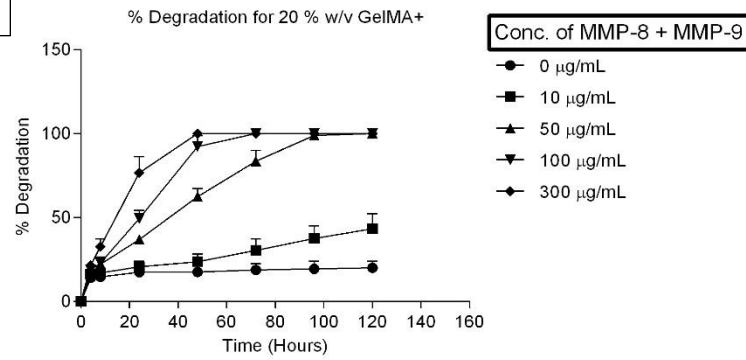
C



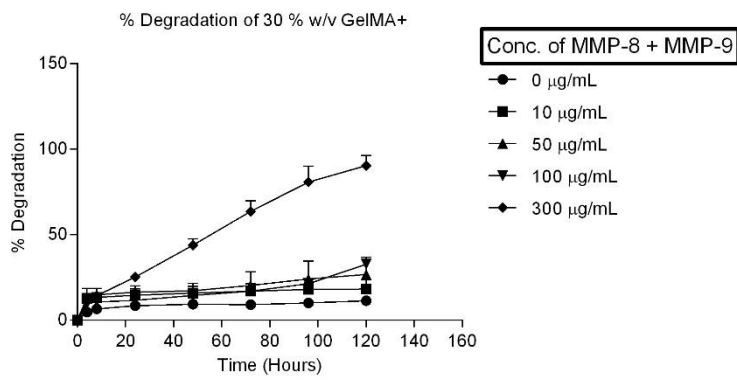
D



E



F



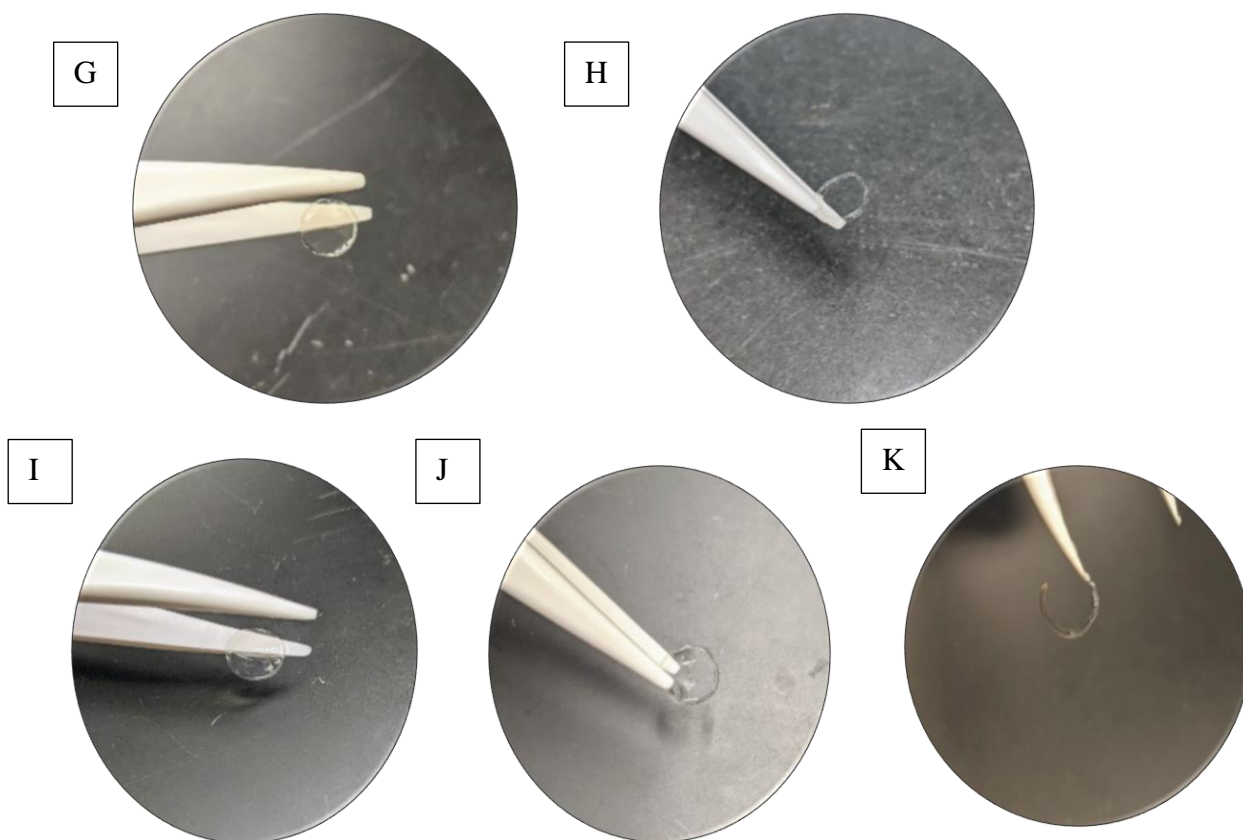


**Figure 3-4:** Degradation profile (n=4) of (A) 20% w/v GelMA+ in varying MMP-9 concentrations, (B) 30% w/v GelMA+ in varying MMP-9 concentrations, (C) 20% w/v GelMA+ in varying MMP-8 concentrations, (D) 30% w/v GelMA+ in varying MMP-8 concentrations, (E) 20% w/v GelMA+ in varying MMP-8+ MMP-9 concentrations, (F) 30% w/v GelMA+ in varying MMP-8+ MMP-9 concentrations; The shape of (G) 20% w/v GelMA+ in PBS (0  $\mu\text{g/mL}$  of MMP-9) after 48 hours, (H) 20% w/v GelMA+ in 100  $\mu\text{g/mL}$  of MMP-9 after 48 hours, (I) the shape of 30% w/v GelMA+ in PBS (0  $\mu\text{g/mL}$  of MMP-9) after 144 hours, (J) the shape of 30% w/v GelMA+ in 100  $\mu\text{g/mL}$  of MMP-9 after 144 hours, (K) the shape of 30% w/v GelMA+ in 300  $\mu\text{g/mL}$  of MMP-9 after 144 hours

### 3.4.1.3 Swelling profile and Water Content

Figure 3-5 shows the swelling ratio of 20% w/v and 30% w/v GelMA+ hydrogels (n=4) (experiments were repeated on different days). Both formulations of GelMA+ swelled up completely within an hour, but to ensure equilibrium was reached, the gels were incubated in the PBS for 24 hours. After 24 hours, it was observed that the 20% w/v GelMA+ gels swelled more than the 30% w/v GelMA+. The results showed that with an increase in the GelMA concentration, there was a significant reduction in the swelling ratio ( $p < 0.05$ ). Table 3-1 lists the water content of both the formulations of GelMA+ hydrogel. The water content (n=4) of 20% w/v GelMA+ gels was significantly higher as compared to 30% w/v GelMA+ gels ( $p < 0.05$ ).

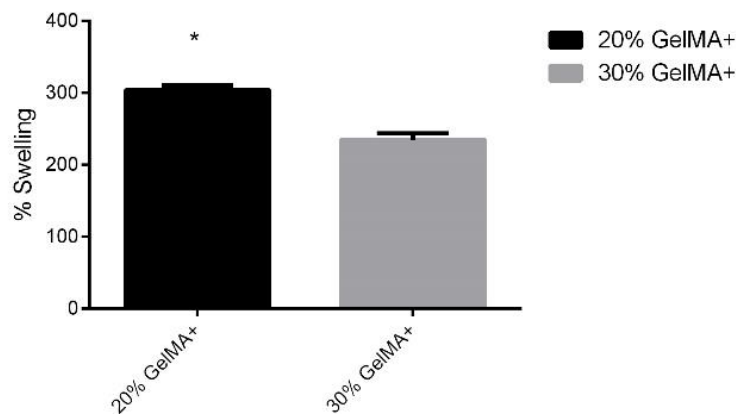


**Figure 3-5:** The swelling ratio (n=4) of 20% w/v and 30% w/v GelMA+ hydrogels after immersion in 1X PBS for 24 hours

**Table 3-1:** Water Content of GelMA+ (n=4)

<b>20% w/v GelMA+</b>	<b>30% w/v GelMA+</b>
74.85 ± 0.67%	70.85 ± 1.81%

### **3.4.1.4 Tensile test**

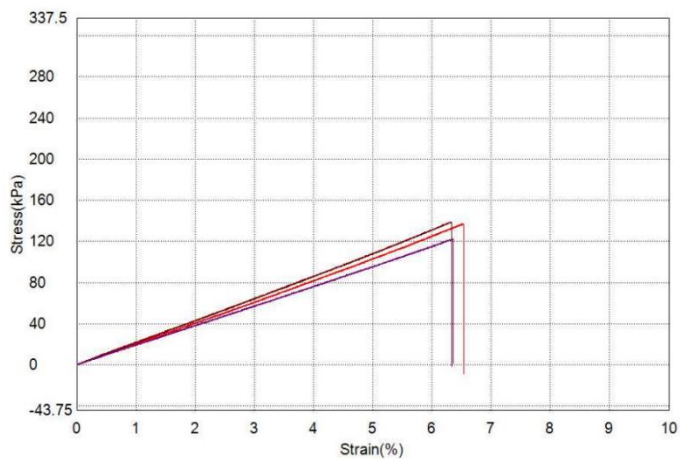
Table 3-2 and figure 3-6 (A-D) shows the influence of increasing GelMA+ concentration on the tensile strength and Young's Modulus (n=3) (experimental data were obtained from 3 samples on the same day). The higher GelMA+ concentration (30% w/v GelMA) resulted in an increase in the tensile strength values (p<0.05). The 20% w/v GelMA+ gels were softer with a Young's modulus value of 2.04 MPa. The 30% w/v GelMA+ gels were stiffer with a Young's modulus value of 2.80 MPa.

**Table 3-2:** Tabular data of tensile strength and Young's modulus of both the GelMA+ formulations (n=3)

<b>GelMA+ formulation</b>	<b>Tensile strength (kPa)</b>	<b>Young's modulus (MPa)</b>
<b>20% w/v GelMA+</b>	133.1 ± 8.8	2.0 ± 0.2
<b>30% w/v GelMA+</b>	181.8 ± 25.3	2.8 ± 0.8



A



B

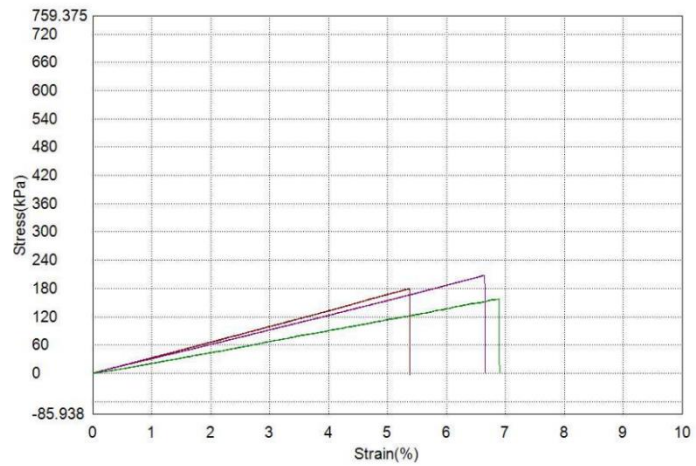


**Figure 3-6:** (A) Tensile stress-strain curves (n=3) of 20% w/v GelMA+, (B) Tensile stress-strain curves of 30% w/v GelMA+

### 3.4.1.5 Optical transmittance

The optical clarity (n=5) (figure 3-7) of both the 20% w/v GelMA+ and 30% w/v GelMA+ gels were measured in the visible light wavelength range of 450 nm and 700 nm using UV spectrophotometer of Citation 5. The transmittances of the 30% w/v GelMA+ decreased significantly ( $p < 0.0001$ ). The 20% w/v GelMA+ gels exhibited about  $89.98 \pm 2.3\%$  transmittance at 450 nm. At 630 nm, the transmittance of 20% w/v GelMA+ was  $95.59 \pm 1.8\%$ . At 450 nm, the 30% w/v GelMA+ gels exhibited about  $86.07 \pm 3.8\%$  transmittance and at 630 nm, the transmittance was  $92.69 \pm 2.9\%$ . The transmittance was measured using the gels kept in 1X PBS in the 48 well plate at room temperature ( $22\text{ }^{\circ}\text{C} - 24\text{ }^{\circ}\text{C}$ ).

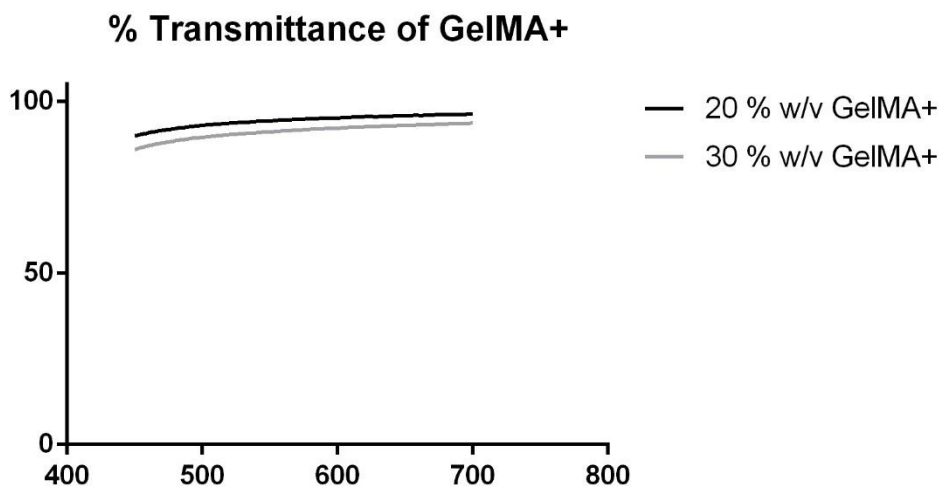


**Figure 3-7:** Optical transmittance of both the formulations of GelMA+ (n=5) measured at wavelength range of 450 nm to 700 nm.

### 3.5 Discussion

Gelatin is a biopolymer and an amphoteric protein<sup>131, 332</sup> and is derived from hydrolysis of collagen,<sup>333</sup> a naturally occurring polymer in the human cornea and the major component derived after collagen hydrolysis in most tissues.<sup>334, 335</sup> Gelatin-based hydrogels are water-soluble, non-cytotoxic, have low immunogenicity, biodegradable and highly biocompatible<sup>173, 336, 337</sup> and contain a high amount of bioactive sequences, such as arginine-glycine-aspartic acid, which provides a favourable condition for cell viability.<sup>131, 132, 338-340</sup> For these reasons, gelatin-based hydrogels have found wide uses in drug delivery and tissue engineering applications.<sup>341-344</sup> This property of gelatin makes it a suitable candidate for corneal wound healing treatment.<sup>338</sup>

GelMA, a gelatin-based hydrogel polymer, is prepared by photo-crosslinking with a photoinitiator and exposing to UV radiation to produce a stronger permanent gel with tunable mechanical properties.<sup>131</sup> The chemical modification of the gelatin by methacrylic anhydride affects only 5% of the amino acid sensitive sites implying that the chemical modification does not influence most of the functional amino acid sensitive sites favourable for cell growth.<sup>143</sup> However, GelMA lacks tunable mechanical and biodegradable properties.<sup>201</sup> This improved GelMA hydrogel, termed GelMA+, has a significantly higher mechanical strength (eight fold)<sup>201</sup> as compared to GelMA. The extra incubation period at 4 °C in GelMA+ formation leads to improved triple helix and physical network formation which in turns improves the mechanical strength of the bioactive hydrogel. GelMA+ also exhibits slower biodegradation kinetics (both in vitro and in vivo) than GelMA due to an increase in crosslinking.<sup>201</sup>

In this study, two formulations of GelMA+ gels, 20% w/v and 30% w/v, were synthesized and evaluated to assess their suitability to be used as a polymer for a degradable therapeutic bandage contact lens for the treatment of recurrent corneal erosion. During initial release study experiments (mentioned in Chapter 5) with model drug (FITC-dextran) from GelMA+ material in the presence of MMP-9, three different formulations of GelMA+ were studied, viz: 10% w/v, 20% w/v and 30% w/v GelMA+. But, during the experiments, it was observed that the 10% w/v GelMA+ gels were fragile and difficult to

handle as they were too soft and tore easily. Hence, for the rest of the experiments involving the physical characterization and cytotoxicity assays, 20% w/v and 30% w/v GelMA+ gels were evaluated.

The physical characterization (porosity, tensile modulus, and water swelling) and biological parameters (cell viability and spreading mentioned in Chapter 4) of GelMA+ hydrogels are essential to determine the suitability of these hydrogel polymers for different biomedical applications. The SEM images (Figure 3-3A – 3-3C) showed the porous nature of the GelMA+ hydrogel. The porosity is an important criterion for drug delivery.<sup>345</sup> The porosity of the hydrogel helps with drug uptake and slow release over time. Previous studies on GelMA have shown the hydrogel's porous nature, with pore sizes ranging from 50  $\mu\text{m}$  to 77  $\mu\text{m}$ .<sup>145,346</sup> The pore size of the fully crosslinked GelMA+ was considerably less when compared to the pre-polymerized GelMA. The pore size of pre-polymerized GelMA was around 150  $\mu\text{m}$  to 300  $\mu\text{m}$ , whereas the pore sizes for 20% and 30% w/v GelMA+ were around 30  $\mu\text{m}$  to 90  $\mu\text{m}$  and 0.078  $\mu\text{m}$  to 0.8  $\mu\text{m}$  in thickness respectively. With an increase in the concentration of the polymer, there was an increase in the crosslinking density. The increase in cross-linking density concurrently leads to a decrease in pore size.

The Young's modulus and tensile strength of GelMA hydrogels can be modified by varying the hydrogel concentration.<sup>163</sup> Similar results were observed with the tensile strength of GelMA+ when the hydrogel concentration increased from 20% to 30%. The 30% w/v GelMA+ was stiffer and stronger compared to 20% w/v GelMA+ ( $p < 0.05$ ) (Figures 3-6A-3-6D). The 30% w/v GelMA+ was stiffer with a Young's modulus of 2.8 MPa as compared to the 20% w/v GelMA, which had a tensile modulus of 2.0 MPa (Table 3-2). This shows that the mechanical property of the GelMA+ hydrogel could be effectively regulated by increasing the GelMA+ concentration. To prepare GelMA+ gels with tensile moduli values of commercial soft contact lens materials, which are around 0.3 to 0.6 MPa,<sup>347</sup> tuning of the GelMA+ material is needed which can be done in future experiments.

The swelling behaviour of hydrogels is dependent on the inter polymeric network and the degree of crosslinking.<sup>133</sup> Hydrogels with smaller pore sizes, due to a dense inter polymeric network, have lower swelling ratios.<sup>348</sup> As expected, the 20% w/v GelMA+, which had a lower cross-linking density and high pore sizes, swelled more than the 30% w/v GelMA+ (303.7% ± 6.9 vs 234.7% ± 8.9). Increasing the crosslinking densities limits the water content of the hydrogel.<sup>349</sup> Hence, 30% w/v GelMA+ exhibited less water content (p<0.05) as compared to 20% w/v GelMA+.

During corneal injury, it has been found that there is an upregulation of a specific matrix metalloproteinase enzyme - MMP-9.<sup>350-352</sup> Several previous studies have shown the biodegradation of GelMA in the presence of collagenase enzymes, particularly MMP-2 and MMP-8.<sup>146, 149, 353-355</sup> The primary enzyme of focus for this thesis was MMP-9 as it has been found that there is an upregulation of MMP-9 as discussed in the section 1.7 of the introduction chapter. Hence the degradation and BLF release profile of GelMA+ (Chapter 5) was done in the presence of MMP-9. However, studies have shown the presence of other MMPs such as MMP-2, MMP-8 in RCE or corneal injury.<sup>146, 149, 353-355 356, 357</sup> To understand the effect of other enzymes beside MMP-9, MMP-8 was chosen to study its effect on the degradation profile on the two formulations 20% and 30% w/v of GelMA+. As there are a combination of MMPs expression during corneal wound healing,<sup>266</sup> it was interesting to study the effect of a combination of MMP-9 and MMP-8 on the degradation profile of GelMA+ gels and if there was any effect on the degradation of GelMA+ due to the presence of two MMPs (MMP-9 + MMP-8) together as opposed to the effect of only one enzyme (MMP-9 or MMP-8). Crosslinking density also affects the rate of degradation of the GelMA+ gels. In this study, the degradation was also dependent on the presence of collagenase enzymes such as MMPs. With an increase in the enzyme concentration, the degradation rate also increased. With an increase in the concentration of all the MMPs, the degradation rate increased (p<0.0001). More studies are needed to study the effect of other enzymes such as MMP-2 which is expressed in RCE<sup>34</sup> and in combination with other MMPs to study the combined effect on the GelMA+ degradation.

The transmittance of contact lenses should be above 90% for optical clarity.<sup>358</sup> It is evident from figure 3-7 that the transmittance of both GelMA+ formulations is above 90% in the visible light range.

However, the 30% w/v GelMA+ gels exhibited lower ( $p < 0.0001$ ) transmittance compared to 20% w/v GelMA+. This is probably due to the higher concentration of polymer in the 30% w/v GelMA+. The commercial biweekly or monthly contact lenses have a central and peripheral thickness around  $0.243 \pm 0.002$  mm and  $0.231 \pm 0.015$  mm respectively.<sup>359</sup> The GelMA+ gels in this project had a thickness of 0.65 mm. The transmittance value of both the GelMA+ formulations would further increase if the gels are formulated thinner in future. As mentioned, the transmittance of GelMA+ gels from both the formulations were measured in the visible light range. It would be interesting to study in future about the transmittance of these GelMA+ gels in the ultraviolet (UV) A (315-400 nm) and UV B (280-315 nm) and test whether it follows the ISO standards<sup>360</sup> for spectral transmittance of contact lenses in the UV a and UV B wavelength range.

However, cytotoxicity of the GelMA+ gels must be evaluated in order to select the suitable formulation of GelMA+ to be employed for researching the MMP-9 triggered therapeutic agents release (in vitro), another crucial characteristic for the biomedical enzyme triggered drug releasing device. The biocompatibility of the two GelMA+ formulations is examined in the following chapter, and we determine whether either formulation is more cytotoxic than the other.

## Chapter 4: Cytotoxicity of GelMA+

### 4.1 Introduction

A biomaterial is “*an object or a substance that is natural or synthetic in nature devised to function in close contact with the living tissues of the human body for therapeutic or diagnostic purposes*”.<sup>361</sup> The most important criterion for a biomaterial is to coexist with the human biological system without causing any unacceptable damage to the body. The assessment of a biomaterial's biocompatibility at the cellular and tissue levels is one of the key requirements for its suitability for therapeutic use. Cytotoxicity testing, which illustrates how cultured cells are exposed directly to the test material or to the test material's extract, is a fundamental and required component of biocompatibility assessment.<sup>362</sup> The choice of a series of steps that are based on the type of biomaterial, the location, and the nature of its application determines whether or not a biomaterial is confirmed to be cytotoxic. All biomaterials, implants, and raw materials for medical devices that are anticipated to come into contact with patients are subjected to cytotoxicity tests as a screening procedure.<sup>363, 364</sup>

Cell viability and/or proliferation rates are reliable measures of a cell's health.<sup>365</sup> Cell health and metabolism can be affected by physical and chemical factors. These substances have the potential to be toxic to cells through a variety of processes, including the destruction of cell membranes, the inhibition of protein synthesis, irreversible binding to receptors, and irreversible binding to polydeoxynucleotides, elongation, and enzymatic reactions.<sup>366</sup> Cheap, dependable, and reproducible short-term cytotoxicity and cell viability tests are required to identify the cell death caused by biomaterials.

Cell-based assays are commonly employed for evaluating substances to determine if the test molecules have an impact on cell growth or exhibit direct cytotoxic effects that ultimately result in cell death.<sup>362, 365-367</sup> It is crucial to know how many viable cells are left at the conclusion of the experiment, regardless of the type of cell-based assay being used. Although cytotoxicity and cell viability assays have different classifications, broadly these assays are categorized based on the kinds of end points that are measured (color changes, fluorescence, luminescence, etc.),<sup>362, 365, 367</sup>

- A. **Dye exclusion:** Trypan blue, eosin, Congo red, erythrosine B assays.
- B. **Colorimetric assays:** MTT (3-(4,5-dimethylthiazol-2-yl)-2,5-diphenyltetrazolium bromide) assay, MTS (5-(3-carboxymethoxyphenyl)-2-(4,5-dimethyl-thiazoly)-3-(4-sulfophenyl) tetrazolium, inner salt assay) assay, XTT (2,3-bis(2-methoxy-4-nitro-5-sulphophenyl)-5-carboxanilide-2H-tetrazolium, monosodium salt) assay, WST-1 (2-(4-iodophenyl)-3-(4-nitrophenyl)-5-(2,4-disulfophenyl)-2H-tetrazolium monosodium salt) assay, WST-8 (2-(2-methoxy-4-nitrophenyl)-3-(4-nitrophenyl)-5-(2,4-disulfophenyl)-2H tetrazolium, monosodium salt) assay, LDH (lactate dehydrogenase) assay, SRB (Sulforhodamine B) assay, NRU (neutral red uptake) assay and crystal violet assay.
- C. **Fluorometric assays:** alamarBlue assay and CFDA-AM (5-carboxyfluorescein diacetate, acetoxymethyl ester) assay.
- D. **Luminometric assays:** ATP (adenosine triphosphate) assay and real-time viability assay.

Gelatin methacrylate (GelMA) has been proven to be one of the most versatile hydrogel biomaterials used for bioprinting and 3D cell culture.<sup>147, 189, 368, 369</sup> As described in Chapter 3, GelMA is a semi-synthetic hydrogel formed by synthesizing primary amine groups of gelatins with methacrylic anhydride, resulting in the modification of lysine and hydroxyl molecules with the methacrylamide and methacrylate molecules. Even after derivatization, GelMA retains most of the essential properties of gelatin.<sup>131</sup> This makes the polymer unique, with the advantages of having tunable mechanical properties along with biocompatibility and biodegradability. GelMA inherits the valuable amino acid sensitive sites from the gelatin: (Arg-Gly-Asp (RGD)) sensitive sites and the metalloprotease degradation sensitive sites. These properties of GelMA help provide an favourable environment for the animal cells to thrive, enabling their growth, adhesion, proliferation, and migration.<sup>145, 146, 155, 194, 198</sup> The transparency of the GelMA hydrogel also facilitates more accessible microscopic analysis of the cells growing.<sup>131</sup>

GelMA is gaining popularity in 3D cell culture technology and tissue engineering platforms due to its low cost, biocompatible and biodegradable features.<sup>154, 163, 370</sup> Several studies suggest that different cells grow on GelMA substrates with excellent viability.<sup>371-373</sup> The essential parameters of GelMA are the concentration of the polymer, degree of functionalization, cross-linking density, ultraviolet intensity,



and ultraviolet exposure time.<sup>173, 374-376</sup> In Chapter 3, it was demonstrated that with an increase in the degree of functionalization and cross-linking density, the swelling, porosity, and degradation of the hydrogel decreases.

In this chapter, the cytotoxicity of both 20% and 30% w/v GelMA+ will be discussed. To determine this, immortalized Human Corneal Epithelial Cells (HCEC) were cultured in the presence of 20% w/v GelMA+ and 30% w/v GelMA+ to observe whether cells could proliferate in the presence of the polymer. After that, a cell mortality assay with alamarBlue was performed to estimate the percentage of cells viable after exposure to GelMA+ after a certain number of days. Then a live/dead assay was conducted to observe qualitative data of viable and dead cells after exposure to the varying GelMA+ formulations.

## **4.2 Materials and Methods**

### **4.2.1 Materials**

The HPV immortalized HCECs were obtained from the Centre for Ocular Research & Education (CORE), School of Optometry & Vision Science, University of Waterloo. The EpiGRO™ Human Ocular Epithelia Complete Media Kit was obtained from Millipore Sigma (Burlington, MA, USA). The LIVE/DEAD™ Viability/Cytotoxicity Kit for mammalian cells and the AlamarBlue™ Cell Viability Reagent was purchased from Invitrogen™ by Thermo Fisher Scientific (Eugene, OR, USA).

### **4.2.2 Biological Characterizations**

#### **4.2.2.1 Cell Culture**

The HPV immortalized HCEC cells were cultured in Corning® tissue culture treated cell culture flasks with a canted neck plug seal cap and a surface area of 25 cm<sup>2</sup>. The nutrient media consisted of EpiGRO™ Human Ocular Epithelia Complete Media along with supplements of L-Glutamine, Epifactor O, Epifactor P, Epinephrine, rh Insulin, Apo transferrin, and Hydrocortisone hemisuccinate (Millipore Sigma, Burlington, MA, USA). The cells were seeded at a ratio of 1:2 and grown in an incubator at 37 °C and 5% carbon dioxide.

#### **4.2.2.2 Cell Culture in the presence of GelMA+ hydrogels**

Once the HCEC cells reached 90% confluency, they were seeded on 48 well tissue culture treated plates at a cell density of  $5 \times 10^4$  cells/cm<sup>2</sup>. The cells were grown in the nutrient media, as described above. Freshly prepared and sterile GelMA+ hydrogels (prepared following section 3.2.2) of both the 20% w/v and 30% w/v formulations were used for this study. Since the GelMA+ gels are fabricated inside the UV chamber (as mentioned in section 3.2.2) and immediately used for the cell culture studies, it was

assumed that the gels were sterile after being taken out from the UV chamber in a glass covered Petri dish. Then the disc shaped gels were placed carefully onto the cells in each well of the 48 well plate and incubated at 37 °C and 5% carbon dioxide. On the 5<sup>th</sup> day, the cell growth on the hydrogels was observed.

#### **4.2.2.3 Cell Viability Assay**

The resazurin reduction test is another name for the alamarBlue assay. The alamarBlue test relies on the transformation of resazurin, a blue non-fluorescent dye, into resorufin, a pink fluorescent dye, by mitochondrial and other enzymes like diaphorases.<sup>377</sup> Resazurin is a phenoxazin-3-one dye and cell permeable redox indicator that can be used with similar protocols to those that use tetrazolium compounds to measure viable cell number.<sup>378</sup> By acting as a substitute for molecular oxygen as an electron acceptor, it serves as an intermediary electron acceptor in the electron transport chain between the final reduction of oxygen and cytochrome oxidase. Resazurin is reduced to resorufin once it enters cells. Resorufin is a highly fluorescent compound that is red in appearance. The overall fluorescence and colour of the cell culture medium are increased as resazurin is constantly converted to resorufin by viable cells. The number of viable cells has an impact on how much resorufin is produced. At excitation and emission wavelength of 570 and 630 nm respectively, the metabolic processes that generate fluorescence signals are observed.<sup>367, 378</sup>

To study the viability of the immortalized HCECs, an alamarBlue<sup>TM</sup> assay was performed. For this assay, freshly prepared disc shaped GelMA+ gels of both formulations (20% and 30% GelMA+) were used GelMA+. It was assumed that the UV sterilization step during the GelMA+ preparation (section 3.2.2) would help to maintain the gels sterile. Immortalized HCECs were seeded on 48 well tissue culture treated plates at a cell density of  $5 \times 10^4$  cells/cm<sup>2</sup> using the growth nutrient media as mentioned in section 4.2.2.1. On each well of the 48 well plate containing the seeded cells, freshly prepared GelMA+ gels of both the formulations were placed over the cells. The disc shaped gels were washed with sterile PBS 1X for 4 minutes inside the cell culture hood prior to exposure to the cells. The gels were washed four times in 5 mL of fresh sterile PBS 1X for 1 minute each time. This was done to

ensure the unreacted photocrosslinker gets washed away. Three sets of 48 well plates with the HCECs and the GelMA+ gels were prepared where the three 48 well plates (containing the cells and the gels) were incubated and cultured for three different time points (1 day, 5 days, and 7 days) at 37 °C and 5% carbon dioxide. The growth media was replaced on alternate days. The alamarBlue™ Cell Viability assay was conducted after 1, 5 and 7 days of incubation of the GelMA+ hydrogels with immortalized HCEC cells. At the end of each time point, the cell culture media was removed from the wells (containing the GelMA+ gels placed over HCECs) and then 0.5 mL of 10% v/v of the alamarBlue™ Cell Viability (Thermo Fischer Scientific, Eugene, OR, USA) reagent prepared with serum free DMEM/F12 media was added to each well containing GelMA+ gels placed over cells. The resulting solution was then incubated at 37 °C and 5% carbon dioxide for 4 hours. 100 µL of the solution from each well was transferred to a new 96 well plate. The fluorescence was measured (excitation 540 nm, emission 590 nm) using the BioTek Citation 5 (BioTek, Winooski, VT, USA). For the control, the fluorescence was measured from the wells which had only immortalized HCEC cells. The percent viability of the immortalized HCECs in the presence of both the formulations of GelMA+ gels were calculated with respect to the control.

#### **4.2.2.4 Live/Dead Assay**

The live/dead fluorescent assay, which is frequently used, offers a quick way for determining the percentage of live and dead cells in cell culture systems or tissues.<sup>379</sup> Live cells can be identified by their ubiquitous intracellular esterase activity, which is revealed by the enzymatic change of the Calcein AM pigment from the nearly nonfluorescent to the highly fluorescent state. In live cells, the polyanionic dye Calcein AM is effectively maintained and emits a strong, uniform green fluorescence (excitation/emission 495 nm/515 nm). Ethidium (EthD)-1 enters cells with damaged membranes and, upon binding to nucleic acids, experiences a 40-fold enhancement of fluorescence, resulting in a bright red fluorescence in dead cells (excitation/emission 495 nm/635 nm). The healthy plasma membrane of living cells keeps out EthD-1. These physical and biochemical characteristics of cells determine the viability of the cell.<sup>380</sup>

To visualize the presence of live and cells in the presence of both the formulations of disc shaped GelMA+ gels, live/dead assay was performed. Immortalized HCECs were seeded on 48 well tissue culture treated plates at a cell density of  $5 \times 10^4$  cells/cm<sup>2</sup> using the growth nutrient media as mentioned in section 4.2.2.1. On each well of the 48 well plate containing the seeded cells, freshly prepared GelMA+ gels of both the formulations were placed over the cells. The disc shaped gels were washed with sterile PBS 1X for 4 minutes inside the cell culture hood prior to exposure to the cells. The gels were washed four times in 5 mL of fresh sterile PBS 1X for 1 minute each time. This was done to ensure the unreacted photocrosslinker gets washed away. The cells were cultured and incubated at 37 °C and 5% carbon dioxide in the presence of the GelMA+ hydrogels for 5 days. The media was changed on alternate days. For the control, the immortalized HCECs were cultured in a 48 well plate without the presence of any GelMA+ gels. The LIVE/DEAD™ Viability/Cytotoxicity Kit (Thermo Fischer Scientific, Eugene, OR, USA) was used to stain the cells and the procedure was performed exactly as described by the manufacturer's instructions.<sup>380</sup> 20 µL of 2 mM of EthD-1 was added to 10 mL of sterile PBS resulting in 4 µM EthD-1 solution. 5 µL of 4 mM calcein AM stock solution to the 10 mL EthD-1 solution. The solution was vortexed to ensure thorough mixing. The growth media was withdrawn from the wells of the 48 well plate containing the cells and the resulting approximately 2 µM Calcein AM and 4 µM EthD-1 working solution was then added directly to cells containing the GelMA+ gels. The cells were incubated with dye at room temperature (22-24 °C) for 20-30 minutes. The images were taken with the Citation 5 (BioTek, Winooski, VT, USA) via fluorescence microscopy.

### **4.3 Statistical Analysis**

Statistical analysis and graphs were plotted using GraphPad Prism 6 software (GraphPad, La Jolla, CA, USA). An analysis of variance (ANOVA) and a post-hoc Tukey's test was performed when necessary to determine the statistical significance between different conditions.

## 4.4 Results

### 4.4.1 Cell Growth with GelMA+ gels

Figure 4-1A and 4-1B show the growth and attachment of the immortalized HCEC cells in the presence of both the formulations of GelMA+ gels (n=4). The experiment was repeated on different days. With 30% w/v GelMA+ gels, more cell growth and attachment was observed compared to 20% w/v GelMA+. The images were observed phase-contrast microscopy with 20 X objective. The images were captured using Zeiss AxioVision Software (White Plains, NY, USA).

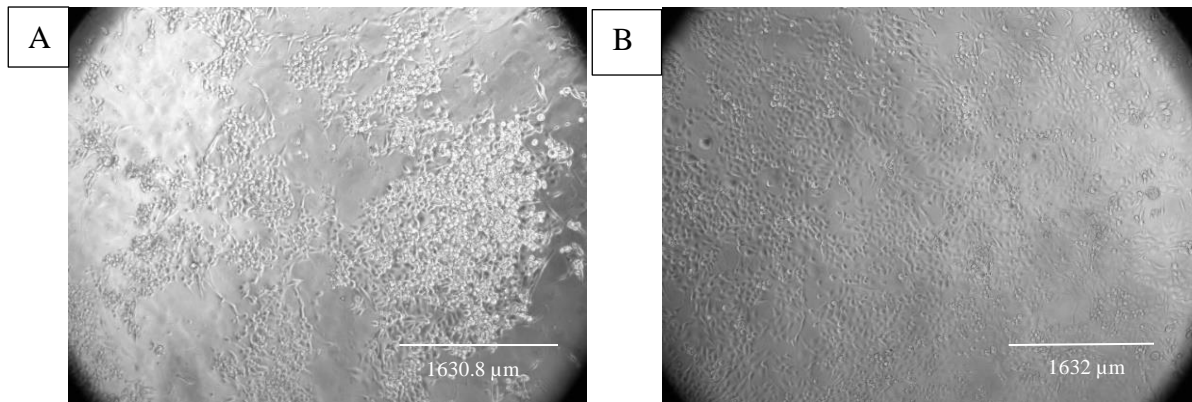


**Figure 4-1:** (A) Growth of immortalized HCEC cells in the presence of 20% w/v GelMA+ gels, (B) Growth of immortalized HCEC cells in the presence of 30% w/v GelMA+ gels

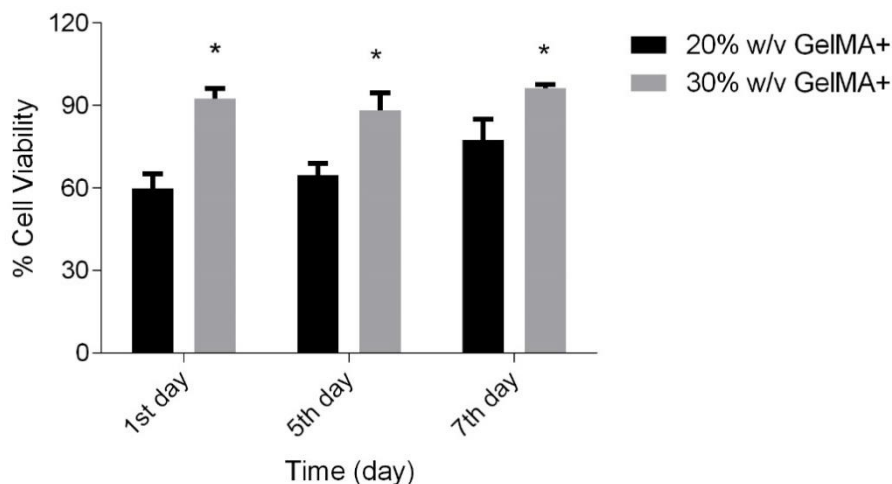
### 4.4.2 Cell Viability Assay

Figure 4-2 shows the percentage of cells viable in the presence of the GelMA+ hydrogels (n=4) on the 1, 5 and 7 days of incubation as measured by the alamarBlue™ assay. The experiments were repeated on different days. The cell viability of HCECs in the presence of GelMA+ gels was compared with the

control where the cells were grown in the absence of the GelMA+ gels, only in the presence of EpiGRO media. The controls were prepared for each time point (1 day, 5 days and 7 days). The cells in the control were seeded on day 0 and proliferated till the mentioned time points (1 day, 5 days and 7 days) for the alamarBlue test. In line with the data observed in the cell growth on GelMA+ gels, more cells were viable in the presence of 30% w/v GelMA+ gels ( $p < 0.0001$ ), which indicates cells prefer or like the presence of GelMA+. On the 7<sup>th</sup> day, 20% w/v GelMA+ hydrogel showed 80% cell viability, whereas the 30% w/v GelMA+ showed almost 95% cell viability. With an increase in the number of days, the percentage of cell viability increased for both GelMA+ formulations ( $p < 0.0001$ ). The increase in the percent viability of HCECs in the presence of 20% and 30% GelMA+ gels with increase in days suggests that with time the cells proliferated in the presence of the GelMA+.

**Table 4-1:**Percentage of cell viability of 20% and 30% w/v GelMA+ when compared to control (n=4)

No. of days	20% w/v GelMA+	30% w/v GelMA+
1	59.9 ± 5.1	92.4 ± 3.7
5	64.7 ± 4.2	88.2 ± 6.3
7	77.5 ± 7.5	96.2 ± 1.3



**Figure 4-2:** Percentage of HCEC cell viability in the presence of different formulations of GelMA+ in comparison to control (HCECs were not exposed to GelMA+ gels) (n=4)

#### 4.4.3 Live/Dead assay

Figure 4-3(A-C) shows the live and dead cells distribution after 5 days in the culture media control (no GelMA+), cells incubated with 20% w/v GelMA+ and cells incubated with 30% w/v GelMA+ (n=4). The experiments were repeated on different days. Cells that were stained green (Calcein-AM) were live cells whereas the cells that were stained red (EthD-1) were dead cells. For both formulations of GelMA+, a large number of cells remained alive with no signs of cytotoxicity (as evident from the green colour of Calcein-AM) when compared to the control after a period of 5-day incubation. There were no studies (negative control) done to show the presence of dead cells or red colour from EthD-1. However, from figures 4-3 (B-C) it can be observed that almost all the cells are viable after a 5-day incubation period. The results show that GelMA+ presents a favorable environment for cell growth and survival.



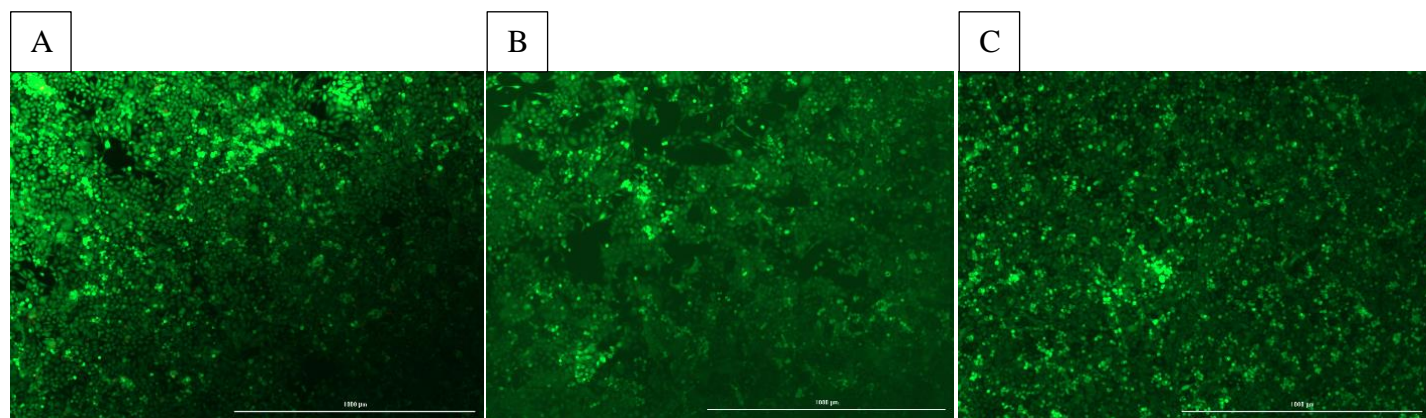


**Figure 4-3:** Live/Dead cells distribution on (A) Control (No GelMA+), (B) 20% w/v GelMA+, (C) 30% w/v GelMA+. The green fluorescence (calcein AM) denotes the presence of live cells, and the red fluorescence (EthD-1) denotes the presence of dead cells. A negative control with all dead HCEC cells was not studied.

## 4.5 Discussion

Several papers have shown that GelMA is a favourable biopolymer for cell adhesion and growth.<sup>159, 346, 381-383</sup> Thus, we hypothesized that GelMA+ would also be a favourable biomaterial for growth of the immortalized HCEC. Figures 4-1A and 4-1B show the cells to thrive and proliferate in the presence of GelMA+, with an increase in the cell growth and proliferation on the 30% w/v GelMA+ hydrogel, indicating that 30% w/v GelMA+ is more favourable for the HCECs. Furthermore, the higher concentration of GelMA+ is also associated with increased stiffness, which is required as an adequate surface/matrix for HCEC growth.<sup>384</sup>

AlamarBlue is a non-toxic cell permeable dye.<sup>367, 377</sup> It is blue in colour and non-fluorescent.<sup>385</sup> AlamarBlue assay is ubiquitous as it is less toxic than other techniques, and considering it can be used to perform lengthy experiments without harming the cells. Resazurin is a water-soluble, non-radioactive molecule with great stability in cell culture.<sup>386</sup> From the alamarBlue assay, it was observed that HCECs cultured with 30% w/v GelMA+ showed improved viability as compared to the 20% w/v (Table 4A). With an increasing number of days, the percentage of viable cells increased for both GelMA+ formulations, demonstrating cell proliferation with time. But the viability of the cells on day 5 in presence of 20% GelMA+ was around 64% which indicates that the 20% GelMA+ may not be favourable for the cell proliferation. Whereas on day 5, the cell viability was above 80% in presence of 30% GelMA+ gels indicating that 30% GelMA+ provided a favourable environment for the cells to thrive. At the end of the 7-day study, the 30% w/v GelMA+ proved to be better for the HCEC cells than the 20% w/v GelMA+ (Table 4-1). The reason for the cells to thrive in the presence of 30% GelMA+ as opposed to 20% GelMA+ can be due to the presence of arginine-glycine-aspartic sequence present in GelMA+ which provides a favourable environment for the cells to proliferate. More number of arginine-glycine-aspartic sequences are present in 30% GelMA+ as opposed to 20% GelMA+. This might be a reason why cells proliferated more in the presence of 30% GelMA+.

The live/dead cell assay data (Figure 4-3A – 4-3C) was not consistent with the alamarBlue data. The majority of the cells were viable for 5 days, as indicated by the green fluorescence (Calcein AM) in the

live/dead cell assay images. The live/dead cell assay images for both formulations of GelMA+ (Figures 4-3B and 4-3C) almost mimic the control (Figure 4-3A), which is devoid of any polymer. But on comparing with the alamarBlue data for 20% GelMA+ on day 5 where the cell viability was around 64%, the live/dead cell data for 20% GelMA+ was not consistent with the alamarBlue assay. On day 5, the live/dead assay for HCECs in the presence of 20% GelMA+ should have shown red dots (EthD-1) due to the presence of dead cells. But the live/dead cell assay image for HCECs in the presence of 20% GelMA+ (Figure 4-3B) showed green (Calcein AM) which indicated almost all the cells were alive which is contradicting the alamarBlue data. This can be due to the fact that the growth media was changed every alternate days during the study period which might have washed away or removed the dead cells when the existing growth media in the 48 well plate was replaced with the fresh media. This might be a reason why red stained dead cells were not visible in the live/dead assay. However, future study with a positive control is needed to show the presence of dead cells for comparison with the test samples. Overall, these data suggest that 30% GelMA+ formulation is non-cytotoxic and can allow cell growth for a week. The results suggest that the immortalized HCEC could proliferate under the 30% w/v GelMA+ for 5 days, and thus 30% w/v is more favourable for the HCECs. The reason for the increased growth of HCECs on 30% w/v GelMA+ as compared to 20% w/v could be the increased stiffness in 30% w/v GelMA+. Several studies have shown that increasing the stiffness of the polymer results in increased cell spreading.<sup>387, 388 389, 390</sup>

Chemical signals can cause changes in cellular activity, such as differentiation, proliferation, and directional migration. These signals include signaling molecules, growth factors, and chemo-attractants. It is now widely acknowledged that in addition to these chemical signals, cells can also react to mechanical signals.<sup>391</sup> These mechanical signals can either result from the mechanical characteristics of the environment cells reside on or in or they can be a stimulus from the environment cells are exposed to, such as shear flow on endothelial cells.<sup>392</sup> The main mechanical characteristic known to influence cellular activity is substrate stiffness (elastic modulus).<sup>393, 394</sup> According to a new study by Cameron et al., loss modulus also affects the differentiation and proliferation of stem cells.<sup>395</sup> Molladavoodi et al. investigated the response of immortalized HCECs on polyacrylamide substrate stiffness.<sup>389</sup> It was observed that with increase in substrate stiffness, there was an increase in the proliferation and

migration speed of HCECs.<sup>389</sup> Masterton et al. also demonstrated that with increase in polydimethylsiloxane substrate stiffness, there was an increase in the proliferation of HCECs.<sup>390</sup> The stiffness of polydimethylsiloxane increased from 10 kPa to 1500 kPa.<sup>390</sup> The stiffness of 20% GelMA+ was 2000 kPa and that of 30% GelMA+ was around 2800 kPa. This higher stiffness of 30% GelMA+ could be a reason for the higher proliferation of HCEC cells as opposed to 20% GelMA+.

From the cytotoxicity studies, the 30% w/v proved to be a better candidate in terms of providing a favourable condition for the cells to thrive and live for over 5 days. As the 30% w/v GelMA+ showed to be a favourable candidate for the wound healing material in terms of physical properties and biocompatibility, it was chosen as the hydrogel polymer to study the triggered release of the therapeutic agent bovine lactoferrin dispersed in its matrix over a period 5 days in the presence of varying MMP-9 concentrations, which is discussed in the next chapter.

# Chapter 5: In vitro release profile of bovine lactoferrin from GelMA+ gels

## 5.1 Introduction

Local drug distribution can be accomplished effectively using controlled release methods.<sup>396</sup> The main objective of localized drug delivery is to maintain therapeutic amounts of a pharmacological agent at a specific location in the body for an extended length of time. A second objective is to lower systemic toxicity by preventing the distribution of medicines to distant non-target organs.<sup>397</sup> When possible, local release enables the distribution of most drug molecules at or close to the site of action, lowering drug toxicity. Therefore, localized drug delivery is a desirable substitute for systemic delivery to avoid insufficient dosages of the medication at the target location and avoid systemic toxicity.<sup>398,399</sup> Polymeric delivery systems that may be implanted or injected are therefore being extensively researched for the local therapy of conditions like brain tumours, vascular illnesses, ophthalmic diseases, reproductive health, and wound healing.<sup>400-403</sup> The interesting problem for these delivery methods is producing a localized, persistent chemical release without impairing the nearby, healthy environment.

Controlled drug release using gelatin methacrylate (GelMA) is gaining momentum in the academic research world.<sup>151, 404-406</sup> A previous study shows controlled release of a  $\beta$  lactam antibiotic using GelMA and polyacrylamide (PAA) hybrid hydrogels, with the release of the antibiotic being fine-tuned by adjusting the composition of PAA.<sup>407</sup> GelMA has also been shown to be usable for controlled release of cefazolin.<sup>408</sup> Another study demonstrated the sustained release of encapsulated cells from the GelMA matrix.<sup>147</sup> GelMA hydrogels, if properly functionalized, can be used as a non-viral gene delivery vehicle.<sup>409,410</sup>

GelMA degrades in the presence of matrix metalloproteinase enzymes such as MMP-9.<sup>346, 353</sup> MMP-9 is highly upregulated during corneal injury.<sup>324-326</sup> Therefore, GelMA could also be used to entrap a particular drug or drug-nanoparticles and enhance the release of these compounds when the upregulated MMPs degrade the gel.<sup>411-413</sup> Chapter 3 describes a unique formulation of GelMA material, GelMA+,

that was shown to have improved mechanical strength compared with conventional GelMA.<sup>201</sup> In this chapter, the release of a model compound is evaluated, fluorescein isothiocyanate FITC-Dextran, and a potential corneal wound healing therapeutic, bovine lactoferrin (BLF), from different formulations of GelMA+, at varying temperatures and in the presence of varying concentrations of MMP-9.

## **5.2 Materials and Methods**

### **5.2.1 Materials**

Gelatin Type A, and bovine lactoferrin (80 kDa) were obtained from Sigma Aldrich (St. Louis, MO, USA). MMP-9 (92 kDa Type IV Collagenase) was obtained from Gibco Thermo Fisher Scientific (Grand Island, NY, USA). The bovine lactoferrin ELISA kit was obtained from Bethyl laboratories Inc. (Montgomery, TX, USA). The methacrylic anhydride and Irgacure 2959 was obtained from Sigma Aldrich (St. Louis, MO, USA). The Spectrum™ Spectra/Por™ 4 RC Dialysis Membrane Tubing 12,000 to 14,000 Dalton MWCO was purchased from Fisher Scientific (Carlsbad, CA, USA).

### **5.2.2 Gelatin methacrylate synthesis**

The method for the synthesis of GelMA+ has been previously described in section 3.2.2. In brief, 5 g of gelatin (type A) was dissolved in 50 mL of phosphate buffered saline 1X (PBS) (10% w/v) with continuous magnetic stirring at 50-60 °C to fasten the formation of the gelatin solution. 10 mL of methacrylic anhydride (20% v/v) was then added dropwise at 50-60 °C with continuous magnetic stirring. The reaction was continued for 1 hour. The resulting mixture was diluted with PBS and dialyzed in deionized (DI) water for 5 days at 40 °C using 12-14 kDa cut-off dialysis membrane tubes. The GelMA solution was then frozen at -80°C and lyophilized.

### **5.2.3 Preparation of BLF or FITC-dextran loaded GelMA+ hydrogel**

Lyophilized GelMA was mixed together in a 1X PBS solution containing 0.5% w/v Irgacure 2959 to obtain mixtures with 10%, 20%, and 30% w/v of GelMA. The mixture was incubated at 60°C for 48 hours. A stock solution of 50 mg/mL FITC-dextran in 1X PBS was prepared and stored at 4 °C. For preparing FITC-dextran loaded GelMA+ gels, 60 µL of 50 mg/mL FITC-dextran was then added to the mixture and centrifuged for 10 mins at 5000 rpm. The mixtures were further incubated for 30 minutes at 60 °C before carefully pipetting into an acrylic mold consisting of circular hollows (thickness ~ 0.65

mm). The samples were then incubated at 4 °C for 1 hour, before being exposed to UV radiation (360-420 nm) at an intensity of 32 mW/cm<sup>2</sup> and polymerized in Dymax Ultraviolet (UV) Curing Chamber (Torrington, CT, USA) for 5 minutes to create GelMA+ gels containing either FITC-dextran or BLF. The resultant circular shaped GelMA+ gels were of diameter ~ 6 mm. For preparing BLF loaded GelMA+ gels, lyophilized GelMA was mixed together with 1X PBS containing the same photoinitiator concentration to prepare 30% w/v of GelMA+. A stock solution of 50 µg/mL BLF in 1X PBS was prepared and stored at 4 °C. To the mixture, 60 µL of 50 µg/mL of BLF was added and then similar steps were followed for the fabrication of BLF loaded GelMA+ gels.

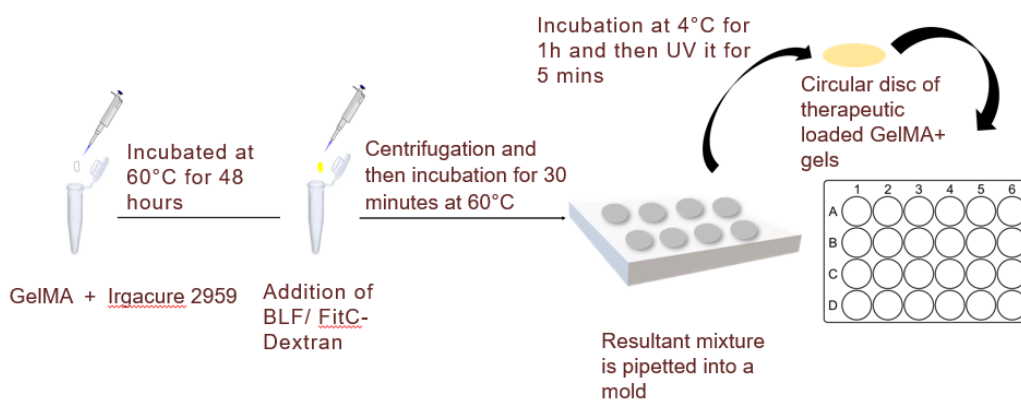


**Figure 5-1:** Schematic representation of the BLF / FITC-dextran loaded GelMA+ gels

#### 5.2.4 In vitro release study of FITC-dextran and BLF at room temperature (23 °C – 25 °C)

The GelMA+ gels disc shaped samples were washed in 1 mL of PBS for 24 hours to remove any loosely bound drug. To understand the release profile of FITC-dextran in low concentration of MMP-9 (nanogram range) to higher concentration of MMP-9 (microgram range), the samples were placed in a 48 well plate containing varying concentrations of MMP-9: 0 µg/mL, 0.25 µg/mL, 1 µg/mL, 10 µg/mL, 50 µg/mL, 100 µg/mL, and 300 µg/mL at room temperature (23°C - 25°C). At t = 0, 0.5, 1, 2, 4, 6, 8,



12, and 24 hour, 100  $\mu\text{L}$  of the release media was withdrawn and the fluorescence was read using a spectrophotometer (Cytation 5, BioTek, VT, USA) at an excitation and emission wavelength of 490 nm and 520 nm respectively. At each time point, after withdrawing 100  $\mu\text{L}$  of release media, 100  $\mu\text{L}$  of fresh release media was added back to the well. For the second study, the 30% w/v GelMA+ samples containing BLF were placed in three concentrations of MMP-9: 0  $\mu\text{g}/\text{mL}$ , 100  $\mu\text{g}/\text{mL}$ , and 300  $\mu\text{g}/\text{mL}$ . At  $t = 0.5, 12,$  and 24 hour, the samples were analyzed using the BLF ELISA kit. The ELISA plate was a 96 well plate where the anti BLF antibodies were bound to the solid phase. 100  $\mu\text{L}$  of the test sample and the standard were added to the 96-well ELISA plate. This leads to a complex formation between the BLF and the anti BLF. Then the unbound sample proteins are washed using the wash buffer. Anti BLF-HRP (streptavidin-conjugated horseradish peroxidase) was added which leads to a complex formation among the anti BLF-HRP, BLF and anti BLF antibodies. Unbound anti BLF HRP were again washed using the wash buffer. Chromogenic substrate TMB (3,3',5,5'-tetramethylbenzidine) was added to each well to produce a colorimetric reaction. The degree of yellow colour, proportional to the lactoferrin present in the sample, was measured at an absorbance of 450 nm.

### **5.2.5 In vitro release study of BLF at 37 °C**

The in vitro release of bovine lactoferrin from 30% w/v GelMA+ gels was undertaken in the presence of varying concentrations of MMP-9 at 37 °C. The samples were washed in 2 mL of 1X PBS for 1 hour to remove any loosely bound BLF. For the BLF release, the samples were placed in three concentrations of MMP-9: 0  $\mu\text{g}/\text{mL}$ , 100  $\mu\text{g}/\text{mL}$ , and 300  $\mu\text{g}/\text{mL}$ . At  $t = 0, 1, 12, 24, 48, 72, 96,$  and 120 hours, the samples were analyzed using the BLF ELISA kit. At each time point, 100  $\mu\text{L}$  of the release media was withdrawn and replaced with fresh release media. In brief, 100  $\mu\text{L}$  of the test sample and the standard were added to the 96-well ELISA plate. HRP (streptavidin-conjugated horseradish peroxidase) and TMB (3,3',5,5'-tetramethylbenzidine) reagents from the kit is added to each well to produce a colorimetric reaction. The degree of yellow colour, proportional to the lactoferrin present in the sample, was measured at an absorbance of 450 nm.

### **5.2.6 Optical Transmittance of BLF loaded GelMA+ gels**

The optical transmittance of BLF loaded 30% w/v GelMA+ hydrogel in 1X PBS were measured UV spectrophotometer of Biotek Citation 5 (Winooski, VT, USA). The GelMA+ disc shaped gels were placed in 1 mL 1X PBS in a 48 well plate and the measurements were performed at the wavelength range of 450 nm to 700 nm. For the blank measurement, the wavelength of the PBS 1X was measured at the wavelength range of 450 nm to 700 nm. The transmittance value of BLF loaded 30% w/v GelMA+ were obtained by subtracting the value GelMA+ gels in 1X PBS with 1X PBS.

### **5.3 Statistical analysis**

Statistical analysis and graphs were plotted using GraphPad Prism 6 software (GraphPad, La Jolla, CA). A repeated measure analysis of variance (rmANOVA) was performed to determine the differences over time, between gel types, and concentrations of MMP-9. A one-way ANOVA was used to determine the differences between various concentrations of MMP-9. The experiments were repeated on different days.

## **5.4 Results**

### **5.4.1 In vitro release kinetics of FITC-dextran and BLF at room temperature (23 °C – 25 °C)**

Figures 5-2, 5-3 and 5-4 show the release kinetics of FITC-dextran from 10%, 20% and 30% GelMA+ formulations respectively in varying concentrations of MMP-9 over 24 hours at room temperature (23 °C – 25 °C) (n=3). In Dr Evelyn Yim's lab at the Chemical Engineering department at the university of Waterloo, they studied the release of FITC-dextran in MMP-9 from 10%, 20% and 30% w/v of GelMA+ gels. Thus, these three formulations of GelMA+ were chosen for the initial study of the release profile of FITC-dextran in MMP-9. The release of the FITC-dextran was sustained over the 24 hours for all the three different formulations of GelMA+ gels in the presence of varying concentrations of MMP-9 ( $p < 0.0001$ ). There were no significant differences in the amount of FITC-dextran released at room temperature between the three formulations ( $p > 0.05$ ). However, the 10% w/v GelMA+ were fragile compared to the 20% and 30% w/v GelMA+ gels.

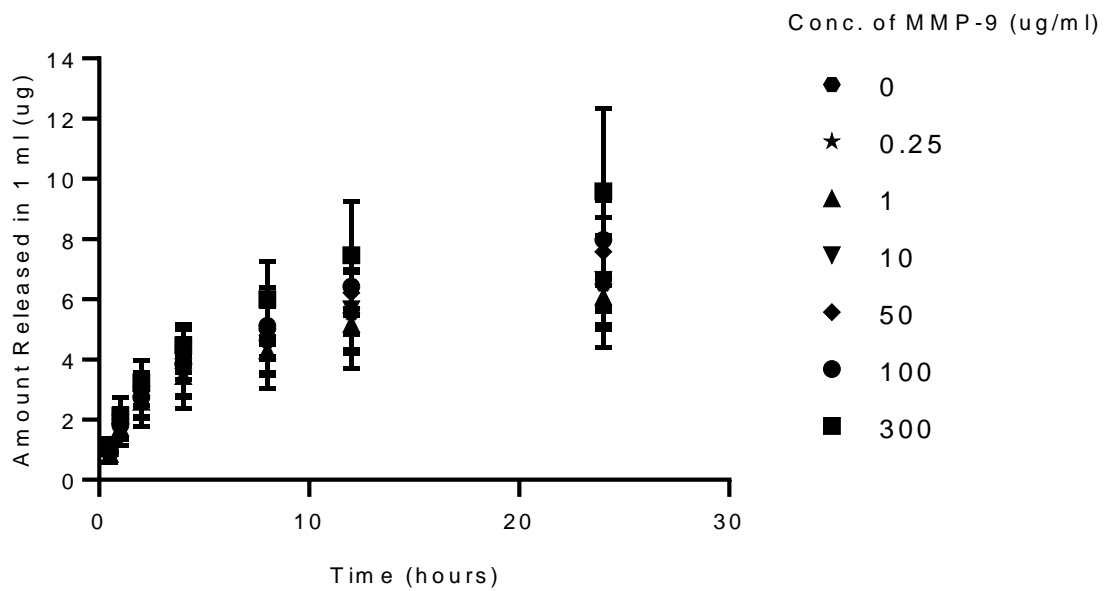


**Figure 5-2:** Release of FITC-dextran from 10% w/v GelMA+ formulation in varying concentrations of MMP-9 over 24 hours

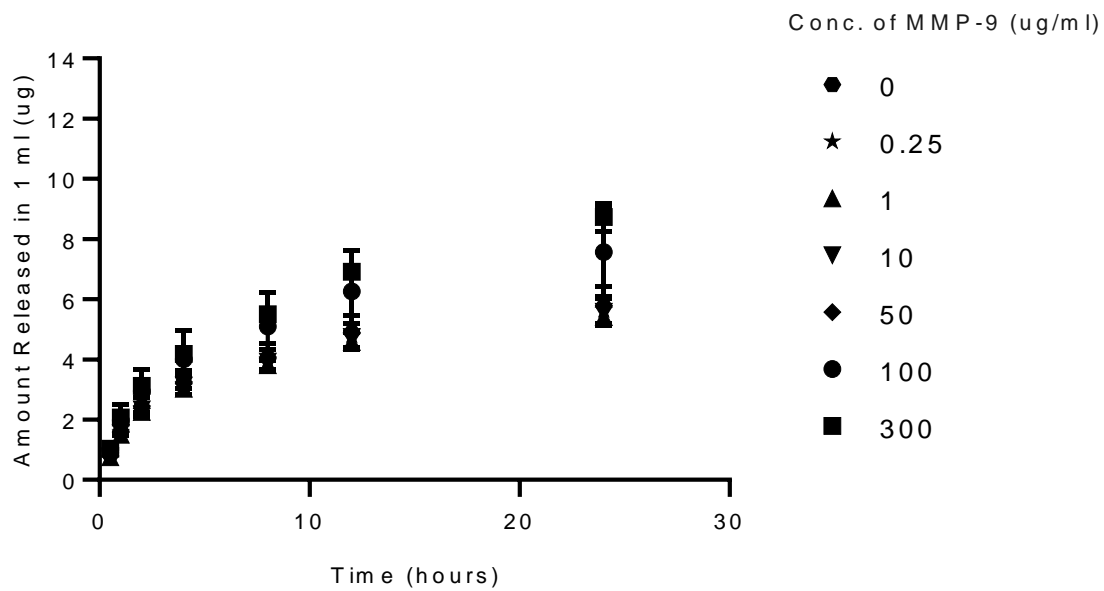


**Figure 5-3:** Release of FITC-dextran from 20% w/v GelMA+ formulation in varying concentrations of MMP-9 over 24 hours (n=3)

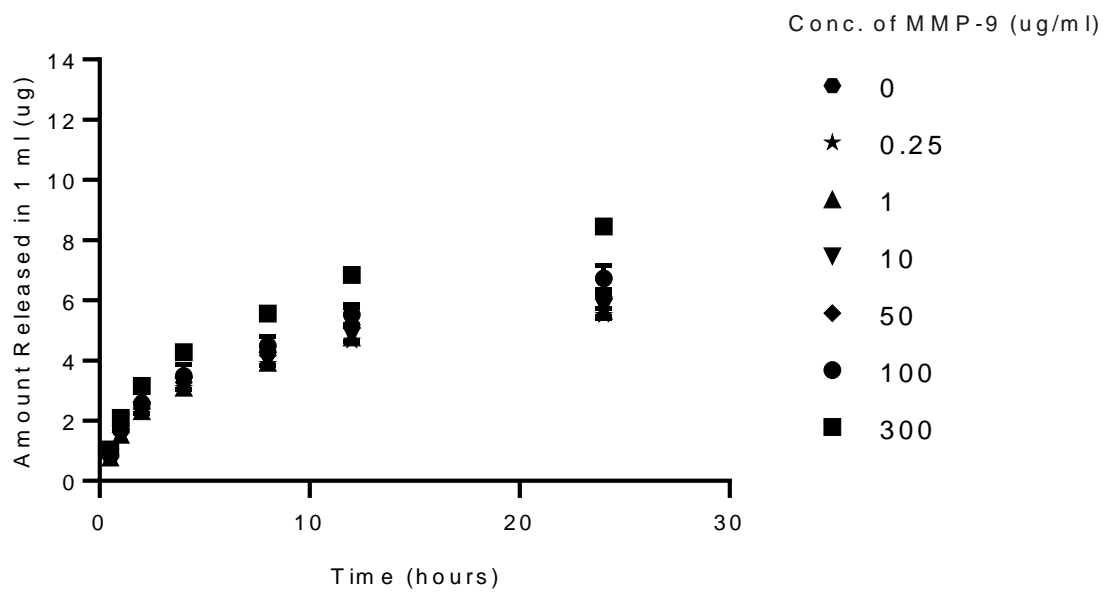


**Figure 5-4:** Release of FITC-dextran from 30% w/v GelMA+ formulation in varying concentrations of MMP-9 over 24 hours (n=3)

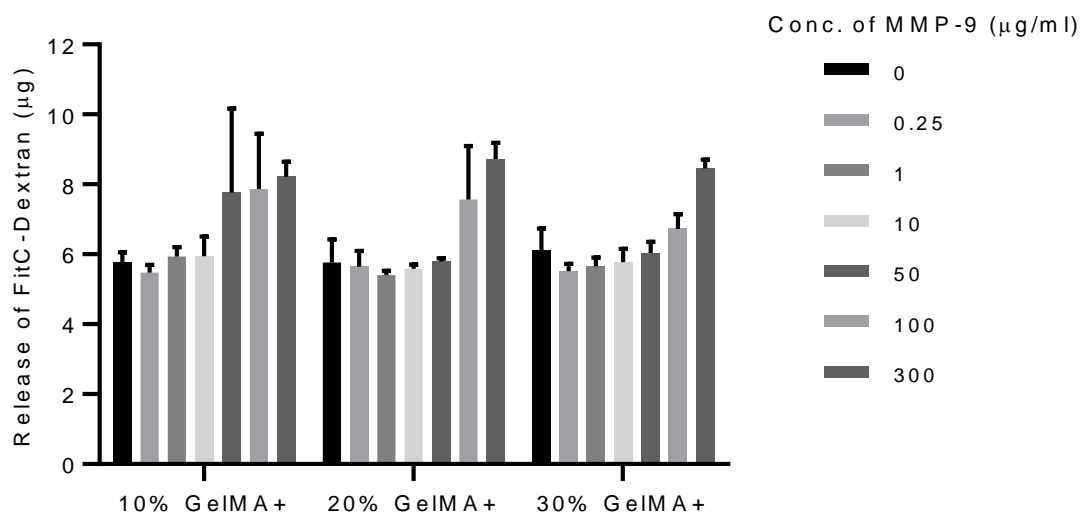


**Figure 5-5:** Release of FITC-dextran from 10%, 20% and 30% w/v GelMA+ in varying concentrations of MMP-9 at 24 hours (n=3)

The cumulative amount of FITC-dextran released after 24 hours at room temperature (23 °C – 25 °C) is shown in Figure 5-5. The release of FITC-dextran increased significantly in the presence of 300 µg/mL of MMP-9 for all gel types ( $p < 0.05$ ). There were, however, no significant differences in the amount of FITC-dextran released between the control (0 µg/mL) and 100 µg/mL of MMP-9 ( $p > 0.05$ ).

Table 5-1 shows the amount of FITC-dextran released during the wash period. The slow release of FITC-dextran at room temperature is likely due to the passive diffusion of the molecule from within the polymer matrix.

**Table 5-1:** The amount of FITC-dextran ( $\mu\text{g}$ ) released during the wash period (24 hours) from different formulations of GelMA+ gels in phosphate buffered saline (n=3)

<b>GelMA+ formulations</b>	<b>Amount of FITC-dextran (<math>\mu\text{g}</math>)</b>
10% w/v GelMA+	$1.7 \pm 0.5$
20% w/v GelMA+	$1.0 \pm 0.5$
30% w/v GelMA+	$1.3 \pm 0.4$

The results for FITC-dextran release with varying concentrations of MMP-9 suggest that there was no significant difference in the release of FITC-dextran for low concentrations of MMP-9 during a 24-hour release period ( $p > 0.05$ ) at room temperature ( $23\text{ }^{\circ}\text{C} - 25\text{ }^{\circ}\text{C}$ ). This indicates that the release of FITC-dextran was mainly due to passive diffusion at room temperature. However, for  $300\text{ }\mu\text{g/mL}$  of MMP-9, there was a significant increase in the release of FITC-dextran at 24 hours ( $p < 0.05$ ). We speculate that the increase in release of FITC-dextran for the  $300\text{ }\mu\text{g/mL}$  was due to degradation of the GelMA+ gels by MMP-9 at this concentration.

The release of bovine lactoferrin over 24 hours for 30% w/v GelMA+ at room temperature ( $23\text{ }^{\circ}\text{C} - 25\text{ }^{\circ}\text{C}$ ) is shown in Figure 5-6 (n=4). From the release profile of FITC-dextran, it was observed that at lower concentration of MMP-9 below  $100\text{ }\mu\text{g/mL}$ , there was no difference in the FITC-dextran release over 24 hours at room temperature. Thus for the BLF release profile, only three concentrations of MMP-9 were chosen (0, 100,  $300\text{ }\mu\text{g/mL}$ ). The release of the BLF at  $23\text{ }^{\circ}\text{C} - 25\text{ }^{\circ}\text{C}$  increased during the 24-hour period for MMP-9 concentrations ( $p < 0.0001$ ). For the control group, there was no difference in the amount of release of BLF between 12 hours and 24 hours at  $23\text{ }^{\circ}\text{C} - 25\text{ }^{\circ}\text{C}$  ( $p > 0.05$ ). There were also no statistically significant differences in the release at 0.5 and 12 hours between the different concentrations of MMP-9 and the control group at  $23\text{ }^{\circ}\text{C} - 25\text{ }^{\circ}\text{C}$  ( $p > 0.05$ ). At 24 hours, there was a



higher release of BLF for the MMP-9 conditions, but there were no significant differences between 100  $\mu\text{g/mL}$  and 300  $\mu\text{g/mL}$  of MMP-9 at 23  $^{\circ}\text{C}$  – 25  $^{\circ}\text{C}$  ( $p>0.05$ ).

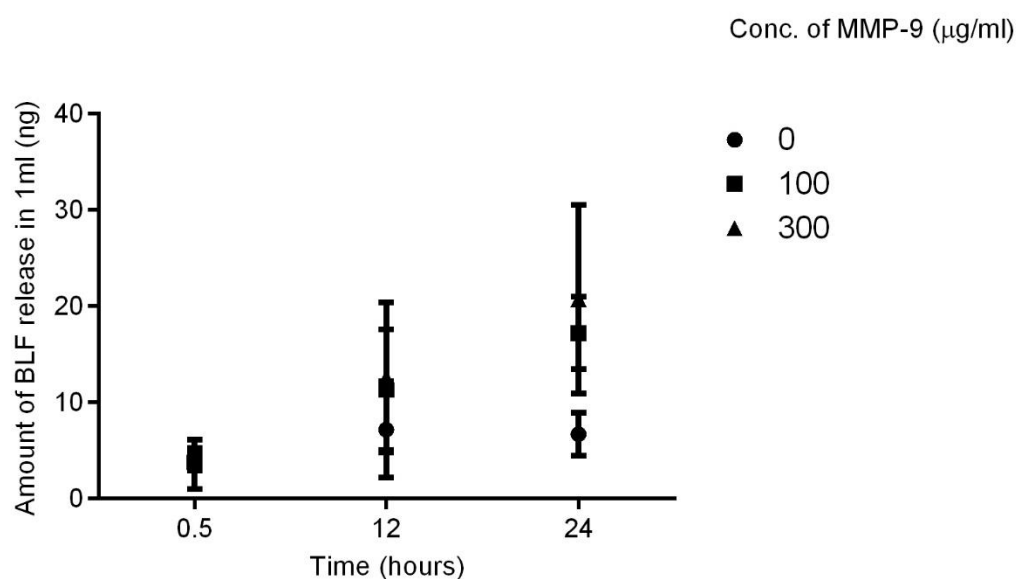


**Figure 5-6:** Release of BLF from 30% w/v GelMA+ at 23  $^{\circ}\text{C}$  – 25  $^{\circ}$  in varying concentrations of MMP-9 over 24 hours ( $n=4$ )

The cost-effectiveness and simplicity of the 70 kDa FITC-dextran model molecule led to its selection as the model molecule to determine drug release rate. It was found that FITC-dextran was sensitive to UV radiation, the GelMA precursor solution, and the photoinitiator. Phase separation between the FITC-dextran and GelMA polymers and dynamic quenching between the fluorophores are considered to be the principal causes of the decreased intensity. Thus, it was assumed the theoretical amount of FITC-dextran might get quenched during UV radiation and might lead to inaccurate calculation of percent release of FITC-dextran. Hence the release profile was estimated as the ‘amount release’ as opposed to ‘percent release’. Regardless of the quenching, FITC-dextran release pattern proved to be predictable of the BLF release profile at room temperature.

## 5.4.2 In vitro release study of BLF at 37 °C

The cumulative in vitro release kinetics of the BLF at 37 °C is shown in Figure 5-7 (n=4) to understand the drug release behaviour around ocular surface temperature and the influence of temperature on the BLF release profile.<sup>414</sup> At 37 °C, the release of BLF from the 30% w/v GelMA+ hydrogel matrix significantly increased with an increase in the MMP-9 concentration (p<0.0001). The amount of BLF released increased over time for all MMP-9 concentrations (p<0.0001). Due to the initial washing of the gels for an hour, no burst release was observed. The results show that the release of BLF from the gels was primarily driven by the enzyme present in the solution. Equation 4 was used for figure 5-7.

$$\text{Equation 4: Percent release of BLF} = \frac{\text{Amount of BLF released at each time point}}{\text{Theoretical amount of BLF loaded in each disc shaped gel}} \times 100\%$$

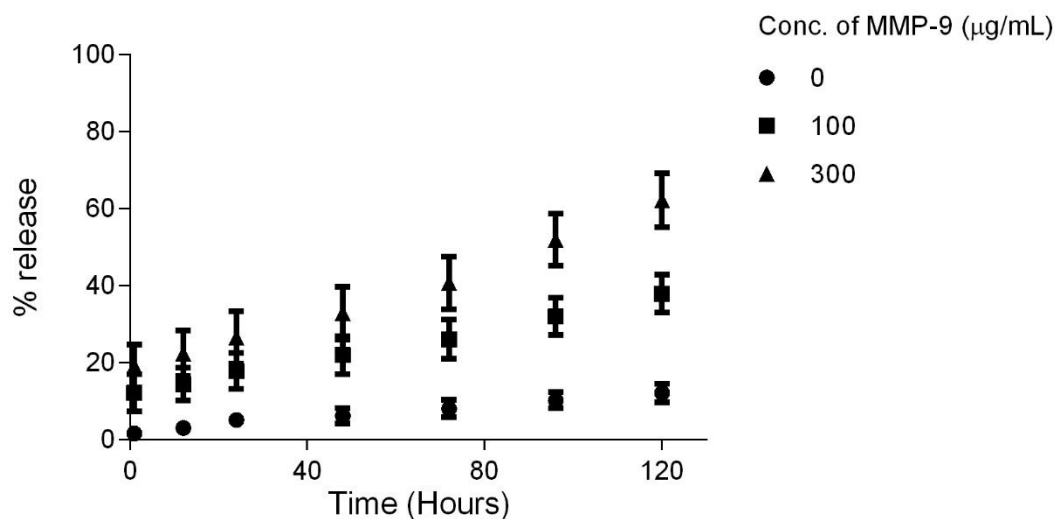


**Figure 5-7:** In vitro release of BLF from 30% w/v GelMA+ at 37 °C in the presence of varying MMP-9 concentrations (n=4)

### 5.4.3 Optical transmittance of BLF loaded GelMA+

To study the influence on BLF on the optical transmittance of GelMA+ hydrogel, the optical clarity (n=5) (Figure 5-8) of BLF loaded 30% w/v GelMA+ gels was measured in the visible light wavelength range of 450 nm and 700 nm using UV spectrophotometer of Citation 5. At 450 nm, the BLF loaded 30% w/v GelMA+ gels exhibited about  $78.2 \pm 2.6\%$  transmittance as opposed to  $86.07 \pm 3.88\%$  of blank 30% w/v GelMA+ hydrogel. At 630 nm, the transmittance was  $89.5 \pm 1.3\%$  as opposed to the transmittance of  $92.7 \pm 3.0\%$  of blank hydrogel. The transmittance was measured using the gels kept in 1X PBS in the 48-well plate at room temperature ( $22\text{ }^{\circ}\text{C}$  -  $24\text{ }^{\circ}\text{C}$ ). It can be observed that the transmittance of BLF loaded GelMA+ was less as compared to blank hydrogel. This suggest that the presence of BLF act as a hindrance to the optical transmittance. Further studies are required to formulate a therapeutic loaded GelMA+ that has an optical transmittance of more than 95% in the visible light range.

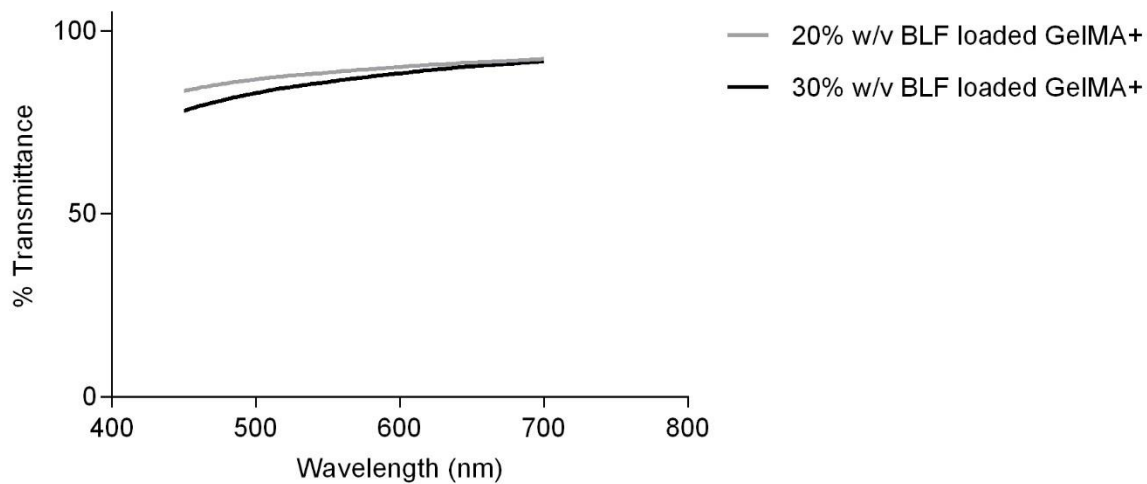


**Figure 5-8:** Optical transmittance of BLF loaded 30% w/v GelMA+ hydrogel in the visible light range of 450 nm to 700 nm

## 5.5 Discussion

The GelMA+ gels in the current study were able to release FITC-dextran over the 24-hour testing period (Figures 5-2, 5-3, 5-4). The release kinetics of FITC-dextran from the gels did not show a burst release within the first hour (Figure 5-2, 5-3, 5-4), which is generally observed in drug release studies from hydrogels.<sup>75, 78, 149, 318, 319</sup> All gels exhibited a slow-release profile for the entire 24-hour period (Figures 5-2, 5-3, 5-4) at room temperature. We hypothesize that the initial wash step removed most of the loosely bound FITC-dextran on the surface or sub-surface of the gels that could have contributed to a burst release.

The molecular weight of the FITC-dextran used in the current study was 70 kDa, which is similar to several therapeutics that could be used for corneal wound healing. For instance, BLF, which has a molecular weight of approximately 87 kDa, is a protein that promotes wound closure.<sup>149, 213, 218</sup> Lactoferrin has also been reported to promote wound healing.<sup>217, 218, 415</sup> Consequently, bovine lactoferrin was selected as the corneal wound healing therapeutic to be evaluated with GelMA+ in the second release study.

Based on the porosity of the GelMA+ gels, a high molecular weight compound would be an ideal candidate for entrapment and release from the gel when degraded by collagenase enzymes. We hypothesize that smaller molecules could simply diffuse from the gels at a faster rate than the rate of degradation. For this study, BLF was used as a model therapeutic for wound healing with a molecular weight of around 80 kDa.<sup>218</sup> Lactoferrin, an iron-binding monomeric glycoprotein,<sup>416</sup> is produced by the epithelial cells of different mammalian organs and found in several secretions, including milk,<sup>206</sup> saliva,<sup>207</sup> tears,<sup>235</sup> digestive secretions,<sup>205</sup> nasal secretions,<sup>417</sup> colostrum.<sup>208</sup> It can be obtained from several mammalian species.<sup>206, 418, 419</sup> The single polypeptide chain of BLF consists of two globular lobes, named as N-terminal or N-lobe and C-terminal or C-lobe.<sup>215, 420, 421</sup> It is antimicrobial,<sup>224, 422, 423</sup> antifungal,<sup>223</sup> antioxidant and anti-inflammatory.<sup>424-427</sup> BLF has also been reported to promote wound healing.<sup>217, 218, 415</sup> BLF has shown promising results in the closure of alkali wounded corneal epithelial cells.<sup>218, 415</sup>

The release of BLF (Figure 5-6) at room temperature (23 °C – 25 °C) and at an elevated temperature of 37 °C was evaluated using the 30% w/v formulation GelMA+, which was determined to have the most appropriate physical characteristics and better cell viability, as established in chapters 3 and 4. At room temperature (23 °C – 25 °C), the release profile for BLF from GelMA+ was similar to that of the FITC-dextran. The results suggest that the release of BLF from these gels was controlled mainly by passive diffusion at room temperature. It was only after 24 hours that the release was significantly higher for the MMP-9 solutions (100 µg/mL and 300 µg/mL) than the control ( $p < 0.05$ ). These results suggest that there may be a lag period before the MMP-9 can degrade the gels to release the matrix-bound BLF at room temperature.

The kinetic release of BLF studied from the 30% w/v GelMA+ at 37 °C over a period 5 days in the presence of varying MMP-9 concentrations (Figure 5-7) showed that GelMA+ was able to release BLF over the specified study period in a linear manner at the elevated temperature over 120 hours. Increasing the enzyme concentration resulted in increased BLF being released over time. Again, no burst release was observed, even though the BLF loaded gels were washed for 1 hour only. We hypothesize that the initial 1-hour wash step is sufficient to remove most of the loosely bound BLF (around 14%) on the surface or sub-surface of the gels that could have contributed to a burst release. Another reason for the absence of burst release from the 30% w/v formulation can be attributed to the small pore size of the 30% w/v GelMA+, which was found to be less than 1 micron. These results reveal that the controlled release from the GelMA+ is temperature dependent, as the enzyme (MMP-9) needs an elevated temperature for catalytic activation so that it can degrade the GelMA+ and release BLF from its hydrogel matrix. It has been reported that the catalytic activity of MMP-9 is a temperature dependent process.<sup>428</sup>

MMPs play an important role in wound healing and inflammation.<sup>429</sup> These enzymes are responsible for cleaving and remodelling of epithelial basement components and tight junction proteins.<sup>430, 431</sup> MMPs are proteolytic enzymes which are produced when ocular surfaces are stressed.<sup>432, 433</sup> Pro MMP-9 is the inactive enzyme or inactive zymogen which is proteolytically converted to active MMP-9.<sup>246</sup> The presence of pro MMP-9 (inactive zymogen or inactive enzyme precursor of MMP-9) in the tears

of healthy patients' was found at a concentration of  $20.3 \pm 5.2$  ng/mL.<sup>412</sup> However, patients suffering from conjunctivochalasis exhibited a pro MMP-9 concentration of  $223.4 \pm 74.5$  ng/mL.<sup>412</sup> In another study, active MMP-9 (active zymogen of active enzyme precursor of MMP-9) among healthy patients were found to be  $8.4 \pm 4.7$  ng/mL,<sup>434</sup> while patients suffering from severe dysfunctional tear syndrome showed a very high MMP-9 activity of  $381.2 \pm 142.8$  ng/mL.<sup>434</sup> MMP-9 levels found in human tears in various ocular disease conditions are detailed in Tables 5-2 and 5-3. The concentrations of MMP-9 can be utilized to enhance the release of active therapeutic agents from MMP-9 triggered GelMA+ to aid in corneal wound healing. Here, as a proof of concept, we chose a higher level of enzymatic concentration for the BLF release from the 30% w/v GelMA+ to show the correlation between the enzymatic concentration and the release of the therapeutic agent. However, more work will be needed to design materials that exhibit the same degradation kinetics at more physiologically relevant concentrations of MMP-9.

**Table 5-2:** Pro MMP-9 levels in ocular diseases

<b>Clinical conditions</b>	<b>Pro MMP-9 levels in healthy patients</b>	<b>Pro MMP-9 levels in diseased patients</b>
Blepharitis	$23.61 \pm 17.4$ ng/mL <sup>435</sup>	$58.56 \pm 30.1$ ng/mL <sup>435</sup>
Dry eye	$23.61 \pm 17.4$ ng/mL <sup>435</sup>	$97.25 \pm 49.5$ ng/mL <sup>435</sup>
Conjunctivochalasis	$23.61 \pm 17.4$ ng/mL <sup>435</sup> , $20.32 \pm 5.2$ ng/mL <sup>412</sup>	$126.40 \pm 101.9$ ng/mL <sup>435</sup> , $223.4 \pm 74.5$ ng/mL <sup>412</sup>
Allergic eye disease	$23.61 \pm 17.4$ ng/mL <sup>435</sup>	$132.33 \pm 78$ pg/mL <sup>435</sup>
Ocular rosacea	$0.2930 \pm 0.1$ ng/mL <sup>258</sup> , $0.2$ ng/mL <sup>436</sup>	$1.1796 \pm 1.2$ g/mL <sup>258</sup> , $26.7$ ng/mL <sup>436</sup>
Vernal Keratoconjunctivitis	$0.5 \pm 0.2$ ng/mL <sup>268</sup>	$16.6 \pm 13.8$ ng/mL <sup>268</sup>

**Table 5-3:** MMP-9 levels in ocular diseases

<b>Clinical conditions</b>	<b>MMP-9 levels in healthy patients</b>	<b>MMP-9 levels in diseased patients</b>
Severe Keratoconus	6.1 ng/mL <sup>437</sup>	171.2 ng/mL <sup>437</sup>
Moderate Keratoconus	6.1 ng/mL <sup>437</sup>	42.7 ng/mL <sup>437</sup>
Mild Keratoconus	6.1 ng/mL <sup>437</sup> , 6.1 ng/mL <sup>438</sup>	58.5 ng/mL <sup>437</sup> , 59.4 ng/mL <sup>438</sup>
Severe dysfunctional tear syndrome	8.39 ± 4.7 ng/mL <sup>434</sup>	381.24 ± 142.8 ng/mL <sup>434</sup>

One advantage of an enzyme degradable biomaterial is that it does not need to be removed while it degrades in-situ. It can be used for sustained and controlled drug delivery to deliver drug to the site of action in the body.<sup>439, 440</sup> As observed from the lactoferrin release profile, the release of the therapeutic agent is directly proportional to the presence of MMP-9. This implies that the drug release will respond to the wound's severity. Large wounds will have higher MMP levels<sup>411, 441</sup> and this in turn will degrade the GelMA+ faster, leading to a higher release of the therapeutic agents. The main disadvantage of GelMA+ bandage contact lenses is that they could cause vision problems as it degrades. One alternative is incorporating this material as a contact lens skirt, ring implant or implant under the lower eyelid.

The gels in this study were fairly thick (~ 600 µm) in comparison to a bandage contact lens, which are typically 100-200 µm thick.<sup>359, 442</sup> Depending on the enzymes available at the wounded site, the GelMA+ gels can be formulated so that it degrades completely in-situ, releasing the therapeutic or drug intended to aid in the wound healing process. More work, however, is required to tune these gels to degrade faster at lower concentrations of MMP-9. Overall, the 30% w/v GelMA+ gels in this study show promise as potential biomaterials for corneal wound healing.



## **Chapter 6: Bovine Lactoferrin-induced corneal epithelial wound healing**

### **6.1 Introduction:**

The corneal epithelium serves as an ocular barrier to protect the integrity of the ocular surface.<sup>23</sup> Damage to this corneal layer can affect vision and expose the internal layers of the cornea to the external environment, potentially resulting in serious infections.<sup>23, 443, 444</sup> Trauma, microbiological or chemical injury, contact lens use, or procedures like photorefractive keratectomy can all harm the corneal epithelium.<sup>445</sup> The majority of minor corneal epithelial wounds heal quickly.<sup>446</sup> The corneal epithelium does, however, take longer to repair under some clinical circumstances, such as chemical injury or mechanical injury, leaving the underlying stroma open to infection and ulceration.<sup>218</sup>

One of the most frequent eye injuries is a corneal abrasion.<sup>447</sup> It results in severe pain, erythema (red eye), and photophobia (light sensitivity), as the corneal epithelium is damaged.<sup>41</sup> Eye complaints account for 2% of primary care clinics, while traumatic disorders and foreign bodies account for 8% of visits.<sup>448</sup> Redness, light sensitivity, increased lacrimation, and impaired visual acuity can all be symptoms of corneal abrasions.<sup>449</sup> In extreme situations, this results in corneal ulcers, perforation, scarring, and irreversible vision loss.<sup>41</sup> To keep the integrity of the corneal epithelium and to protect the eye, the corneal epithelium must repair itself quickly.<sup>284</sup>

Lactoferrin (80 kDa) is present in bodily secretions.<sup>205</sup> It acts as an anti-inflammatory<sup>450</sup>, regulates the immune system, and acts as an antibacterial agent.<sup>451</sup> Lactoferrin may offer a potential treatment for corneal wounds.<sup>213, 218</sup> In both healthy and diabetic mice with full-thickness wounds, therapy with recombinant lactoferrin enhanced skin wound closure.<sup>452</sup> In various organs, lactoferrin has been demonstrated to promote the proliferation of epithelial cells.<sup>453</sup> The fact that it can shield corneal cells from harm by ultraviolet B radiation suggests that it might be used on the cornea.<sup>216</sup> Several studies have demonstrated lactoferrin's ability to promote corneal epithelial alkali wound healing in vitro.<sup>213,</sup>

One of the oldest techniques to analyze directional cell migration in vitro is the wound-healing assay, which is easy, and economical.<sup>454</sup> This process imitates in vivo wound healing cell movement. In this study, we investigated the effect of bovine lactoferrin (BLF) on immortalized human corneal epithelial cells' (HCECs) ability to repair in vitro following a scratch injury using the scratch wound assay method.

## **6.2 Materials and Methods**

### **6.2.1 Materials**

The HPV immortalized HCECs were obtained from the Centre for Ocular Research & Education (CORE), School of Optometry & Vision Science, University of Waterloo, Waterloo, ON, Canada. The EpiGRO™ Human Ocular Epithelia Complete Media Kit was obtained from Millipore Sigma (Burlington, MA, USA). The 80 kDa BLF was obtained from Sigma Aldrich (St. Louis, MO, USA)

### **6.2.2 Cell Culture**

HCECs were cultured in Corning® tissue culture treated cell culture flasks with a canted neck plug seal cap and a surface area of 25 cm<sup>2</sup> in a serum free growth media. The growth nutrient media consisted of EpiGRO™ Human Ocular Epithelia Complete Media along with supplements of L-Glutamine, Epifactor O, Epifactor P, Epinephrine, rh Insulin, Apo transferrin, and Hydrocortisone hemisuccinate (Millipore Sigma, Burlington, MA, USA). The cells were seeded at a ratio of 1:2 and grown in an incubator at 37 °C and 5% carbon dioxide. Unless otherwise stated, all investigations involving the cultivation of HCECs were conducted at 37 °C in a 5% carbon dioxide atmosphere.

### **6.2.3 Making a scratch induced wound on HCEC monolayer**

To study the effect of BLF on scratch induced wounded HCECs, the immortalized HCECs were cultured as described in the previous section. Briefly, immortalized HCECs were maintained on a tissue culture treated 96-well plate at  $2.5 \times 10^4$  cells/cm<sup>2</sup> in EpiGRO™ Human Ocular Epithelia Complete Media along with supplements of L-Glutamine, Epifactor O, Epifactor P, Epinephrine, rh Insulin, Apo transferrin, and Hydrocortisone hemisuccinate (Millipore Sigma, Burlington, MA, USA). Once the HCECs achieved a confluent monolayer, the cells were manually scratched using a 200 µL pipette tip (p200). The debris from the scratch was immediately removed by washing cells in the 96-well plate four times with 250 µL of the growth medium (EpiGRO™ Human Ocular Epithelia Complete Media). After the washing step, 250 µL of the growth media was added to each well containing wounded HCECs.

### **6.2.4 Effect of BLF on HCEC Wound Healing of Scratch-Induced Wound Model**

In previous work on alkali induced corneal epithelial wound healing, 5 mg/mL of BLF was able to induce wound healing.<sup>218</sup> Since this was a scratch wound healing assay, which has not been studied before in presence of BLF as compared to alkali induced wound healing assay, a concentration of 5 mg/mL of BLF and more than 5 mg/mL of BLF were chosen. To determine the effect of BLF on the healing of a scratch induced wound, a scratch was made on the confluent monolayer of HCECs using a p200 pipette tip, as discussed in the previous section. After wounding, the cells were immediately washed, as mentioned in the last step. The growth medium containing 0, 5, 7.5, and 10 mg/mL BLF was added to the wounded cells and incubated at 37 °C in a 5% carbon dioxide atmosphere to determine the therapeutic window. The control was the growth medium devoid of BLF. The study was conducted for 6 days. Wounds were visually examined to compare almost identical wound areas using a phase contrast microscope at 20X magnification. On days 0, 1, 2, 4, and 6, wound closure was observed in response to the treatment. Wounds were photographed at 20X magnification using Zeiss AxioVision Software (White Plains, NY, USA), and the area of the wound was determined using an image analysis

system (Image J version 1.33, National Institutes of Health, Bethesda, MD, USA). To capture the images of a specific wounded site on the cells, the bottom of the wells of a 96 well plate was marked with a sharpie. At each time point, based on the marked location, the image of the wounded cells were captured. The percentage reduction in wound area relative to the initial wounding at day 0 was used to calculate the degree of wound closure in response to the BLF treatment. The same procedure was repeated to find the wounding response to the same concentration of BLF for 4 days at several time points (0, 4, 8, 24, 48, 72, 96 hours).

### **6.3 Statistical Analysis**

Statistical analysis and graphs were plotted using GraphPad Prism 6 software (GraphPad, La Jolla, CA, USA). An analysis of variance (ANOVA) and a post-hoc Tukey's test were performed when necessary to determine the statistical significance between different conditions. The studies were repeated on different days.

## **6.4 Results**

### **6.4.1 Effect of BLF on HCEC Wound Healing of Scratch-Induced Wound Model for 6 days**

The treatment showed BLF could heal mechanically injured HCECs (n=4). With the increase in the concentrations of BLF, the wound closure significantly improved ( $p < 0.0001$ ) compared to the control. With the increase in time (number of days), the wound closure significantly improved for all the concentrations of BLF ( $p < 0.0001$ ) until day 4. There was no significant difference in percent wound closure ( $p > 0.05$ ) for all the BLF concentrations from day 4 to day 6. Figure 6-1 shows the percent wound closure for all the concentrations of BLF. On day 6, the treatment with 5mg/mL BLF resulted in 1.50 times wound closure ( $85.41 \pm 3.14\%$  wound closure compared to  $56.89 \pm 1.93\%$  in the control) (Figure 6-1). Treatment with 7.5 mg/mL BLF resulted in 1.65 times wound closure compared to control ( $93.76 \pm 1.90\%$  wound closure as compared to  $56.89 \pm 1.93\%$  in the control) (Figure 6-1). 10 mg/mL BLF resulted in 1.75 times wound closure when compared to the wound closure measured in the control ( $99.36 \pm 0.84\%$  wound closure) (Figure 6-1). No significant difference ( $p > 0.05$ ) was observed in the treatment between 7.5 mg/mL and 10 mg/mL BLF on day 4 and day 6. However, the percent wound closure by 10 mg/mL BLF was higher ( $p < 0.001$ ) than 5 mg/mL BLF throughout the entire study period. Figure 6-2 shows images of the scratched wound closure in response to BLF treatment (0, 5, 7.5, and 10 mg/mL).

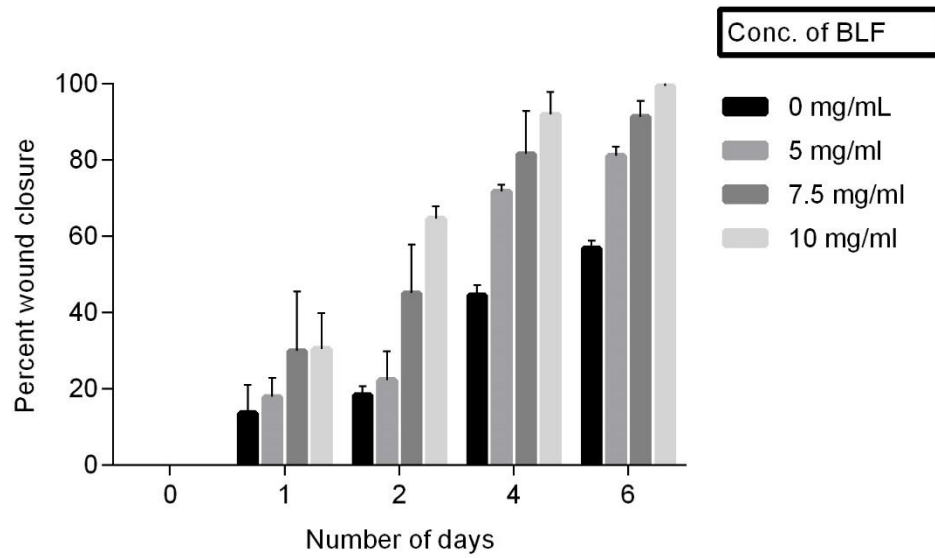


**Figure 6-1:** Percent closure of scratch induced HCEC wounds in response to treatment with BLF (0, 5, 7.5, 10 mg/mL) (n=4)

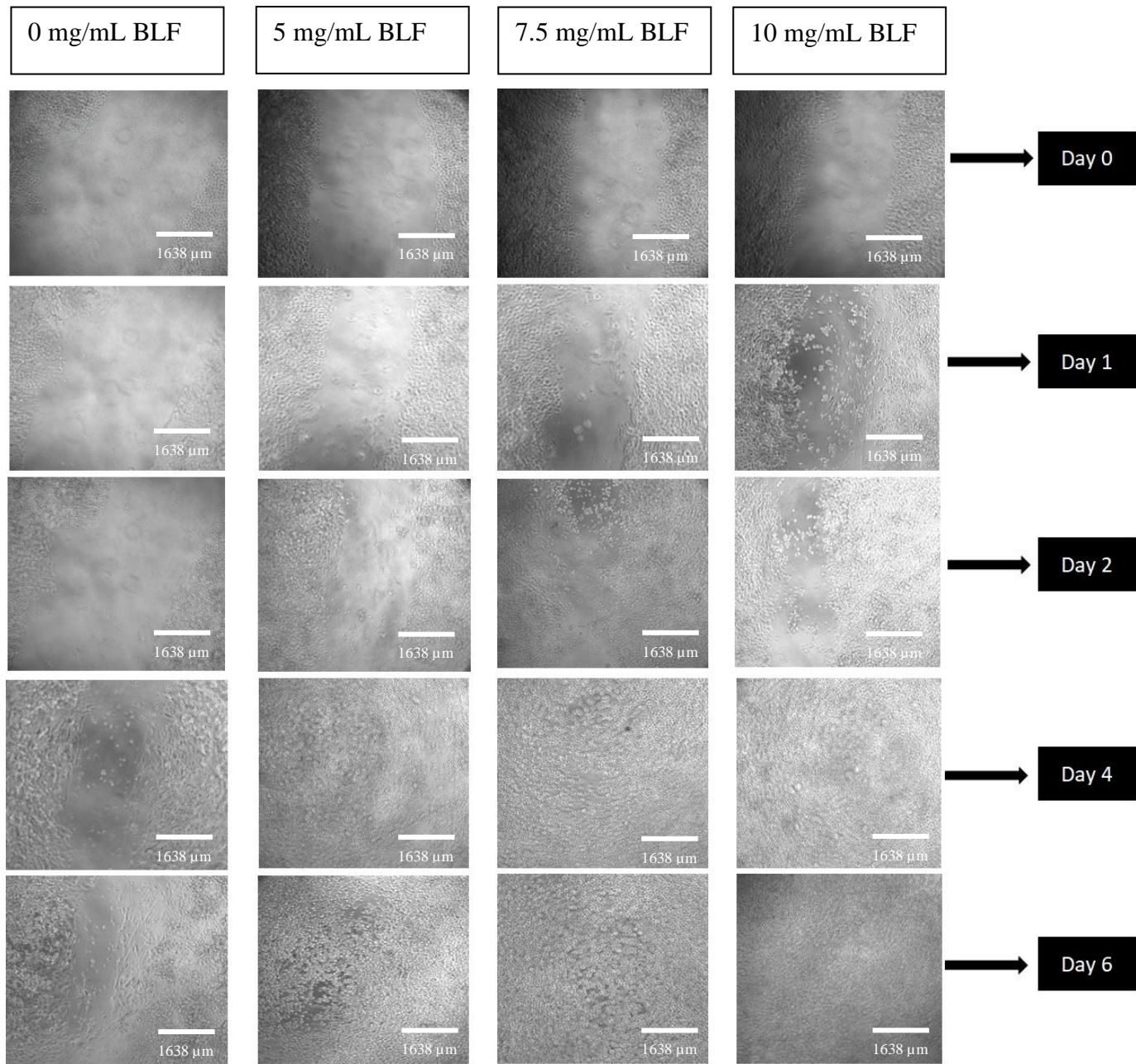


**Figure 6-2:** Images of wound closure of scratch induced HCEC wounds in response to treatment with BLF (0, 5, 7.5, 10 mg/mL) with Day 0 showing the original wound size (n=4)

#### **6.4.2 Effect of BLF on HCEC Wound Healing of Scratch-Induced Wound Model for 4 days (96 hours)**

From the previous study following the treatment of BLF, it was observed that 91% of the wound closure was achieved by day 4 when treated with 10 mg/mL BLF and approximately 100% by day 6. These results suggest that treatment with 10 mg/mL BLF was able to achieve complete wound closure by day 4. To observe the wound healing at shorter time intervals (0, 4, 8, 24, 48, 72, 96 hours) at specific hours, the same study was repeated, but the study duration shortened to 96 hours (4 days) (n=4). As expected, the percent wound closure was similar to the results obtained in the previous experiment. With the increase in time, the wound closure significantly increased for all concentrations of BLF ( $p < 0.0001$ ). Figure 6-3 shows the percent wound closure for all the concentrations of BLF. 5mg/mL BLF resulted in  $77.10 \pm 1.38\%$  wound closure compared to  $51.28 \pm 3.05\%$  for the control at 96 hours (Figure 6-3). 7.5 mg/mL BLF resulted in  $88.96 \pm 1.38\%$  wound closure as compared to  $51.28 \pm 3.05\%$  in the control at 96 hours (Figure 6-3). 10 mg/mL BLF resulted in  $95.76 \pm 1.29\%$  wound closure at 96 hours (Figure 6-3). The percent wound closure following treatment with 10 mg/mL BLF was significantly higher ( $p < 0.001$ ) than the other treatments of BLF at 96 hours. Figure 6-4 shows images of the scratched wound closure in response to BLF treatment (0, 5, 7.5, and 10 mg/mL).



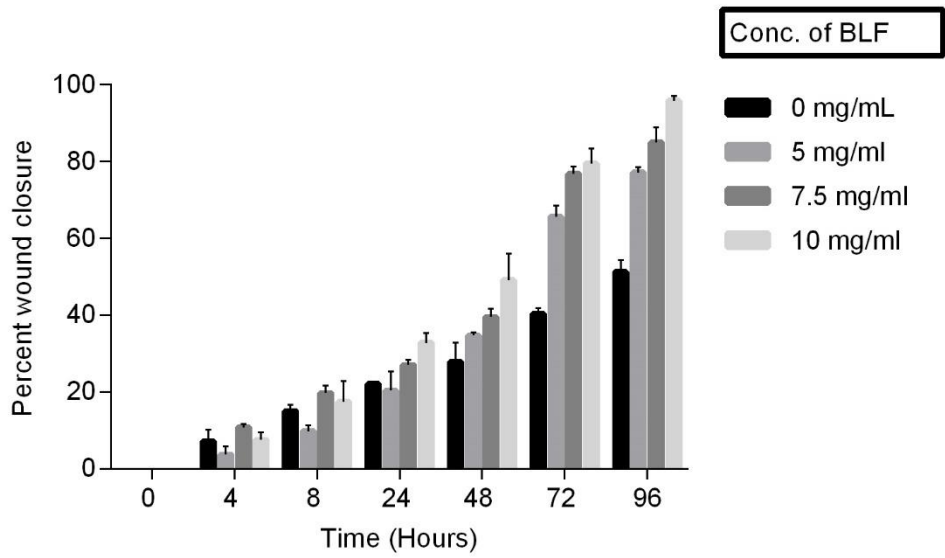


**Figure 6-3:** Percent closure of scratch induced HCEC wounds in response to treatment with BLF (0, 5, 7.5, 10 mg/mL) (n=4)

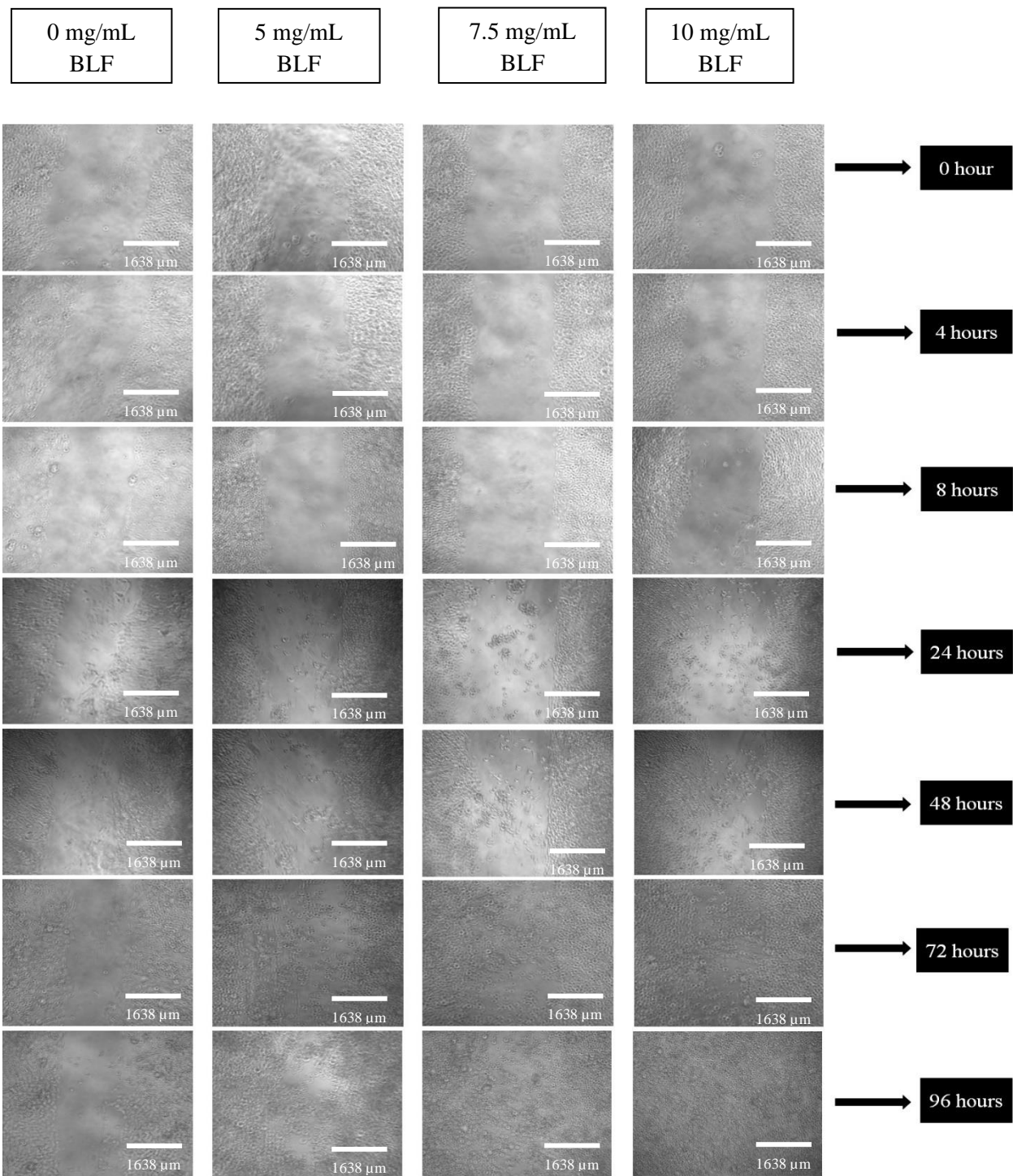


**Figure 6-4:** Images of wound closure of scratch induced HCEC wounds in response to treatment with BLF (0, 5, 7.5, 10 mg/mL) with Day 0 showing the original wound size (n=4)

## 6.5 Discussion

The preservation of a transparent, functional cornea depends on the integrity of the corneal epithelium.<sup>23</sup> Corneal injury has several problems that prevent the cornea from healing, causing scarring, persistent inflammation, and repeated erosions.<sup>455</sup> In this study, BLF was found to promote the healing of HCEC cells following an in vitro scratch-induced wound. Treatment with 10 mg/mL BLF promoted healing in the scratch induced corneal epithelial wound (95% wound closure) within four days (Figures 6-1 and 6-3).

The migration and proliferation of epithelial cells characterize the stages of corneal epithelial wound healing.<sup>456,457</sup> The wound healing process can be broken down into the latent and closure phases. In the latent phase, the cells undergo cellular and subcellular changes to remove debris from the wounded area and prepare for the closure phase.<sup>457-459</sup> The closure phase involves the migration and adhesion of the cells into the deprived area.<sup>460</sup> To cover the wound, there is a rapid migration of adherent basal cells, followed by the differentiation, proliferation, and stratification of limbal stem cells to reinstate the original multi-layered epithelial structure.<sup>290</sup> Lamellipodial extensions, cell-to-cell junctional proteins, and actin microfilament cables exaggerated in the cells at the forefront of the wound are all used to drive migration mechanically. After migration, the cells proliferate over many days to cover the wounded area completely.<sup>457,461</sup>

Each 2D wound healing assay's fundamental premise is the purposeful destruction of a confluent cell monolayer, leaving a cell-free area that cells can use to bridge and repair. As a result, the majority of 2D wound healing assays consist of three fundamental steps: cell injury (wounding), observation of the healing process and data acquisition (using, for example, a microscope), and lastly, data evaluation.<sup>462</sup> In a scratch wound healing assay, a confluent epithelium is scratched to physically remove a "strip of cells" from the monolayer using a tool like a pipette tip or a razor blade. The remaining cells' development during the "healing" of this "wound" is then monitored under a microscope for periods of time varying from a few hours to a few days, and the analysis of the cells' development offers crucial clues about the cells' motile phenotype.<sup>463</sup> There are two primary wound healing processes.<sup>464</sup> The first

type, referred to as "purse-string" closure, happens when comparatively small wounds are closed off by a pluricellular continuous actin belt. The contraction of this band via myosin motors then induces healing.<sup>465,466</sup> The second healing process, which is more pertinent to this piece, is driven by the border cells' acquired motility, which allows them to spread out and crawl collectively on the new surface while preserving the epithelium's integrity.<sup>467</sup> Actually, these two processes can coexist in the same wound and are not mutually exclusive.<sup>468</sup> It is unclear what causes this learned motility to occur when crawling is involved. As a consequence of the brutal tearing off of the adhesive junctions they keep with their neighbors, these border cells may in fact become partially permeable. These cells may be induced to migrate if there is an abrupt inflow of extracellular medium. Of course, it's also conceivable that a free edge could cause a motile reaction on its own.<sup>463</sup> Numerous studies have made this assumption, but only a very small number of investigations involving corneal epithelia<sup>469</sup> or endothelial cells have provided evidence to support it.<sup>470</sup>

Growth factors and cytokines are crucial for the healing of corneal wounds. Some growth factors that promote corneal wound healing are epidermal growth factor (EGF),<sup>471</sup> keratinocyte growth factor,<sup>472</sup> and platelet-derived growth factor (PDGF).<sup>473</sup> A series of epithelial wound-healing events can start when interleukin-1 (IL-1) and IL-6 levels are elevated in injured corneas. In vivo studies have demonstrated that IL-6 encourages corneal epithelial cell migration and wound healing.<sup>474, 475</sup> For treating corneal epithelial lesions, numerous exogenous growth factors, cytokines, and matrix proteins have been employed.<sup>476</sup>

Lactoferrin has anti-inflammatory<sup>450</sup> and antibacterial properties.<sup>219, 422</sup> A C-lobe and an N-lobe are parts of lactoferrin. It has been demonstrated that the bovine glycoprotein as a whole molecule can speed corneal epithelial wound healing in vitro, even though only the C-lobe is the active group in corneal wound healing.<sup>213, 218</sup> It has been reported that the effect of lactoferrin on cell migration depends on the cell type. In vitro studies have shown that lactoferrin inhibits the migration of gastrointestinal<sup>477</sup> and epidermal Langerhans cells,<sup>478</sup> whereas it promotes the migration of fibroblasts in a wound healing assay.<sup>479</sup> In corneal epithelial wound healing, BLF improved wound healing by reducing inflammation.<sup>213</sup>

Lactoferrin influences cytokine expression such as Interleukin-6 (IL-6) and platelet-derived growth factor (PDGF).<sup>480, 481</sup> The modulation of IL-6 by lactoferrin depends on the cell and injury type. It has been found that lactoferrin increases the production of IL-6 in peritoneal and alveolar cells obtained from cyclophosphamide mice.<sup>482</sup> In comparison, it decreased serum IL-6 in vivo during endotoxemia with complex temporal regulation.<sup>483</sup> IL-6 acts as a regulator of epithelial cell growth and cellular adhesion<sup>484</sup> and is reported to be involved in corneal wound healing.<sup>474, 475</sup> IL-6 helps facilitate wound closure of wounded rabbit corneas thorough upregulation of integrins.<sup>474, 475</sup> A study reported that following BLF treatment of corneal wounds induced by alkali exposure, there was a significant increase in the production of IL-6 and PDGF.<sup>218</sup> PDGF has an essential role in promoting corneal wound healing.<sup>473, 485</sup> The increased percent wound closure correlated with the increase in IL-6 and PDGF.<sup>218</sup> However, IL-6 and PGDF alone do not induce cell migration in the wounded corneal cells. Instead, IL-6 and PDGF enhance fibronectin's effect, which significantly increases corneal epithelial cell migration in wounded cells.<sup>218, 485</sup> It has been reported that fibronectin expression happens in response to initial wounding.<sup>486, 487</sup> Fibronectin expression increases after injuries such as mechanical epithelial debridement,<sup>488</sup> alkali burns<sup>218</sup> and keratectomy.<sup>489</sup> An increase in wound closure of wounded corneal epithelial cells following BLF treatment can presumably be attributed to the synergistic activity of IL-6 and PDGF with fibronectin.

There are very few published studies examining the effect of BLF on scratch-induced corneal epithelial wounds.<sup>355</sup> Our results showed that BLF promotes corneal epithelial wound closure (Figures 6-1 and 6-3). Consistent with the studies done on BLF promoting corneal epithelial wound healing in alkali induced injury,<sup>213, 218</sup> our results show that even in scratch-induced wounding, BLF was able to promote wound closure by more than 1.5 times as compared to the control. BLF at all three concentrations (5, 7.5, and 10 mg/mL) showed a significant increase in corneal wound healing closure as compared to a control ( $p < 0.001$ ). In the 4-day study (96 hours) (Figure 6-2), the percent wound closure increased with BLF concentrations. The findings reported that BLF at 10 mg/mL was able to induce complete wound closure in four days, and 7.5 mg/mL completely closed the wound in six days, suggesting that BLF might be an excellent therapeutic option for corneal abnormalities brought on by mechanical injury.

In conclusion, a concentration of 7.5 mg/mL or 10 mg/mL BLF would be an appropriate choice of a therapeutic for addition to 30% w/v GelMA+. The wound closure for these two concentrations within 7 days is complementary with the concept of using the enzyme responsive bandage contact lenses for a week. The 30% w/v GelMA+ is degraded completely by 6 days in 300  $\mu$ g/mL, thereby releasing the matrix bound BLF, which promotes corneal epithelial wound healing.

## Chapter 7: Conclusions and Recommendations

### 7.1 Conclusions:

This thesis investigated the novel gelatin methacrylate (GelMA+), an enzyme responsive therapeutic releasing material developed for a potential bandage contact lens (BCL) material to treat recurrent corneal erosion (RCE) syndrome. No previous studies have reported yet of using an enzyme responsive BCL for RCE treatment or corneal injury treatment. BCLs are usually worn for 2-3 months<sup>18</sup> which is a lengthy duration treatment and can be patient incompliant. The concept for this project was to use the MMP responsive GelMA+ hydrogel loaded with a potential therapeutic bovine lactoferrin for a period of 5 days or a week. The efficacy of this treatment approach depending on the efficacy of bovine lactoferrin in wound closure and catalytic activity of the MMPs (present at the wound site) in degrading the hydrogel and aid in therapeutic release. The first aim of the thesis was to prepare two different formulations of GelMA+ and characterize both to determine the appropriate formulation for further studying the release of bovine lactoferrin (BLF). The results demonstrated that by tuning the GelMA+ concentration, desired porosity and tensile strength can be achieved. Increasing the GelMA+ concentration resulted in a reduction in the pore size. The 30% w/v GelMA+ showed higher tensile strength than 20% w/v GelMA+ gels, and this higher mechanical strength would enable the 30% gels to better withstand the shear force generated from blinking. One of the important experiments in chapter 3 was to determine the degradation profile of both GelMA+ formulations in varying matrix metalloproteinase (MMPs) enzymes. As mentioned in the introduction and chapter 1, there is an upregulation of MMPs during wounding.<sup>262,351</sup> The concept for the enzyme degradable and therapeutic releasing bandage contact lens was to utilize the highly upregulated MMPs present at the wound site to degrade the GelMA+ and release the matrix-bound wound healing agent on the surface of the corneal epithelium for the treatment of RCE. Several studies have mentioned the presence of MMP-8 and MMP-9 during corneal wounding.<sup>351,357,411,412,490</sup> The degradation was studied in MMP-9, MMP-8, and a combination of both MMP-8 + MMP-9. All three enzyme variations showed similar degradation profiles. The degradation of the gels was dependent on the concentration of MMPs. However, a large amount of MMPs (more than the physiologically relevant amount which is below 400 ng/mL<sup>434</sup>) was

needed to achieve complete degradation of the gels. It was noted that 20% gels completely degraded in two days in 300  $\mu\text{g/mL}$  MMP-9, whereas 30% gels took almost six days to achieve the same.

Chapter 4 focused on assessing the cytotoxicity of both formulations of GelMA+. The growth of immortalized human corneal epithelial cell (HCEC) on 30% w/v GelMA+ was greater than 20% w/v GelMA+. Higher concentration of GelMA+ is also associated with increased stiffness, which influence the proliferation of HCECs in the presence of GelMA+ substrate.<sup>384, 389, 390</sup> Most of the studies have reported the use of GelMA as a scaffold for corneal implant<sup>491</sup> or equivalent of corneal stroma<sup>492</sup> or cornea regeneration.<sup>493</sup> However, no studies have reported yet the influence of GelMA stiffness on a 2D monolayer of human corneal epithelial cells. In this chapter, it was observed that with increase in tensile strength and Young's modulus of the GelMA+ substrate, cell proliferation increased. An alamarBlue assay supported that HCECs cultured with 30% w/v GelMA+ showed more viability as compared to the 20% w/v. With increasing time, the percentage of viable cells in the presence of the hydrogel substrates increased for 30% GelMA+ formulation, demonstrating cell growth and proliferation with time. This indicates that 30% GelMA+ provided a favourable environment for the cells to thrive. The live/dead assay suggested that 30% GelMA+ formulation is non cytotoxic, and can sustain cell growth for a week. The results indicated that the immortalized HCECs could proliferate in the presence of 30% w/v GelMA+ for five days, and thus 30% w/v is more favourable for the HCECs.

A high molecular weight compound was selected because of the porous nature of GelMA+ gels. Because of the porous nature of GelMA+, there was a high probability of the low molecular weight drug to diffuse out in the release media even before the catalytic activity of MMP-9 happens and degrade the hydrogel. Since the thesis focused on the enzyme responsivity of GelMA+ and the release of therapeutic should be enzyme and time dependent, a high molecular weight drug was chosen. Bovine lactoferrin (BLF) (~80 kDa) was the choice of therapeutic for the studying the release profile in the presence of MMP-9. At first, a model compound FITC-dextran (70 kDa) was studied to determine the release pattern from three different formulations of GelMA+ (10%, 20% and 30% w/v) at room temperature in the presence of varying concentrations of MMP-9. At low enzyme concentrations, there was no difference in the FITC-Dextran release, indicating that the release of FITC-dextran was mainly



due to passive diffusion at room temperature. The cost-effectiveness and simplicity of the 70 kDa FITC-dextran model molecule led to its selection as the model molecule to determine drug release rate. Regardless of the quenching, FITC-dextran due to UV radiation, the release pattern proved to be predictable for the BLF release profile at room temperature. At 300  $\mu\text{g/mL}$  of MMP-9, there was significant difference in the release of FITC-dextran over 24 hours at room temperature. The release profile at room temperature was a combination of passive diffusion and release due to enzyme degradation. This served as a proof of concept that there was more FITC-dextran release at high MMP-9 (300  $\mu\text{g/mL}$ ) concentration with time. However, at a higher temperature (37 °C), BLF was released linearly with increasing time and MMP-9 concentrations. These results suggested that the controlled release from the GelMA+ is temperature dependent, as the enzyme (MMP-9) needs an elevated temperature to become catalytically activated so that it can degrade the GelMA+ and release BLF from the hydrogel matrix. BLF release is dependent on both diffusion and enzyme concentration, but with a higher impact from the latter. Thus, it is possible to control the release of the drug from the GelMA+ by adjusting the polymer and enzyme concentration. Depending on the enzymes available at the wounded site, the GelMA+ gels can be formulated in a similar fashion so that it degrades completely in-situ, releasing the therapeutic or drug to assist in wound healing.

BLF was shown to aid in corneal epithelial wound healing following scratch induced wound assay. No studies have previously shown the influence of BLF on scratch induced wound in vitro. The idea or concept for this project was to develop an enzyme responsive therapeutic loaded BCL that can aid corneal wound healing within a week. Thus, it was important to determine the optimal concentration of BLF which can achieve wound closure within a week. Here, three different concentrations (5, 7.5, 10 mg/mL) of BLF were tested on a scratch-induced corneal wound model. Both 7.5 mg/mL and 10 mg/mL of BLF achieved complete wound closure within a week. Based on the previous studies on BLF promoting corneal wound healing,<sup>213, 218</sup> it can be speculated that BLF promotes epithelial wound healing by reducing inflammatory responses following a scratch wound. BLF can be a potential therapeutic of choice for future studies for the treatment of RCE.

The main advantage of this novel approach of using enzyme degradable biomaterial as a BCL is that it does not need to be removed while it degrades in-situ. It can be used for sustained and controlled drug delivery to deliver drug to the site of action in the body.<sup>439, 440</sup> As observed from the lactoferrin release profile, the release of a therapeutic agent is directly proportional to the presence of MMP-9. This implies that the drug release will respond to the wound's severity. Large wounds will have higher MMP levels<sup>411, 441</sup> and this in turn will degrade the GelMA+ faster, leading to a higher release of any incorporated therapeutic agent.

There are several **limitations** for this project:

- i. The first and important limitation was the use of high concentrations of MMP-9 and MMP-8 for the GelMA+ degradation study and high concentration of MMP-9 for the BLF release study from GelMA+ matrix. The enzyme concentration used here was in the microgram range as opposed to the physiologically relevant MMP-9 concentration (mentioned in section 5.5).
- ii. Another important limitation was the thickness of the disc shaped GelMA+ gels. The thickness of the gels used in this project were ~ 0.65 mm. However, the thickness of the marketed contact lenses are less than 0.2 mm. The thickness of the gels also plays a role in the degradation of the polymer. Increasing thickness will slow down the GelMA+ degradation and will require more enzyme to release the matrix bound therapeutic. Thus, it will be interesting to tune the thickness of the gels and observe if enzyme concentration at the nanogram range can degrade GelMA+ gels.
- iii. Another limitation of the study was the optical transmittance of the BLF loaded 30% w/v GelMA+ gels. The optical transmittance of the gels was less than 90% which is not ideal. Hence, it is important to tune with the therapeutic loaded gels so that the optical transmittance in the visible wavelength range is above 90% for optical clarity.

## **7.2 Recommendations:**

Based on the research work performed, recommendations for future work benefitting the field of therapeutic releasing enzyme responsive contact lenses for the treatment of corneal wounds are presented in the following section. Along with the potential improvements to the current work, the constraints of the current work will be considered.

### **7.2.1 Studying the effect of lipids and protein deposition on GelMA+ lens**

Previous studies have mentioned the deposition of proteins and lipids on contact lenses.<sup>494, 495</sup> A study found that drug release from contact lenses slowed down in the presence of artificial tear solution (ATS) compared to phosphate buffered saline (PBS).<sup>496</sup> Here, the release of both the model compound and BLF was tested in PBS. It would be interesting to test the controlled release kinetics from GelMA+ lenses in ATS, as this would mimic the in vivo environment containing tear film lipids and proteins. This will determine if tear film components may impact the degradation of the material as it becomes covered by tear film deposits, potentially hindering the enzymes from encountering the GelMA+. Deposits on the lens surface may also affect the drug release profile.

### **7.2.2 Degradation of GelMA+ gels in a physiologically relevant MMP-9 concentration**

MMP-9 levels among healthy patients was found to be  $8.39 \pm 4.70$  ng/mL, while patients suffering from severe dry eye showed a very high MMP-9 activity of  $381.24 \pm 142.83$  ng/mL.<sup>434</sup> In another study, the presence of pro MMP-9 in the tears of healthy patients was found to be around  $20.32 \pm 5.21$  ng/mL. However, patients suffering from conjunctivochalasis reported pro MMP-9 (inactive zymogen of inactive enzyme precursor of MMP-9) concentrations around  $223.4 \pm 74.53$  ng/mL.<sup>412</sup> Thus, the concentration of MMPs in the human tear fluid is typically in the nanogram range. For this study, micrograms of MMP-9 were used to achieve complete degradation of both formulations of GelMA+.

To enable the enzyme responsive biomaterial, degrade in-situ, future work should focus on preparing a thin and mechanically strong GelMA+ lens (withstanding the blinking friction). This lens should be capable of undergoing similar degradation in physiological concentrations of MMPs to match the human ocular conditions.

### **7.2.3 Incorporation of GelMA+ into the commercial contact lenses**

The main disadvantage of GelMA+ bandage contact lenses is that it could cause vision problems as it degrades. One alternative is to incorporate this material as a contact lens skirt on the commercial bandage contact lenses. Another possible future study could incorporate the drug loaded GelMA+ on the edges of commercial lenses, leaving the lens's center blank so that vision is not affected.

### **7.2.4 Incorporation of GelMA+ as lid implant**

To avoid any vision-related issues due to GelMA+, it can also be fabricated as an ocular drug-loaded implant placed at the lower eyelid. Ocusert<sup>®</sup> was one of the first commercialized implants for sustained drug delivery to treat glaucoma.<sup>497, 498</sup> The implant released the drug pilocarpine for a week at zero-order rate. The implant was inserted by the patient into the inferior conjunctival fornix.<sup>498</sup> Later, another implant was commercialized under the name Lacrisert<sup>®</sup> for dry eye treatment. The Lacrisert rod is inserted into the lower conjunctival sac using an applicator. The polymer disintegrates as it absorbs water and gels. Lacrisert thickens and stabilises the precorneal tear film to extend the duration before tears break up in individuals with moderate to severe dry eye.<sup>498, 499</sup> However, both products were unsuccessful due to patient compliance.<sup>498, 499</sup> Drug-loaded GelMA+ can be used in a similar pattern to treat corneal injury. With time, the GelMA+ would slowly degrade in-situ in the lower eyelid to provide a sustained release of the therapeutic. The released therapeutic then spreads over the injured cornea with the help of tear fluids and aid in wound healing.

### **7.2.5 Testing the enzyme responsive drug delivery system in vivo**

A vital concept related to this project is to test the behaviour of the therapeutic releasing enzyme responsive hydrogel in an in vivo setting. It is recommended to study the degradation profile of GelMA+ gels in situ. As mentioned previously, one of the main concerns with the enzyme degradable polymer is the hindrance to vision. It will be interesting to observe what happens to the degraded GelMA+ in tears and how it affects the vision as the degradation proceeds. It will also be interesting to note the controlled release profile of therapeutics and how long it takes to heal the corneal wound in vivo.

The project successfully put forth GelMA+, an improved version of GelMA (in terms of physical properties) and was evaluated as a potential enzyme-triggered drug releasing platform for the treatment of RCE. More work, however, is required to tune these gels to degrade faster at lower, and physiologically relevant, concentrations of MMP-9. Nevertheless, the studies completed in this thesis demonstrated the GelMA+ gels in this study show promise as potential biomaterials that could be used as a hydrogel polymer for a therapeutic releasing bandage contact lens for corneal wound healing.

## References

1. Miller DD, Hasan SA, Simmons NL, Stewart MW. Recurrent Corneal Erosion: A Comprehensive Review. *Clinical Ophthalmology (Auckland, NZ)* 2019;13:325.
2. Whitcher JP, Srinivasan M, Upadhyay MP. Prevention of Corneal Ulceration in the Developing World. *International Ophthalmology Clinics* 2002;42:71-7.
3. Whitcher JP, Srinivasan M, Upadhyay MP. Corneal Blindness: A Global Perspective. *Bulletin of the world health organization* 2001;79:214-21.
4. Calder L, Balasubramanian S, Stiell I. Lack of Consensus on Corneal Abrasion Management: Results of a National Survey. *Canadian Journal of Emergency Medicine* 2004;6:402-7.
5. Hykin P, Foss A, Pavesio C, Dart J. The Natural History and Management of Recurrent Corneal Erosion: A Prospective Randomised Trial. *Eye* 1994;8:35-40.
6. Ramamurthi S, Rahman M, Dutton G, Ramaesh K. Pathogenesis, Clinical Features and Management of Recurrent Corneal Erosions. *Eye* 2006;20:635-44.
7. Das S, Seitz B. Recurrent Corneal Erosion Syndrome. *Survey of ophthalmology* 2008;53:3-15.
8. Hulbert M. Efficacy of Eyepad in Corneal Healing after Corneal Foreign Body Removal. *The Lancet* 1991;337:643.
9. Kirkpatrick J, Hoh H, Cook S. No Eye Pad for Corneal Abrasion. *Eye* 1993;7:468-71.
10. Patterson J, Fetzer D, Krall J, et al. Eye Patch Treatment for the Pain of Corneal Abrasion. *Southern medical journal* 1996;89:227-9.
11. Kaiser PK, Group CAPS. A Comparison of Pressure Patching Versus No Patching for Corneal Abrasions Due to Trauma or Foreign Body Removal. *Ophthalmology* 1995;102:1936-42.
12. Arbour JD, Brunette I, Boisjoly HM, et al. Should We Patch Corneal Erosions? *Archives of ophthalmology* 1997;115:313-7.
13. King J, Brison R. Do Topical Antibiotics Help Corneal Epithelial Trauma? *Canadian Family Physician* 1993;39:2349.
14. Watson S, Lee H. Interventions for Recurrent Corneal Erosion: A Cochrane Systematic Review. *Eye* 2013;27:1330-1.
15. Arora R, Jain S, Monga S, et al. Efficacy of Continuous Wear Purevision Contact Lenses for Therapeutic Use. *Contact Lens and Anterior Eye* 2004;27:39-43.
16. Blackmore SJ. The Use of Contact Lenses in the Treatment of Persistent Epithelial Defects. *Contact Lens and Anterior Eye* 2010;33:239-44.
17. Reidy JJ, Paulus MP, Gona S. Recurrent Erosions of the Cornea: Epidemiology and Treatment. *Cornea* 2000;19:767-71.
18. Fraunfelder FW, Cabezas M. Treatment of Recurrent Corneal Erosion by Extended-Wear Bandage Contact Lens. *Cornea* 2011;30:164-6.
19. NIH NEI. 2022. Available at: <https://www.nei.nih.gov/learn-about-eye-health/healthy-vision/how-eyes-work>. Accessed: last updated May 2022.
20. Kolb H. *Gross Anatomy of the Eye*. 2011.
21. Bower K, Weichel ED, Kim T. Overview of Refractive Surgery. *American family physician* 2001;64:1183.

22. Rüfer F, Schröder A, Erb C. White-to-White Corneal Diameter: Normal Values in Healthy Humans Obtained with the Orbscan II Topography System. *Cornea* 2005;24:259-61.
23. DelMonte DW, Kim T. Anatomy and Physiology of the Cornea. *Journal of Cataract & Refractive Surgery* 2011;37:588-98.
24. Rowsey TG, Karamichos D. The Role of Lipids in Corneal Diseases and Dystrophies: A Systematic Review. *Clinical and Translational Medicine* 2017;6:30.
25. Farjo A, McDermott M, Soong HK. Corneal Anatomy, Physiology, and Wound Healing. *Ophthalmology* 2009;44:203-8.
26. Sridhar MS. Anatomy of Cornea and Ocular Surface. *Indian journal of ophthalmology* 2018;66:190.
27. Lee TN. The Ins and Outs of Corneal Wound Healing: Learn the Science and Key Clinical Points of Corneal Wound Healing and Adjunct Modalities Such as Amniotic Membranes. *Review of Optometry* 2016;153:44-51.
28. Cameron JD. Corneal Reaction to Injury. *Cornea* 2005;115-33.
29. Eghrari AO, Riazuddin SA, Gottsch JD. Overview of the Cornea: Structure, Function, and Development. *Progress in molecular biology and translational science* 2015;134:7-23.
30. Torricelli AA, Singh V, Santhiago MR, Wilson SE. The Corneal Epithelial Basement Membrane: Structure, Function, and Disease. *Investigative ophthalmology & visual science* 2013;54:6390-400.
31. Mantelli F, Mauris J, Argüeso P. The Ocular Surface Epithelial Barrier and Other Mechanisms of Mucosal Protection: From Allergy to Infectious Diseases. *Current opinion in allergy and clinical immunology* 2013;13.
32. Xu K, Kam KW, Young AL, Jhanji V. Recurrent Corneal Erosion Syndrome. *The Asia-Pacific Journal of Ophthalmology* 2012;1:349-54.
33. Hansen E. Om Den Intermitterende Keratitis Vesicularis Neuralgica Af Traumatisk Opindelse. *Hospitalis-Tidende* 1872;51:201-3.
34. Hadassah J, Bhuvaneshwari N, Rao U, Sehgal P. Evaluation of Succinylated Collagen Bandage Lenses in Corneal Healing by the Expression of Matrix Metalloproteinases (Mmp-2 and Mmp-9) in Tear Fluid. *Ophthalmic Research* 2009;42:64-72.
35. McGrath LA, Lee GA. Techniques, Indications and Complications of Corneal Debridement. *Survey of Ophthalmology* 2014;59:47-63.
36. Hersh PS, Rice BA, Baer JC, et al. Topical Nonsteroidal Agents and Corneal Wound Healing. *Archives of ophthalmology* 1990;108:577-83.
37. Jacobs DS, Trobe J, Bachur R, Wiley J. Corneal Abrasions and Corneal Foreign Bodies: Management. In: *UpToDate*; 2017.
38. Dursun D, Kim MC, Solomon A, Pflugfelder SC. Treatment of Recalcitrant Recurrent Corneal Erosions with Inhibitors of Matrix Metalloproteinase-9, Doxycycline and Corticosteroids. *American journal of ophthalmology* 2001;132:8-13.
39. Kim H-S, Luo L, Pflugfelder SC, Li D-Q. Doxycycline Inhibits Tgf-B1–Induced Mmp-9 Via Smad and Mapk Pathways in Human Corneal Epithelial Cells. *Investigative ophthalmology & visual science* 2005;46:840-8.
40. Laibson PR. Recurrent Corneal Erosions and Epithelial Basement Membrane Dystrophy. *Eye & contact lens* 2010;36:315-7.

41. Wipperman JL, Dorsch JN. Evaluation and Management of Corneal Abrasions. *American family physician* 2013;87:114-20.
42. Wong VW, Chi SC, Lam DS. Diamond Burr Polishing for Recurrent Corneal Erosions: Results from a Prospective Randomized Controlled Trial. *Cornea* 2009;28:152-6.
43. Weiner BM. Therapeutic Bandage Lenses. *Anterior Segment Complications of Contact Lens Wear* Churchill Livingstone, New York 1994:455-71.
44. Karlgard CC, Jones LW, Moresoli C. Survey of Bandage Lens Use in North America, October–December 2002. *Eye & contact lens* 2004;30:25-30.
45. Tighe BJ, Mann A. 2 - Contact Lens Materials. In: Phillips AJ, Speedwell L, eds. *Contact Lenses (Sixth Edition)*. London: Elsevier; 2019:18-31.
46. Alvord L, Davis T, Morgan CF, et al. Oxygen Permeability of a New Type of High Dk Soft Contact Lens Material. *Optometry and vision science: official publication of the American Academy of Optometry* 1998;75:30-6.
47. Tighe B. Silicone Hydrogel Materials-How Do They Work? *Silicone hydrogels: the rebirth of continuous wear contact lenses* 2000.
48. Segal O, Barkana Y, Hourovitz D, et al. Scleral Contact Lenses May Help Where Other Modalities Fail. *Cornea* 2003;22:308-10.
49. Sun Y-Z, Guo L, Zhang F-S. Curative Effect Assessment of Bandage Contact Lens in Neurogenic Keratitis. *International journal of ophthalmology* 2014;7:980.
50. Dua H, Gomes J, Singh A. Corneal Epithelial Wound Healing. *The British journal of ophthalmology* 1994;78:401.
51. Arffa RC, Grayson M. *Grayson's Diseases of the Cornea*: Elsevier España; 1997.
52. Holden BA, Mertz GW. Critical Oxygen Levels to Avoid Corneal Edema for Daily and Extended Wear Contact Lenses. *Investigative ophthalmology & visual science* 1984;25:1161-7.
53. Schein OD, Glynn RJ, Poggio EC, et al. The Relative Risk of Ulcerative Keratitis among Users of Daily-Wear and Extended-Wear Soft Contact Lenses. *New England Journal of Medicine* 1989;321:773-8.
54. Ahmed IIK, Breslin CW. Role of the Bandage Soft Contact Lens in the Postoperative Laser in Situ Keratomileusis Patient. *Journal of Cataract & Refractive Surgery* 2001;27:1932-6.
55. Brilakis HS, Deutsch TA. Topical Tetracaine with Bandage Soft Contact Lens Pain Control after Photorefractive Keratectomy. In: Slack Incorporated Thorofare, NJ; 2000:444-7.
56. Simşek N, Ay GM, Tugal-Tutkun I, et al. An Experimental Study on the Effect of Collagen Shields and Therapeutic Contact Lenses on Corneal Wound Healing. *Cornea* 1996;15:612-6.
57. Hugkulstone C. Use of a Bandage Contact Lens in Perforating Injuries of the Cornea. *Journal of the Royal Society of Medicine* 1992;85:322.
58. Sindt CW. The Compromised Cornea: Take Cover. *Review of Optometry* 2018;155:42-6.
59. Hassan HT. The Evaluation of Bandage Soft Contact Lenses as a Primary Treatment for Traumatic Corneal Abrasions. *Int J Clin Exp Ophthalmol* 2020;4:041-8.
60. Kymionis GD, Liakopoulos DA, Grentzelos MA, et al. Combined Topical Application of a Regenerative Agent with a Bandage Contact Lens for the Treatment of Persistent Epithelial Defects. *Cornea* 2014;33:868-72.
61. Wichterle O, Lim D. Hydrophilic Gels for Biological Use. *Nature* 1960;185:117-8.
62. Sedlacek J. Possibility of the Application of Ophthalmic Drugs with the Use of Gel Contact Lenses. *Ceskoslovenska oftalmologie* 1965;21:509-12.



63. Fonn D, Bruce AS. A Review of the Holden–Mertz Criteria for Critical Oxygen Transmission. *Eye & contact lens* 2005;31:247-51.
64. Holden BA, Sankaridurg PR, Sweeney DF, et al. Microbial Keratitis in Prospective Studies of Extended Wear with Disposable Hydrogel Contact Lenses. *Cornea* 2005;24:156-61.
65. Hsu K-H, Carbia BE, Plummer C, Chauhan A. Dual Drug Delivery from Vitamin E Loaded Contact Lenses for Glaucoma Therapy. *European Journal of Pharmaceutics and Biopharmaceutics* 2015;94:312-21.
66. Paugh JR, Stapleton F, Keay L, Ho A. Tear Exchange under Hydrogel Contact Lenses: Methodological Considerations. *Investigative ophthalmology & visual science* 2001;42:2813-20.
67. Lin MC, Soliman GN, Lim VA, et al. Scalloped Channels Enhance Tear Mixing under Hydrogel Contact Lenses. *Optometry and vision science* 2006;83:874-8.
68. Muntz A, Subbaraman LN, Sorbara L, Jones L. Tear Exchange and Contact Lenses: A Review. *Journal of optometry* 2015;8:2-11.
69. McNamara NA, Polse KA, Brand RJ, et al. Tear Mixing under a Soft Contact Lens: Effects of Lens Diameter. *American journal of ophthalmology* 1999;127:659-65.
70. Creech J, Chauhan A, Radke C. Dispersive Mixing in the Posterior Tear Film under a Soft Contact Lens. *Industrial & engineering chemistry research* 2001;40:3015-26.
71. Hehl E-M, Beck R, Luthard K, et al. Improved Penetration of Aminoglycosides and Fluoroquinolones into the Aqueous Humour of Patients by Means of Acuvue Contact Lenses. *European journal of clinical pharmacology* 1999;55:317-23.
72. Li C-C, Chauhan A. Modeling Ophthalmic Drug Delivery by Soaked Contact Lenses. *Industrial & engineering chemistry research* 2006;45:3718-34.
73. Peng C-C, Kim J, Chauhan A. Extended Delivery of Hydrophilic Drugs from Silicone-Hydrogel Contact Lenses Containing Vitamin E Diffusion Barriers. *Biomaterials* 2010;31:4032-47.
74. Peng C-C, Burke MT, Carbia BE, et al. Extended Drug Delivery by Contact Lenses for Glaucoma Therapy. *Journal of controlled release* 2012;162:152-8.
75. Phan C-M, Subbaraman LN, Jones L. In Vitro Uptake and Release of Natamycin from Conventional and Silicone Hydrogel Contact Lens Materials. *Eye & contact lens* 2013;39:162-8.
76. Hui A, Sheardown H, Jones L. Acetic and Acrylic Acid Molecular Imprinted Model Silicone Hydrogel Materials for Ciprofloxacin-Hcl Delivery. *Materials* 2012;5:85-107.
77. Kim J, Peng C-C, Chauhan A. Extended Release of Dexamethasone from Silicone-Hydrogel Contact Lenses Containing Vitamin E. *Journal of controlled release* 2010;148:110-6.
78. Phan C-M, Subbaraman L, Liu S, et al. In Vitro Uptake and Release of Natamycin Dex-B-Pla Nanoparticles from Model Contact Lens Materials. *Journal of Biomaterials Science, Polymer Edition* 2014;25:18-31.
79. Nasr FH, Khoee S, Dehghan MM, et al. Preparation and Evaluation of Contact Lenses Embedded with Polycaprolactone-Based Nanoparticles for Ocular Drug Delivery. *Biomacromolecules* 2016;17:485-95.
80. Bengani LC, Hsu K-H, Gause S, Chauhan A. Contact Lenses as a Platform for Ocular Drug Delivery. *Expert opinion on drug delivery* 2013;10:1483-96.
81. Peterson RC, Wolffsohn JS, Nick J, et al. Clinical Performance of Daily Disposable Soft Contact Lenses Using Sustained Release Technology. *Contact Lens and Anterior Eye* 2006;29:127-34.
82. Sedlavec J. Possibilities of Application of Ophthalmic Drugs with the Aid of Gel Contact Lens. *Cesk Oftalmol* 1965;21:509-14.

83. Xu W, Jiao W, Li S, et al. Bimatoprost Loaded Microemulsion Laden Contact Lens to Treat Glaucoma. *Journal of Drug Delivery Science and Technology* 2019;54:101330.
84. Li C, Chauhan A. Ocular Transport Model for Ophthalmic Delivery of Timolol through P-Hema Contact Lenses. *Journal of drug delivery science and technology* 2007;17:69-79.
85. Ruben M, Watkins R. Pilocarpine Dispensation for the Soft Hydrophilic Contact Lens. *British Journal of Ophthalmology* 1975;59:455-8.
86. Kim J, Chauhan A. Dexamethasone Transport and Ocular Delivery from Poly (Hydroxyethyl Methacrylate) Gels. *International journal of pharmaceutics* 2008;353:205-22.
87. Schultz CL, Poling TR, Mint JO. A Medical Device/Drug Delivery System for Treatment of Glaucoma. *Clinical and Experimental Optometry* 2009;92:343-8.
88. Soluri A, Hui A, Jones L. Delivery of Ketotifen Fumarate by Commercial Contact Lens Materials. *Optometry and Vision Science* 2012;89:1140-9.
89. García-Millán E, Koprivnik S, Otero-Espinar FJ. Drug Loading Optimization and Extended Drug Delivery of Corticoids from Phema Based Soft Contact Lenses Hydrogels Via Chemical and Microstructural Modifications. *International journal of pharmaceutics* 2015;487:260-9.
90. Desai AR, Maulvi FA, Desai DM, et al. Multiple Drug Delivery from the Drug-Implants-Laden Silicone Contact Lens: Addressing the Issue of Burst Drug Release. *Materials Science and Engineering: C* 2020;112:110885.
91. Maulvi FA, Singhanian SS, Desai AR, et al. Contact Lenses with Dual Drug Delivery for the Treatment of Bacterial Conjunctivitis. *International journal of pharmaceutics* 2018;548:139-50.
92. Galante R, Oliveira AS, Topete A, et al. Drug-Eluting Silicone Hydrogel for Therapeutic Contact Lenses: Impact of Sterilization Methods on the System Performance. *Colloids and Surfaces B: Biointerfaces* 2018;161:537-46.
93. Maulvi FA, Soni TG, Shah DO. Effect of Timolol Maleate Concentration on Uptake and Release from Hydrogel Contact Lenses Using Soaking Method. *J Pharm Appl Sci* 2014;1:17-23.
94. Maulvi FA, Patil RJ, Desai AR, et al. Effect of Gold Nanoparticles on Timolol Uptake and Its Release Kinetics from Contact Lenses: In Vitro and in Vivo Evaluation. *Acta biomaterialia* 2019;86:350-62.
95. Maulvi FA, Soni TG, Shah DO. Extended Release of Hyaluronic Acid from Hydrogel Contact Lenses for Dry Eye Syndrome. *Journal of Biomaterials Science, Polymer Edition* 2015;26:1035-50.
96. González-Chomón C, Concheiro A, Alvarez-Lorenzo C. Soft Contact Lenses for Controlled Ocular Delivery: 50 Years in the Making. *Therapeutic delivery* 2013;4:1141-61.
97. Jung HJ, Abou-Jaoude M, Carbia BE, et al. Glaucoma Therapy by Extended Release of Timolol from Nanoparticle Loaded Silicone-Hydrogel Contact Lenses. *Journal of controlled release* 2013;165:82-9.
98. Maulvi FA, Lakdawala DH, Shaikh AA, et al. In Vitro and in Vivo Evaluation of Novel Implantation Technology in Hydrogel Contact Lenses for Controlled Drug Delivery. *Journal of Controlled Release* 2016;226:47-56.
99. Gulsen D, Chauhan A. Ophthalmic Drug Delivery through Contact Lenses. *Investigative ophthalmology & visual science* 2004;45:2342-7.
100. Bazzaz BSF, Khameneh B, Jalili-Behabadi M-m, et al. Preparation, Characterization and Antimicrobial Study of a Hydrogel (Soft Contact Lens) Material Impregnated with Silver Nanoparticles. *Contact Lens and Anterior Eye* 2014;37:149-52.

101. Gulsen D, Li C-C, Chauhan A. Dispersion of Dmpc Liposomes in Contact Lenses for Ophthalmic Drug Delivery. *Current eye research* 2005;30:1071-80.
102. Danion A, Arsenault I, Vermette P. Antibacterial Activity of Contact Lenses Bearing Surface-Immobilized Layers of Intact Liposomes Loaded with Levofloxacin. *Journal of pharmaceutical sciences* 2007;96:2350-63.
103. Hiratani H, Alvarez-Lorenzo C. The Nature of Backbone Monomers Determines the Performance of Imprinted Soft Contact Lenses as Timolol Drug Delivery Systems. *Biomaterials* 2004;25:1105-13.
104. Varela-Garcia A, Gomez-Amoza JL, Concheiro A, Alvarez-Lorenzo C. Imprinted Contact Lenses for Ocular Administration of Antiviral Drugs. *Polymers* 2020;12:2026.
105. White CJ, Byrne ME. Molecularly Imprinted Therapeutic Contact Lenses. *Expert opinion on drug delivery* 2010;7:765-80.
106. White CJ, McBride MK, Pate KM, et al. Extended Release of High Molecular Weight Hydroxypropyl Methylcellulose from Molecularly Imprinted, Extended Wear Silicone Hydrogel Contact Lenses. *Biomaterials* 2011;32:5698-705.
107. Ali M, Byrne ME. Controlled Release of High Molecular Weight Hyaluronic Acid from Molecularly Imprinted Hydrogel Contact Lenses. *Pharmaceutical research* 2009;26:714-26.
108. White C, Tieppo A, Byrne M. Controlled Drug Release from Contact Lenses: A Comprehensive Review from 1965-Present. *Journal of drug delivery science and technology* 2011;21:369-84.
109. Schrader S, Wedel T, Moll R, Geerling G. Combination of Serum Eye Drops with Hydrogel Bandage Contact Lenses in the Treatment of Persistent Epithelial Defects. *Graefe's Archive for Clinical and Experimental Ophthalmology* 2006;244:1345-9.
110. Byrne ME, Salian V. Molecular Imprinting within Hydrogels Ii: Progress and Analysis of the Field. *International journal of pharmaceutics* 2008;364:188-212.
111. Yu Y, Macoon R, Chauhan A. Improving Wettability and Lubricity of Commercial Contact Lenses by Polymerizing a Thin Film of Dimethylacryamide. *Colloids and Surfaces A: Physicochemical and Engineering Aspects* 2019;583:123974.
112. Lee D, Cho S, Park HS, Kwon I. Ocular Drug Delivery through Phema-Hydrogel Contact Lenses Co-Loaded with Lipophilic Vitamins. *Scientific Reports* 2016;6:1-8.
113. Peng C-C, Chauhan A. Extended Cyclosporine Delivery by Silicone-Hydrogel Contact Lenses. *Journal of Controlled Release* 2011;154:267-74.
114. NAGATA M, KOJIMA M, SASAKI K. Effect of Vitamin E Eye Drops on Naphthalene-Induced Cataract in Rats. *Journal of ocular pharmacology and therapeutics* 1999;15:345-50.
115. Yañez F, Martikainen L, Braga ME, et al. Supercritical Fluid-Assisted Preparation of Imprinted Contact Lenses for Drug Delivery. *Acta biomaterialia* 2011;7:1019-30.
116. Maulvi FA, Soni TG, Shah DO. A Review on Therapeutic Contact Lenses for Ocular Drug Delivery. *Drug delivery* 2016;23:3017-26.
117. Franco P, De Marco I. Contact Lenses as Ophthalmic Drug Delivery Systems: A Review. *Polymers* 2021;13:1102.
118. Costa VP, Braga ME, Guerra JP, et al. Development of Therapeutic Contact Lenses Using a Supercritical Solvent Impregnation Method. *The Journal of Supercritical Fluids* 2010;52:306-16.
119. Yokozaki Y, Sakabe J, Ng B, Shimoyama Y. Effect of Temperature, Pressure and Depressurization Rate on Release Profile of Salicylic Acid from Contact Lenses Prepared by

- Supercritical Carbon Dioxide Impregnation. *Chemical Engineering Research and Design* 2015;100:89-94.
120. Masmoudi Y, Azzouk LB, Forzano O, et al. Supercritical Impregnation of Intraocular Lenses. *The Journal of Supercritical Fluids* 2011;60:98-105.
121. Omranipour HM, Sajadi Tabassi S, Kowsari R, et al. Brimonidine Imprinted Hydrogels and Evaluation of Their Binding and Releasing Properties as New Ocular Drug Delivery Systems. *Curr Drug Deliv* 2015;12:717-25.
122. Yan F, Liu Y, Han S, et al. Bimatoprost Imprinted Silicone Contact Lens to Treat Glaucoma. *Aaps Pharmscitech* 2020;21:1-8.
123. Gonzalez-Chomon C, Silva M, Concheiro A, Alvarez-Lorenzo C. Biomimetic Contact Lenses Eluting Olopatadine for Allergic Conjunctivitis. *Acta Biomaterialia* 2016;41:302-11.
124. Xue Y, Zhang W, Lei Y, Dang M. Novel Polyvinyl Pyrrolidone-Loaded Olopatadine HCl-Laden Doughnut Contact Lens to Treat Allergic Conjunctivitis. *Journal of pharmaceutical sciences* 2020;109:1714-24.
125. Jung HJ, Chauhan A. Temperature Sensitive Contact Lenses for Triggered Ophthalmic Drug Delivery. *Biomaterials* 2012;33:2289-300.
126. Zhu Q, Cheng H, Huo Y, Mao S. Sustained Ophthalmic Delivery of Highly Soluble Drug Using Ph-Triggered Inner Layer-Embedded Contact Lens. *International Journal of Pharmaceutics* 2018;544:100-11.
127. Wei N, Dang H, Huang C, Sheng Y. Timolol Loaded Microemulsion Laden Silicone Contact Lens to Manage Glaucoma: In Vitro and in Vivo Studies. *Journal of Dispersion Science and Technology* 2021;42:742-50.
128. Yang M, Yang Y, Lei M, et al. Experimental Studies on Soft Contact Lenses for Controlled Ocular Delivery of Pirfenidone: In Vitro and in Vivo. *Drug Delivery* 2016;23:3538-43.
129. Horne RR, Judd KE, Pitt WG. Rapid Loading and Prolonged Release of Latanoprost from a Silicone Hydrogel Contact Lens. *Journal of Drug Delivery Science and Technology* 2017;41:410-8.
130. Ross AE, Bengani LC, Tulsan R, et al. Topical Sustained Drug Delivery to the Retina with a Drug-Eluting Contact Lens. *Biomaterials* 2019;217:119285.
131. Yue K, Trujillo-de Santiago G, Alvarez MM, et al. Synthesis, Properties, and Biomedical Applications of Gelatin Methacryloyl (Gelma) Hydrogels. *Biomaterials* 2015;73:254-71.
132. Nichol JW, Koshy ST, Bae H, et al. Cell-Laden Microengineered Gelatin Methacrylate Hydrogels. *Biomaterials* 2010;31:5536-44.
133. Peppas NA, Hoffman AS. Hydrogels. In. *Biomaterials Science: Elsevier*; 2020:153-66.
134. Hoffman AS. Hydrogels for Biomedical Applications. *Advanced drug delivery reviews* 2012;64:18-23.
135. Naahidi S, Jafari M, Logan M, et al. Biocompatibility of Hydrogel-Based Scaffolds for Tissue Engineering Applications. *Biotechnology advances* 2017;35:530-44.
136. Deligkaris K, Tadele TS, Olthuis W, van den Berg A. Hydrogel-Based Devices for Biomedical Applications. *Sensors and Actuators B: Chemical* 2010;147:765-74.
137. Miri AK, Hosseinabadi HG, Cecen B, et al. Permeability Mapping of Gelatin Methacryloyl Hydrogels. *Acta biomaterialia* 2018;77:38-47.
138. Sun M, Sun X, Wang Z, et al. Synthesis and Properties of Gelatin Methacryloyl (Gelma) Hydrogels and Their Recent Applications in Load-Bearing Tissue. *Polymers* 2018;10:1290.

139. Ahadian S, Sadeghian RB, Salehi S, et al. Bioconjugated Hydrogels for Tissue Engineering and Regenerative Medicine. *Bioconjugate Chemistry* 2015;26:1984-2001.
140. Young S, Wong M, Tabata Y, Mikos AG. Gelatin as a Delivery Vehicle for the Controlled Release of Bioactive Molecules. *Journal of controlled release* 2005;109:256-74.
141. Xia W, Liu W, Cui L, et al. Tissue Engineering of Cartilage with the Use of Chitosan-Gelatin Complex Scaffolds. *Journal of Biomedical Materials Research Part B: Applied Biomaterials: An Official Journal of The Society for Biomaterials, The Japanese Society for Biomaterials, and The Australian Society for Biomaterials and the Korean Society for Biomaterials* 2004;71:373-80.
142. Ayvazyan A, Morimoto N, Kanda N, et al. Collagen-Gelatin Scaffold Impregnated with Bfgf Accelerates Palatal Wound Healing of Palatal Mucosa in Dogs. *Journal of Surgical Research* 2011;171:e247-e57.
143. Van Den Bulcke AI, Bogdanov B, De Rooze N, et al. Structural and Rheological Properties of Methacrylamide Modified Gelatin Hydrogels. *Biomacromolecules* 2000;1:31-8.
144. Ludwig PE, Huff TJ, Zuniga JM. The Potential Role of Bioengineering and Three-Dimensional Printing in Curing Global Corneal Blindness. *Journal of Tissue Engineering* 2018;9:2041731418769863.
145. Noshadi I, Hong S, Sullivan KE, et al. In Vitro and in Vivo Analysis of Visible Light Crosslinkable Gelatin Methacryloyl (Gelma) Hydrogels. *Biomaterials science* 2017;5:2093-105.
146. Modaresifar K, Hadjizadeh A, Niknejad H. Design and Fabrication of Gelma/Chitosan Nanoparticles Composite Hydrogel for Angiogenic Growth Factor Delivery. *Artificial cells, nanomedicine, and biotechnology* 2018;46:1799-808.
147. Pepelanova I, Kruppa K, Scheper T, Lavrentieva A. Gelatin-Methacryloyl (Gelma) Hydrogels with Defined Degree of Functionalization as a Versatile Toolkit for 3d Cell Culture and Extrusion Bioprinting. *Bioengineering* 2018;5:55.
148. Mertz L. What Is Biocompatibility?: A New Definition Based on the Latest Technology. *IEEE pulse* 2013;4:14-5.
149. Tse JW, Rizwan M, Rasmussen J, et al. Gelatin Methacrylate as an Enzyme-Controlled Release Vehicle of Hyaluronic Acid for the Treatment of Recurrent Corneal Erosion. *ACS Applied Bio Materials* 2020;3:6214-23.
150. Bose S, Phan CM, Yim E, Jones LW. Fabrication of a Mmp-9 Triggered Biomaterial for Corneal Wound Healing. *Investigative Ophthalmology & Visual Science* 2021;62:674-.
151. Lai T, Yu J, Tsai W. Gelatin Methacrylate/Carboxybetaine Methacrylate Hydrogels with Tunable Crosslinking for Controlled Drug Release. *Journal of Materials Chemistry B* 2016;4:2304-13.
152. Zoratto N, Di Lisa D, de Rutte J, et al. In Situ Forming Microporous Gelatin Methacryloyl Hydrogel Scaffolds from Thermostable Microgels for Tissue Engineering. *Bioengineering & Translational Medicine* 2020;5:e10180.
153. Fares MM, Sani ES, Lara RP, et al. Interpenetrating Network Gelatin Methacryloyl (Gelma) and Pectin-G-Pcl Hydrogels with Tunable Properties for Tissue Engineering. *Biomaterials science* 2018;6:2938-50.
154. Loessner D, Meinert C, Kaemmerer E, et al. Functionalization, Preparation and Use of Cell-Laden Gelatin Methacryloyl-Based Hydrogels as Modular Tissue Culture Platforms. *Nature protocols* 2016;11:727-46.
155. Shirahama H, Lee BH, Tan LP, Cho N-J. Precise Tuning of Facile One-Pot Gelatin Methacryloyl (Gelma) Synthesis. *Scientific reports* 2016;6:1-11.

156. Piao Y, You H, Xu T, et al. Biomedical Applications of Gelatin Methacryloyl Hydrogels. *Engineered Regeneration* 2021;2:47-56.
157. Sun X, Lang Q, Zhang H, et al. Electrospun Photocrosslinkable Hydrogel Fibrous Scaffolds for Rapid in Vivo Vascularized Skin Flap Regeneration. *Advanced Functional Materials* 2017;27:1604617.
158. Li X, Chen S, Li J, et al. 3d Culture of Chondrocytes in Gelatin Hydrogels with Different Stiffness. *Polymers* 2016;8:269.
159. Wang H, Zhou L, Liao J, et al. Cell-Laden Photocrosslinked Gelma–Dexma Copolymer Hydrogels with Tunable Mechanical Properties for Tissue Engineering. *Journal of Materials Science: Materials in Medicine* 2014;25:2173-83.
160. Ding H, Illsley NP, Chang RC. 3d Bioprinted Gelma Based Models for the Study of Trophoblast Cell Invasion. *Scientific Reports* 2019;9:1-13.
161. Nazir F, Ashraf I, Iqbal M, et al. 6-Deoxy-Aminocellulose Derivatives Embedded Soft Gelatin Methacryloyl (Gelma) Hydrogels for Improved Wound Healing Applications: In Vitro and in Vivo Studies. *International Journal of Biological Macromolecules* 2021;185:419-33.
162. Yang Z, Ren X, Liu Y. Multifunctional 3d Printed Porous Gelma/Xanthan Gum Based Dressing with Biofilm Control and Wound Healing Activity. *Materials Science and Engineering: C* 2021;131:112493.
163. Zhao X, Lang Q, Yildirimer L, et al. Photocrosslinkable Gelatin Hydrogel for Epidermal Tissue Engineering. *Advanced healthcare materials* 2016;5:108-18.
164. Zhou J, Yao D, Qian Z, et al. Bacteria-Responsive Intelligent Wound Dressing: Simultaneous in Situ Detection and Inhibition of Bacterial Infection for Accelerated Wound Healing. *Biomaterials* 2018;161:11-23.
165. Jahan I, George E, Saxena N, Sen S. Silver-Nanoparticle-Entrapped Soft Gelma Gels as Prospective Scaffolds for Wound Healing. *ACS Applied Bio Materials* 2019;2:1802-14.
166. Pennisi E. Tending Tender Tendons. *Science* 2002;295:1011-.
167. Yang G, Lin H, Rothrauff BB, et al. Multilayered Polycaprolactone/Gelatin Fiber-Hydrogel Composite for Tendon Tissue Engineering. *Acta biomaterialia* 2016;35:68-76.
168. Visser J, Melchels FP, Jeon JE, et al. Reinforcement of Hydrogels Using Three-Dimensionally Printed Microfibres. *Nature communications* 2015;6:1-10.
169. Rinoldi C, Costantini M, Kijeńska-Gawrońska E, et al. Tendon Tissue Engineering: Effects of Mechanical and Biochemical Stimulation on Stem Cell Alignment on Cell-Laden Hydrogel Yarns. *Advanced healthcare materials* 2019;8:1801218.
170. Kwon S, Lee SS, Sivashanmugam A, et al. Bioglass-Incorporated Methacrylated Gelatin Cryogel for Regeneration of Bone Defects. *Polymers* 2018;10:914.
171. Han L, Xu J, Lu X, et al. Biohybrid Methacrylated Gelatin/Polyacrylamide Hydrogels for Cartilage Repair. *Journal of Materials Chemistry B* 2017;5:731-41.
172. Chen J, Chin A, Almarza AJ, Taboas JM. Hydrogel to Guide Chondrogenesis Versus Osteogenesis of Mesenchymal Stem Cells for Fabrication of Cartilaginous Tissues. *Biomedical Materials* 2020;15:045006.
173. Chen YC, Lin RZ, Qi H, et al. Functional Human Vascular Network Generated in Photocrosslinkable Gelatin Methacrylate Hydrogels. *Advanced functional materials* 2012;22:2027-39.

174. Chen H, Guo L, Wicks J, et al. Quickly Promoting Angiogenesis by Using a Dfo-Loaded Photo-Crosslinked Gelatin Hydrogel for Diabetic Skin Regeneration. *Journal of Materials Chemistry B* 2016;4:3770-81.
175. Jia W, Gungor-Ozkerim PS, Zhang YS, et al. Direct 3d Bioprinting of Perfusable Vascular Constructs Using a Blend Bioink. *Biomaterials* 2016;106:58-68.
176. Coimbra P, Santos P, Alves P, et al. Coaxial Electrospun Pcl/Gelatin-Ma Fibers as Scaffolds for Vascular Tissue Engineering. *Colloids and Surfaces B: Biointerfaces* 2017;159:7-15.
177. Nuutila K, Samandari M, Endo Y, et al. In Vivo Printing of Growth Factor-Eluting Adhesive Scaffolds Improves Wound Healing. *Bioactive materials* 2022;8:296-308.
178. Parthiban SP, Rana D, Jabbari E, et al. Covalently Immobilized Vegf-Mimicking Peptide with Gelatin Methacrylate Enhances Microvascularization of Endothelial Cells. *Acta biomaterialia* 2017;51:330-40.
179. Cao Y, Cheng P, Sang S, et al. 3d Printed Pcl/Gelma Biphasic Scaffold Boosts Cartilage Regeneration Using Co-Culture of Mesenchymal Stem Cells and Chondrocytes: In Vivo Study. *Materials & Design* 2021;210:110065.
180. Ju X, Liu X, Zhang Y, et al. A Photo-Crosslinked Proteinogenic Hydrogel Enabling Self-Recruitment of Endogenous Tgf-B1 for Cartilage Regeneration. *Smart Materials in Medicine* 2022;3:85-93.
181. Daikuara LY, Yue Z, Skropeta D, Wallace GG. In Vitro Characterisation of 3d Printed Platelet Lysate-Based Bioink for Potential Application in Skin Tissue Engineering. *Acta biomaterialia* 2021;123:286-97.
182. Guan G, Lv Q, Liu S, et al. 3d-Bioprinted Peptide Coupling Patches for Wound Healing. *Materials Today Bio* 2022;13:100188.
183. Lee JS, Park HS, Jung H, et al. 3d-Printable Photocurable Bioink for Cartilage Regeneration of Tonsil-Derived Mesenchymal Stem Cells. *Additive Manufacturing* 2020;33:101136.
184. Zhang X, Huang P, Jiang G, et al. A Novel Magnesium Ion-Incorporating Dual-Crosslinked Hydrogel to Improve Bone Scaffold-Mediated Osteogenesis and Angiogenesis. *Materials Science and Engineering: C* 2021;121:111868.
185. Chen J, Huang D, Wang L, et al. 3d Bioprinted Multiscale Composite Scaffolds Based on Gelatin Methacryloyl (Gelma)/Chitosan Microspheres as a Modular Bioink for Enhancing 3d Neurite Outgrowth and Elongation. *Journal of colloid and interface science* 2020;574:162-73.
186. Ansari S, Pouraghaei Sevari S, Chen C, et al. Rgd-Modified Alginate-Gelma Hydrogel Sheet Containing Gingival Mesenchymal Stem Cells: A Unique Platform for Wound Healing and Soft Tissue Regeneration. *ACS Biomaterials Science & Engineering* 2021;7:3774-82.
187. Zhou X, Nowicki M, Sun H, et al. 3d Bioprinting-Tunable Small-Diameter Blood Vessels with Biomimetic Biphasic Cell Layers. *ACS applied materials & interfaces* 2020;12:45904-15.
188. Naderi N, Griffin M, Mosahebi A, et al. Adipose Derived Stem Cells and Platelet Rich Plasma Improve the Tissue Integration and Angiogenesis of Biodegradable Scaffolds for Soft Tissue Regeneration. *Molecular Biology Reports* 2020;47:2005-13.
189. Na K, Shin S, Lee H, et al. Effect of Solution Viscosity on Retardation of Cell Sedimentation in Dlp 3d Printing of Gelatin Methacrylate/Silk Fibroin Bioink. *Journal of Industrial and Engineering Chemistry* 2018;61:340-7.

190. Farasatkia A, Kharaziha M, Ashrafizadeh F, Salehi S. Transparent Silk/Gelatin Methacrylate (Gelma) Fibrillar Film for Corneal Regeneration. *Materials Science and Engineering: C* 2021;120:111744.
191. Lee J, Manoharan V, Cheung L, et al. Nanoparticle-Based Hybrid Scaffolds for Deciphering the Role of Multimodal Cues in Cardiac Tissue Engineering. *ACS nano* 2019;13:12525-39.
192. Ou Q, Huang K, Fu C, et al. Nanosilver-Incorporated Halloysite Nanotubes/Gelatin Methacrylate Hybrid Hydrogel with Osteoimmunomodulatory and Antibacterial Activity for Bone Regeneration. *Chemical Engineering Journal* 2020;382:123019.
193. Zhou X, Cui H, Nowicki M, et al. Three-Dimensional-Bioprinted Dopamine-Based Matrix for Promoting Neural Regeneration. *ACS applied materials & interfaces* 2018;10:8993-9001.
194. Chen P, Xia C, Mei S, et al. Intra-Articular Delivery of Sinomenium Encapsulated by Chitosan Microspheres and Photo-Crosslinked Gelma Hydrogel Ameliorates Osteoarthritis by Effectively Regulating Autophagy. *Biomaterials* 2016;81:1-13.
195. Li Y, Yan D, Fu F, et al. Composite Core-Shell Microparticles from Microfluidics for Synergistic Drug Delivery. *Science China Materials* 2017;60:543-53.
196. Luo Z, Sun W, Fang J, et al. Biodegradable Gelatin Methacryloyl Microneedles for Transdermal Drug Delivery. *Advanced healthcare materials* 2019;8:1801054.
197. Jiang D, Ge P, Wang L, et al. A Novel Electrochemical Mast Cell-Based Paper Biosensor for the Rapid Detection of Milk Allergen Casein. *Biosensors and Bioelectronics* 2019;130:299-306.
198. Topkaya SN. Gelatin Methacrylate (Gelma) Mediated Electrochemical DNA Biosensor for DNA Hybridization. *Biosensors and Bioelectronics* 2015;64:456-61.
199. Bode F, Da Silva MA, Drake AF, et al. Enzymatically Cross-Linked Tilapia Gelatin Hydrogels: Physical, Chemical, and Hybrid Networks. *Biomacromolecules* 2011;12:3741-52.
200. Bode F, Da Silva MA, Smith P, et al. Hybrid Gelation Processes in Enzymatically Gelled Gelatin: Impact on Nanostructure, Macroscopic Properties and Cellular Response. *Soft Matter* 2013;9:6986-99.
201. Rizwan M, Peh GS, Ang H-P, et al. Sequentially-Crosslinked Bioactive Hydrogels as Nano-Patterned Substrates with Customizable Stiffness and Degradation for Corneal Tissue Engineering Applications. *Biomaterials* 2017;120:139-54.
202. Vagge A, Senni C, Bernabei F, et al. Therapeutic Effects of Lactoferrin in Ocular Diseases: From Dry Eye Disease to Infections. *International Journal of Molecular Sciences* 2020;21:6668.
203. González-Chávez SA, Arévalo-Gallegos S, Rascón-Cruz Q. Lactoferrin: Structure, Function and Applications. *International journal of antimicrobial agents* 2009;33:301. e1-. e8.
204. Giansanti F, Panella G, Leboffe L, Antonini G. Lactoferrin from Milk: Nutraceutical and Pharmacological Properties. *Pharmaceuticals* 2016;9:61.
205. Legrand D, Ellass E, Carpentier M, Mazurier J. Lactoferrin. *Cellular and Molecular Life Sciences* 2005;62:2549-59.
206. Masson P, Heremans J. Lactoferrin in Milk from Different Species. *Comparative Biochemistry and Physiology* 1971:119-29.
207. Groenink J, Walgreen-Weterings E, Nazmi K, et al. Salivary Lactoferrin and Low-Mr Mucin Mg2 in Actinobacillus Actinomycetemcomitans-Associated Periodontitis. *Journal of clinical periodontology* 1999;26:269-75.
208. Nagasawa T, Kiyosawa I, Kuwahara K. Amounts of Lactoferrin in Human Colostrum and Milk. *Journal of Dairy Science* 1972;55:1651-9.



209. Kijlstra A, Jeurissen S, Koning K. Lactoferrin Levels in Normal Human Tears. *British Journal of Ophthalmology* 1983;67:199-202.
210. Teng C, Pentecost B, CHEN Y-H, et al. Lactotransferrin Gene Expression in the Mouse Uterus and Mammary Gland. *Endocrinology* 1989;124:992-9.
211. Åbrink M, Larsson E, Gobl A, Hellman L. Expression of Lactoferrin in the Kidney: Implications for Innate Immunity and Iron Metabolism. *Kidney international* 2000;57:2004-10.
212. Fillebeen C, Mitchell V, Dexter D, et al. Lactoferrin Is Synthesized by Mouse Brain Tissue and Its Expression Is Enhanced after Mptp Treatment. *Molecular brain research* 1999;72:183-94.
213. Ashby B, Garrett Q, Willcox M. Bovine Lactoferrin Structures Promoting Corneal Epithelial Wound Healing in Vitro. *Investigative ophthalmology & visual science* 2011;52:2719-26.
214. Superti F. Lactoferrin from Bovine Milk: A Protective Companion for Life. *Nutrients* 2020;12:2562.
215. Moore SA, Anderson BF, Groom CR, et al. Three-Dimensional Structure of Diferric Bovine Lactoferrin at 2.8 Å Resolution. *Journal of molecular biology* 1997;274:222-36.
216. Fujihara T, Nagano T, Endo K, et al. Lactoferrin Protects against Uv-B Irradiation-Induced Corneal Epithelial Damage in Rats. *Cornea* 2000;19:207-11.
217. Engelmayer J, Blezinger P, Varadhachary A. Talactoferrin Stimulates Wound Healing with Modulation of Inflammation. *Journal of Surgical Research* 2008;149:278-86.
218. Pattamatta U, Willcox M, Stapleton F, et al. Bovine Lactoferrin Stimulates Human Corneal Epithelial Alkali Wound Healing in Vitro. *Investigative ophthalmology & visual science* 2009;50:1636-43.
219. Takayama Y, Aoki R. Roles of Lactoferrin on Skin Wound Healing. *Biochemistry and Cell Biology* 2011;90:497-503.
220. Mulder AM, Connellan PA, Oliver CJ, et al. Bovine Lactoferrin Supplementation Supports Immune and Antioxidant Status in Healthy Human Males. *Nutrition Research* 2008;28:583-9.
221. Zhang Y, Lima CF, Rodrigues LR. Anticancer Effects of Lactoferrin: Underlying Mechanisms and Future Trends in Cancer Therapy. *Nutrition reviews* 2014;72:763-73.
222. Conneely OM. Antiinflammatory Activities of Lactoferrin. *Journal of the American College of Nutrition* 2001;20:389S-95S.
223. Fernandes KE, Carter DA. The Antifungal Activity of Lactoferrin and Its Derived Peptides: Mechanisms of Action and Synergy with Drugs against Fungal Pathogens. *Frontiers in microbiology* 2017;8:2.
224. Bruni N, Capucchio MT, Biasibetti E, et al. Antimicrobial Activity of Lactoferrin-Related Peptides and Applications in Human and Veterinary Medicine. *Molecules* 2016;21:752.
225. Takayama Y, Mizumachi K. Effects of Lactoferrin on Collagen Gel Contractile Activity and Myosin Light Chain Phosphorylation in Human Fibroblasts. *FEBS letters* 2001;508:111-6.
226. Grinnell F. Fibroblasts, Myofibroblasts, and Wound Contraction. *The Journal of cell biology* 1994;124:401-4.
227. Takayama Y, Takahashi H, Mizumachi K, Takezawa T. Low Density Lipoprotein Receptor-Related Protein (Lrp) Is Required for Lactoferrin-Enhanced Collagen Gel Contractile Activity of Human Fibroblasts. *Journal of Biological Chemistry* 2003;278:22112-8.
228. Takayama Y, Mizumachi K, Takezawa T. The Bovine Lactoferrin Region Responsible for Promoting the Collagen Gel Contractile Activity of Human Fibroblasts. *Biochemical and Biophysical Research Communications* 2002;299:813-7.

229. Pattamatta U, Willcox M, Stapleton F, Garrett Q. Bovine Lactoferrin Promotes Corneal Wound Healing and Suppresses Il-1 Expression in Alkali Wounded Mouse Cornea. *Current Eye Research* 2013;38:1110-7.
230. Rusciano D, Pezzino S, Olivieri M, et al. Age-Related Dry Eye Lactoferrin and Lactobionic Acid. *Ophthalmic Research* 2018;60:94-9.
231. Danjo Y, Lee M, Horimoto K, Hamano T. Ocular Surface Damage and Tear Lactoferrin in Dry Eye Syndrome. *Acta ophthalmologica* 1994;72:433-7.
232. Sonobe H, Ogawa Y, Yamada K, et al. A Novel and Innovative Paper-Based Analytical Device for Assessing Tear Lactoferrin of Dry Eye Patients. *The Ocular Surface* 2019;17:160-6.
233. Roda M, Corazza I, Bacchi Reggiani ML, et al. Dry Eye Disease and Tear Cytokine Levels—a Meta-Analysis. *International journal of molecular sciences* 2020;21:3111.
234. Baldwin D, Jenny E, Aisen P. The Effect of Human Serum Transferrin and Milk Lactoferrin on Hydroxyl Radical Formation from Superoxide and Hydrogen Peroxide. *Journal of Biological Chemistry* 1984;259:13391-4.
235. Flanagan J, Willcox M. Role of Lactoferrin in the Tear Film. *Biochimie* 2009;91:35-43.
236. Dogru M, Matsumoto Y, Yamamoto Y, et al. Lactoferrin in Sjögren's Syndrome. *Ophthalmology* 2007;114:2366-7. e4.
237. FUJIHARA T, NAGANO T, NAKAMURA M, SHIRASAWA E. Lactoferrin Suppresses Loss of Corneal Epithelial Integrity in a Rabbit Short-Term Dry Eye Model. *Journal of ocular pharmacology and therapeutics* 1998;14:99-107.
238. Gauvin R, Chen Y-C, Lee JW, et al. Microfabrication of Complex Porous Tissue Engineering Scaffolds Using 3d Projection Stereolithography. *Biomaterials* 2012;33:3824-34.
239. Nagase H. Matrix Metalloproteinases. Zinc metalloproteases in health and disease 1996:173-224.
240. Woessner Jr JF. Matrix Metalloproteinases and Their Inhibitors in Connective Tissue Remodeling. *The FASEB Journal* 1991;5:2145-54.
241. Jamerson EC, Elhusseiny AM, ElSheikh RH, et al. Role of Matrix Metalloproteinase 9 in Ocular Surface Disorders. *Eye & Contact Lens* 2020;46:S57-S63.
242. Shi W, Liu J, Li M, et al. Expression of Mmp, Hpse, and Fap in Stroma Promoted Corneal Neovascularization Induced by Different Etiological Factors. *Current Eye Research* 2010;35:967-77.
243. Mulholland B, Tuft S, Khaw P. Matrix Metalloproteinase Distribution During Early Corneal Wound Healing. *Eye* 2005;19:584-8.
244. Park JY, Kim BG, Kim JS, Hwang JH. Matrix Metalloproteinase 9 Point-of-Care Immunoassay Result Predicts Response to Topical Cyclosporine Treatment in Dry Eye Disease. *Translational vision science & technology* 2018;7:31-.
245. Szklarczyk A, Lapinska J, Rylski M, et al. Matrix Metalloproteinase-9 Undergoes Expression and Activation During Dendritic Remodeling in Adult Hippocampus. *Journal of neuroscience* 2002;22:920-30.
246. Dreier R, Grässel S, Fuchs S, et al. Pro-Mmp-9 Is a Specific Macrophage Product and Is Activated by Osteoarthritic Chondrocytes Via Mmp-3 or a Mt1-Mmp/Mmp-13 Cascade. *Experimental cell research* 2004;297:303-12.
247. Cheng C-Y, Hsieh H-L, Hsiao L-D, Yang C-M. Pi3-K/Akt/Jnk/Nf-Kb Is Essential for Mmp-9 Expression and Outgrowth in Human Limbal Epithelial Cells on Intact Amniotic Membrane. *Stem cell research* 2012;9:9-23.

248. Zhou HY, Shin EM, Guo LY, et al. Anti-Inflammatory Activity of 4-Methoxyhonokiol Is a Function of the Inhibition of Inos and Cox-2 Expression in Raw 264.7 Macrophages Via Nf-Kb, Jnk and P38 Mapk Inactivation. *European Journal of Pharmacology* 2008;586:340-9.
249. Moon SK, Cha BY, Kim CH. Erk1/2 Mediates Tnf-A-Induced Matrix Metalloproteinase-9 Expression in Human Vascular Smooth Muscle Cells Via the Regulation of Nf-Kb and Ap-1: Involvement of the Ras Dependent Pathway. *Journal of cellular physiology* 2004;198:417-27.
250. Tseng H-C, Lee I-T, Lin C-C, et al. Il-1 $\beta$  Promotes Corneal Epithelial Cell Migration by Increasing Mmp-9 Expression through Nf-Kb-and Ap-1-Dependent Pathways. *PLoS one* 2013;8:e57955.
251. Gordon GM, Ledee DR, Feuer WJ, Fini ME. Cytokines and Signaling Pathways Regulating Matrix Metalloproteinase-9 (Mmp-9) Expression in Corneal Epithelial Cells. *Journal of cellular physiology* 2009;221:402-11.
252. Seo MJ, Kim JM, Lee MJ, et al. The Therapeutic Effect of Da-6034 on Ocular Inflammation Via Suppression of Mmp-9 and Inflammatory Cytokines and Activation of the Mapk Signaling Pathway in an Experimental Dry Eye Model. *Current eye research* 2010;35:165-75.
253. Bargagna-Mohan P, Strissel KJ, Fini ME. Regulation of Gelatinase B Production in Corneal Cells Is Independent of Autocrine Il-1 $\alpha$ . *Investigative ophthalmology & visual science* 1999;40:784-9.
254. Kim H-S, Shang T, Chen Z, et al. Tgf-B1 Stimulates Production of Gelatinase (Mmp-9), Collagenases (Mmp-1,-13) and Stromelysins (Mmp-3,-10,-11) by Human Corneal Epithelial Cells. *Experimental eye research* 2004;79:263-74.
255. Tao Y, Bazan H, Bazan NG. Platelet-Activating Factor Induces the Expression of Metalloproteinases-1 and-9, but Not-2 or-3, in the Corneal Epithelium. *Investigative ophthalmology & visual science* 1995;36:345-54.
256. Saravani R, Yari D, Saravani S, Hasanian-Langroudi F. Correlation between the Col4a3, Mmp-9, and Timp-1 Polymorphisms and Risk of Keratoconus. *Japanese journal of ophthalmology* 2017;61:218-22.
257. Ottino P, Taheri F, Bazan HE. Platelet-Activating Factor Induces the Gene Expression of Timp-1,-2, and Pai-1: Imbalance between the Gene Expression of Mmp-9 and Timp-1 and-2. *Experimental eye research* 2002;74:393-402.
258. Sobrin L, Liu Z, Monroy DC, et al. Regulation of Mmp-9 Activity in Human Tear Fluid and Corneal Epithelial Culture Supernatant. *Investigative ophthalmology & visual science* 2000;41:1703-9.
259. Kaufman HE. The Practical Detection of Mmp-9 Diagnoses Ocular Surface Disease and May Help Prevent Its Complications. *Cornea* 2013;32:211-6.
260. Petznick A, Madigan MC, Garrett Q, et al. Contributions of Ocular Surface Components to Matrix-Metalloproteinases (Mmp)-2 and Mmp-9 in Feline Tears Following Corneal Epithelial Wounding. *PLoS One* 2013;8:e71948.
261. Ye HQ, Azar DT. Expression of Gelatinases a and B, and Timps 1 and 2 During Corneal Wound Healing. *Investigative ophthalmology & visual science* 1998;39:913-21.
262. Smith V, Rishmawi H, Hussein H, Easty D. Tear Film Mmp Accumulation and Corneal Disease. *British journal of ophthalmology* 2001;85:147-53.
263. Fournié PR, Gordon GM, Dawson DG, et al. Correlations of Long-Term Matrix Metalloproteinase Localization in Human Corneas after Successful Laser-Assisted in Situ

- Keratomileusis with Minor Complications at the Flap Margin. *Archives of Ophthalmology* 2008;126:162-70.
264. Mutoh T, Nishio M, Matsumoto Y, Arai K. Correlation between the Matrix Metalloproteinase-9 Activity and Chondroitin Sulfate Concentrations in Tear Fluid after Laser in Situ Keratomileusis. *Clinical Ophthalmology (Auckland, NZ)* 2010;4:823.
265. Murakami J, Nishida T, Otori T. Coordinated Appearance of B1 Integrins and Fibronectin During Corneal Wound Healing. *The Journal of laboratory and clinical medicine* 1992;120:86-93.
266. Fini ME, Parks WC, Rinehart WB, et al. Role of Matrix Metalloproteinases in Failure to Re-Epithelialize after Corneal Injury. *The American journal of pathology* 1996;149:1287.
267. Kowluru RA, Zhong Q, Santos JM. Matrix Metalloproteinases in Diabetic Retinopathy: Potential Role of Mmp-9. *Expert opinion on investigational drugs* 2012;21:797-805.
268. Leonardi A, Brun P, Abatangelo G, et al. Tear Levels and Activity of Matrix Metalloproteinase (Mmp)-1 and Mmp-9 in Vernal Keratoconjunctivitis. *Investigative ophthalmology & visual science* 2003;44:3052-8.
269. George AK, Homme RP, Majumder A, et al. Effect of Mmp-9 Gene Knockout on Retinal Vascular Form and Function. *Physiological genomics* 2019;51:613-22.
270. Diekmann U, Zarbock R, Hendig D, et al. Elevated Circulating Levels of Matrix Metalloproteinases Mmp-2 and Mmp-9 in Pseudoxanthoma Elasticum Patients. *Journal of molecular medicine* 2009;87:965-70.
271. Pflugfelder SC, Farley W, Luo L, et al. Matrix Metalloproteinase-9 Knockout Confers Resistance to Corneal Epithelial Barrier Disruption in Experimental Dry Eye. *The American journal of pathology* 2005;166:61-71.
272. Lambert V, Wielockx B, Munaut C, et al. Mmp-2 and Mmp-9 Synergize in Promoting Choroidal Neovascularization. *The FASEB journal* 2003;17:2290-2.
273. Rouet-Benzineb P, Buhler J, Dreyfus P. Altered Balance between Matrix Gelatinases (Mmp-2 and Mmp-9) and Their Tissue Inhibitors in Human Dilated Cardiomyopathy. *Potential role of MMP-9 in myosin-heavy chain degradation*;1999:1.
274. Mori S, Pawankar R, Ozu C, et al. Expression and Roles of Mmp-2, Mmp-9, Mmp-13, Timp-1, and Timp-2 in Allergic Nasal Mucosa. *Allergy, asthma & immunology research* 2012;4:231-9.
275. Erlewyn-Lajeunesse MD, Hunt LP, Pohunek P, et al. Bronchoalveolar Lavage Mmp-9 and Timp-1 in Preschool Wheezers and Their Relationship to Persistent Wheeze. *Pediatric research* 2008;64:194-9.
276. Hiratsuka S, Nakamura K, Iwai S, et al. Mmp9 Induction by Vascular Endothelial Growth Factor Receptor-1 Is Involved in Lung-Specific Metastasis. *Cancer cell* 2002;2:289-300.
277. Bergers G, Brekken R, McMahon G, et al. Matrix Metalloproteinase-9 Triggers the Angiogenic Switch During Carcinogenesis. *Nature cell biology* 2000;2:737-44.
278. Yorioka CW, Coletta RD, Alves F, et al. Matrix Metalloproteinase-2 and-9 Activities Correlate with the Disease-Free Survival of Oral Squamous Cell Carcinoma Patients. *International journal of oncology* 2002;20:189-94.
279. Li D-D, Song J-N, Huang H, et al. The Roles of Mmp-9/Timp-1 in Cerebral Edema Following Experimental Acute Cerebral Infarction in Rats. *Neuroscience letters* 2013;550:168-72.
280. Ladwig GP, Robson MC, Liu R, et al. Ratios of Activated Matrix Metalloproteinase-9 to Tissue Inhibitor of Matrix Metalloproteinase-1 in Wound Fluids Are Inversely Correlated with Healing of Pressure Ulcers. *Wound repair and regeneration* 2002;10:26-37.

281. Tian Y-Q, Ning X-H, Yin D-Y, et al. Expression of Mmp-9 and Timp-1 in Rat Models of Pressure Ulcer and Their Significance. *Int J Clin Exp Med* 2019;12:7209-16.
282. Hansen CN, Fisher LC, Deibert RJ, et al. Elevated Mmp-9 in the Lumbar Cord Early after Thoracic Spinal Cord Injury Impedes Motor Relearning in Mice. *Journal of Neuroscience* 2013;33:13101-11.
283. Liu C-Y, Kao WW-Y. Corneal Epithelial Wound Healing. *Progress in molecular biology and translational science* 2015;134:61-71.
284. Lu L, Reinach PS, Kao WW-Y. Corneal Epithelial Wound Healing. *Experimental biology and medicine* 2001;226:653-64.
285. Ljubimov AV, Saghizadeh M. Progress in Corneal Wound Healing. *Progress in retinal and eye research* 2015;49:17-45.
286. Steele C. Corneal Wound Healing: A Review. *Optometry Today* 1999;24:28-32.
287. Clark EA, Brugge JS. Integrins and Signal Transduction Pathways: The Road Taken. *Science* 1995;268:233-9.
288. Schoenwaelder SM, Burridge K. Bidirectional Signaling between the Cytoskeleton and Integrins. *Current opinion in cell biology* 1999;11:274-86.
289. Blanco-Mezquita JT, Hutcheon AE, Stepp MA, Zieske JD. Av $\beta$ 6 Integrin Promotes Corneal Wound Healing. *Investigative ophthalmology & visual science* 2011;52:8505-13.
290. Ljubimov AV, Saghizadeh M. Progress in Corneal Wound Healing. *Prog Retin Eye Res* 2015;49:17-45.
291. Kimura K, Teranishi S, Kawamoto K, Nishida T. Protective Effect of Dexamethasone against Hypoxia-Induced Disruption of Barrier Function in Human Corneal Epithelial Cells. *Experimental eye research* 2011;92:388-93.
292. Gipson I. Cell Biology of the Corneal Epithelium. *Principles and practices of ophthalmology* 1994:3-16.
293. Zagon IS, Sassani JW, McLaughlin PJ. Cellular Dynamics of Corneal Wound Re-Epithelialization in the Rat: I. Fate of Ocular Surface Epithelial Cells Synthesizing DNA Prior to Wounding. *Brain research* 1999;822:149-63.
294. Zieske J, Gipson I. Agents That Affect Corneal Wound Healing: Modulation of Structure and Function. *Principles and Practice of Ophthalmology: Basic Sciences Philadelphia, PA: WB Saunders* 1994:1093-9.
295. Buck RC. Cell Migration in Repair of Mouse Corneal Epithelium. *Investigative ophthalmology & visual science* 1979;18:767-84.
296. Hanna C. Proliferation and Migration of Epithelial Cells: During Corneal Wound Repair in the Rabbit and the Rat. *American journal of ophthalmology* 1966;61:55-63.
297. McCartney MD, Cantu-Crouch D. Rabbit Corneal Epithelial Wound Repair: Tight Junction Reformation. *Current eye research* 1992;11:15-24.
298. Suzuki K, Tanaka T, Enoki M, Nishida T. Coordinated Reassembly of the Basement Membrane and Junctional Proteins During Corneal Epithelial Wound Healing. *Investigative ophthalmology & visual science* 2000;41:2495-500.
299. Khodadoust AA, Silverstein AM, Kenyon KR, Dowling JE. Adhesion of Regenerating Corneal Epithelium: The Role of Basement Membrane. *American journal of ophthalmology* 1968;65:339-48.
300. Gipson IK. Adhesive Mechanisms of the Corneal Epithelium. *Acta Ophthalmologica* 1992;70:13-7.

301. Gipson IK, Spurr-Michaud SJ, Tisdale AS. Hemidesmosomes and Anchoring Fibril Collagen Appear Synchronously During Development and Wound Healing. *Developmental biology* 1988;126:253-62.
302. Gipson IK, Spurr-Michaud S, Tisdale A, Keough M. Reassembly of the Anchoring Structures of the Corneal Epithelium During Wound Repair in the Rabbit. *Investigative ophthalmology & visual science* 1989;30:425-34.
303. Poliseti N, Islam MM, Griffith M. The Artificial Cornea. *Corneal regenerative medicine* 2013;45-52.
304. Ross M, Deschênes J. Practice Patterns in the Interdisciplinary Management of Corneal Abrasions. *Canadian Journal of Ophthalmology* 2017;52:548-51.
305. Liu C, Buckley R. The Role of the Therapeutic Contact Lens in the Management of Recurrent Corneal Erosions: A Review of Treatment Strategies. *The CLAO Journal: Official Publication of the Contact Lens Association of Ophthalmologists, Inc* 1996;22:79-82.
306. Shafran T, Gleason W, Lorenz KO, Szczotka-Flynn LB. Application of Senofilcon a Contact Lenses for Therapeutic Bandage Lens Indications. *Eye & contact lens* 2013;39:315-23.
307. Karlgard C, Wong N, Jones L, Moresoli C. In Vitro Uptake and Release Studies of Ocular Pharmaceutical Agents by Silicon-Containing and P-Hema Hydrogel Contact Lens Materials. *International journal of pharmaceutics* 2003;257:141-51.
308. Busin M, Spitznas M. Sustained Gentamicin Release by Presoaked Medicated Bandage Contact Lenses. *Ophthalmology* 1988;95:796-8.
309. Donnenfeld ED, Selkin BA, Perry HD, et al. Controlled Evaluation of a Bandage Contact Lens and a Topical Nonsteroidal Anti-Inflammatory Drug in Treating Traumatic Corneal Abrasions. *Ophthalmology* 1995;102:979-84.
310. Kanpolat A, Uçakhan ÖÖ. Therapeutic Use of Focus® Night & Day™ Contact Lenses. *Cornea* 2003;22:726-34.
311. Ahad MA, Anandan M, Tah V, et al. Randomized Controlled Study of Ocular Lubrication Versus Bandage Contact Lens in the Primary Treatment of Recurrent Corneal Erosion Syndrome. *Cornea* 2013;32:1311-4.
312. Peng C-C, Ben-Shlomo A, Mackay EO, et al. Drug Delivery by Contact Lens in Spontaneously Glaucomatous Dogs. *Current eye research* 2012;37:204-11.
313. Xu J, Xue Y, Hu G, et al. A Comprehensive Review on Contact Lens for Ophthalmic Drug Delivery. *Journal of controlled release* 2018;281:97-118.
314. Holgado M, Anguiano-Domínguez A, Martín-Banderas L. Contact Lenses as Drug-Delivery Systems: A Promising Therapeutic Tool. *Archivos de la Sociedad Española de Oftalmología (English Edition)* 2020;95:24-33.
315. Filipe HP, Henriques J, Reis P, et al. Contact Lenses as Drug Controlled Release Systems: A Narrative Review. *Revista Brasileira de Oftalmologia* 2016;75:241-7.
316. dos Santos J-FR, Alvarez-Lorenzo C, Silva M, et al. Soft Contact Lenses Functionalized with Pendant Cyclodextrins for Controlled Drug Delivery. *Biomaterials* 2009;30:1348-55.
317. Jaanus SD, Blaho KE. *Clinical Ocular Pharmacology*: Butterworth-Heinemann; 2001.
318. Bajgrowicz M, Phan C-M, Subbaraman LN, Jones L. Release of Ciprofloxacin and Moxifloxacin from Daily Disposable Contact Lenses from an in Vitro Eye Model. *Investigative ophthalmology & visual science* 2015;56:2234-42.

319. Hui A, Bajgrowicz-Cieslak M, Phan C-M, Jones L. In Vitro Release of Two Anti-Muscarinic Drugs from Soft Contact Lenses. *Clinical Ophthalmology (Auckland, NZ)* 2017;11:1657.
320. Meadows DL, Paugh JR, Joshi A, Mordaunt J. A Novel Method to Evaluate Residence Time in Humans Using a Nonpenetrating Fluorescent Tracer. *Investigative ophthalmology & visual science* 2002;43:1032-9.
321. Knopf-Marques H, Barthes J, Wolfova L, et al. Auxiliary Biomembranes as a Directional Delivery System to Control Biological Events in Cell-Laden Tissue-Engineering Scaffolds. *ACS omega* 2017;2:918-29.
322. Maitra J, Shukla VK. Cross-Linking in Hydrogels-a Review. *Am J Polym Sci* 2014;4:25-31.
323. Jia X, Kiick KL. Hybrid Multicomponent Hydrogels for Tissue Engineering. *Macromolecular bioscience* 2009;9:140-56.
324. Van den Steen PE, Dubois B, Nelissen I, et al. Biochemistry and Molecular Biology of Gelatinase B or Matrix Metalloproteinase-9 (Mmp-9). *Critical reviews in biochemistry and molecular biology* 2002;37:375-536.
325. Xu F, Inci F, Mullick O, et al. Release of Magnetic Nanoparticles from Cell-Encapsulating Biodegradable Nanobiomaterials. *ACS nano* 2012;6:6640-9.
326. Xiao W, He J, Nichol JW, et al. Synthesis and Characterization of Photocrosslinkable Gelatin and Silk Fibroin Interpenetrating Polymer Network Hydrogels. *Acta biomaterialia* 2011;7:2384-93.
327. Caley MP, Martins VL, O'Toole EA. Metalloproteinases and Wound Healing. *Advances in wound care* 2015;4:225-34.
328. Sabino F, Keller U. Matrix Metalloproteinases in Impaired Wound Healing. *Metalloproteinases Med* 2015;2:1-8.
329. Sivak JM, Fini ME. Mmps in the Eye: Emerging Roles for Matrix Metalloproteinases in Ocular Physiology. *Progress in retinal and eye research* 2002;21:1-14.
330. Matsubara M, Girard MT, Kublin CL, et al. Differential Roles for Two Gelatinolytic Enzymes of the Matrix Metalloproteinase Family in the Remodelling Cornea. *Developmental biology* 1991;147:425-39.
331. Fini ME, Girard MT, Matsubara M. Collagenolytic/Gelatinolytic Enzymes in Corneal Wound Healing. *Acta ophthalmologica* 1992;70:26-33.
332. Koshy ST, Desai RM, Joly P, et al. Click-Crosslinked Injectable Gelatin Hydrogels. *Advanced healthcare materials* 2016;5:541-7.
333. Ward AG, Courts A. *Science and Technology of Gelatin*: Academic press; 1977.
334. Frantz C, Stewart KM, Weaver VM. The Extracellular Matrix at a Glance. *Journal of cell science* 2010;123:4195-200.
335. Zimmermann DR, Trüeb B, Winterhalter KH, et al. Type Vi Collagen Is a Major Component of the Human Cornea. *FEBS letters* 1986;197:55-8.
336. Barbetta A, Dentini M, Zannoni EM, De Stefano ME. Tailoring the Porosity and Morphology of Gelatin-Methacrylate Polyhipe Scaffolds for Tissue Engineering Applications. *Langmuir* 2005;21:12333-41.
337. Singh D, Tripathi A, Nayak V, Kumar A. Proliferation of Chondrocytes on a 3-D Modelled Macroporous Poly (Hydroxyethyl Methacrylate)-Gelatin Cryogel. *Journal of Biomaterials Science, Polymer Edition* 2011;22:1733-51.

338. Gómez-Guillén MC, Turnay J, Fernández-Díaz M, et al. Structural and Physical Properties of Gelatin Extracted from Different Marine Species: A Comparative Study. *Food Hydrocolloids* 2002;16:25-34.
339. Zhao X, Liu S, Yildirimer L, et al. Injectable Stem Cell-Laden Photocrosslinkable Microspheres Fabricated Using Microfluidics for Rapid Generation of Osteogenic Tissue Constructs. *Advanced Functional Materials* 2016;26:2809-19.
340. Kurian AG, Singh RK, Patel KD, et al. Multifunctional Gelma Platforms with Nanomaterials for Advanced Tissue Therapeutics. *Bioactive materials* 2022;8:267-95.
341. Gnani S, Di Blasio L, Tonda-Turo C, et al. Gelatin-Based Hydrogel for Vascular Endothelial Growth Factor Release in Peripheral Nerve Tissue Engineering. *Journal of tissue engineering and regenerative medicine* 2017;11:459-70.
342. Sharifi S, Islam MM, Sharifi H, et al. Tuning Gelatin-Based Hydrogel Towards Bioadhesive Ocular Tissue Engineering Applications. *Bioactive materials* 2021;6:3947-61.
343. Tronci G, Neffe AT, Pierce BF, Lendlein A. An Entropy–Elastic Gelatin-Based Hydrogel System. *Journal of Materials Chemistry* 2010;20:8875-84.
344. Shin SR, Bae H, Cha JM, et al. Carbon Nanotube Reinforced Hybrid Microgels as Scaffold Materials for Cell Encapsulation. *ACS nano* 2011;6:362-72.
345. Anglin EJ, Cheng L, Freeman WR, Sailor MJ. Porous Silicon in Drug Delivery Devices and Materials. *Advanced drug delivery reviews* 2008;60:1266-77.
346. ur Rehman SR, Augustine R, Zahid AA, et al. Reduced Graphene Oxide Incorporated Gelma Hydrogel Promotes Angiogenesis for Wound Healing Applications. *International journal of nanomedicine* 2019;14:9603.
347. Bhamra TS, Tighe BJ. Mechanical Properties of Contact Lenses: The Contribution of Measurement Techniques and Clinical Feedback to 50 Years of Materials Development. *Contact Lens and Anterior Eye* 2017;40:70-81.
348. Yacob N, Hashim K. Morphological Effect on Swelling Behaviour of Hydrogel. In: *AIP Conference Proceedings*. American Institute of Physics; 2014:153-9.
349. Sung Y, Gregonis D, John M, Andrade J. Thermal and Pulse Nmr Analysis of Water in Poly (2-Hydroxyethyl Methacrylate). *Journal of Applied Polymer Science* 1981;26:3719-28.
350. Isnard N, Robert L, Renard G. Effect of Sulfated Gags on the Expression and Activation of Mmp-2 and Mmp-9 in Corneal and Dermal Explant Cultures. *Cell biology international* 2003;27:779-84.
351. Li D-Q, Lokeshwar BL, Solomon A, et al. Regulation of Mmp-9 Production by Human Corneal Epithelial Cells. *Experimental eye research* 2001;73:449-59.
352. Sakimoto T, Shoji J, Yamada A, Sawa M. Upregulation of Matrix Metalloproteinase in Tear Fluid of Patients with Recurrent Corneal Erosion. *Japanese journal of ophthalmology* 2007;51:343-6.
353. Kim P, Yuan A, Nam K-H, et al. Fabrication of Poly (Ethylene Glycol): Gelatin Methacrylate Composite Nanostructures with Tunable Stiffness and Degradation for Vascular Tissue Engineering. *Biofabrication* 2014;6:024112.
354. Koshy ST, Ferrante TC, Lewin SA, Mooney DJ. Injectable, Porous, and Cell-Responsive Gelatin Cryogels. *Biomaterials* 2014;35:2477-87.
355. Tse J. Gelatin Methacrylate as a Controlled Release Vehicle for Treatment of Recurrent Corneal Erosion. University of Waterloo; 2018.



356. Bian F, Wang C, Tukler-Henriksson J, et al. Mmp-8 Is Critical for Dexamethasone Therapy in Alkali-Burned Corneas under Dry Eye Conditions. *Journal of cellular physiology* 2016;231:2506-16.
357. Kuo IC. Corneal Wound Healing. *Current opinion in ophthalmology* 2004;15:311-5.
358. Wang Z, Li X, Zhang X, et al. Novel Contact Lenses Embedded with Drug-Loaded Zwitterionic Nanogels for Extended Ophthalmic Drug Delivery. *Nanomaterials* 2021;11:2328.
359. Lira M, Pereira C, Oliveira ME, Castanheira EM. Importance of Contact Lens Power and Thickness in Oxygen Transmissibility. *Contact Lens and Anterior Eye* 2015;38:120-6.
360. Standardization IOF, . I. Ophthalmic Optics—Contact Lenses—Part 1: Vocabulary, Classification System and Recommendations for Labelling Specifications. In: International Organization for Standardization Geneva, Switzerland; 2010.
361. Williams DF. On the Mechanisms of Biocompatibility. *Biomaterials* 2008;29:2941-53.
362. Komeri R, Kasoju N, Kumar PA. In Vitro Cytotoxicity and Cytocompatibility Assays for Biomaterial Testing under Regulatory Platform. In. *Biomedical Product and Materials Evaluation*: Elsevier; 2022:329-53.
363. Li W, Zhou J, Xu Y. Study of the in Vitro Cytotoxicity Testing of Medical Devices. *Biomedical reports* 2015;3:617-20.
364. Wang MO, Etheridge JM, Thompson JA, et al. Evaluation of the in Vitro Cytotoxicity of Cross-Linked Biomaterials. *Biomacromolecules* 2013;14:1321-9.
365. Borra RC, Lotufo MA, Gagioti SM, et al. A Simple Method to Measure Cell Viability in Proliferation and Cytotoxicity Assays. *Brazilian oral research* 2009;23:255-62.
366. Ishiyama M, Tominaga H, Shiga M, et al. A Combined Assay of Cell Viability and in Vitro Cytotoxicity with a Highly Water-Soluble Tetrazolium Salt, Neutral Red and Crystal Violet. *Biological and Pharmaceutical Bulletin* 1996;19:1518-20.
367. Adan A, Kiraz Y, Baran Y. Cell Proliferation and Cytotoxicity Assays. *Current pharmaceutical biotechnology* 2016;17:1213-21.
368. Ye W, Li H, Yu K, et al. 3d Printing of Gelatin Methacrylate-Based Nerve Guidance Conduits with Multiple Channels. *Materials & Design* 2020;192:108757.
369. Xu W, Molino BZ, Cheng F, et al. On Low-Concentration Inks Formulated by Nanocellulose Assisted with Gelatin Methacrylate (Gelma) for 3d Printing toward Wound Healing Application. *ACS applied materials & interfaces* 2019;11:8838-48.
370. Nikkhah M, Eshak N, Zorlutuna P, et al. Directed Endothelial Cell Morphogenesis in Micropatterned Gelatin Methacrylate Hydrogels. *Biomaterials* 2012;33:9009-18.
371. Ramón-Azcón J, Ahadian S, Obregón R, et al. Gelatin Methacrylate as a Promising Hydrogel for 3d Microscale Organization and Proliferation of Dielectrophoretically Patterned Cells. *Lab on a Chip* 2012;12:2959-69.
372. Shah N, Hallur PM, Ganesh RA, et al. Gelatin Methacrylate Hydrogels Culture Model for Glioblastoma Cells Enriches for Mesenchymal-Like State and Models Interactions with Immune Cells. *Scientific reports* 2021;11:1-18.
373. Kang H, Shih Y-RV, Hwang Y, et al. Mineralized Gelatin Methacrylate-Based Matrices Induce Osteogenic Differentiation of Human Induced Pluripotent Stem Cells. *Acta biomaterialia* 2014;10:4961-70.
374. Schuurman W, Levett PA, Pot MW, et al. Gelatin-Methacrylamide Hydrogels as Potential Biomaterials for Fabrication of Tissue-Engineered Cartilage Constructs. *Macromolecular bioscience* 2013;13:551-61.

375. Klotz BJ, Gawlitta D, Rosenberg AJ, et al. Gelatin-Methacryloyl Hydrogels: Towards Biofabrication-Based Tissue Repair. *Trends in biotechnology* 2016;34:394-407.
376. Colosi C, Shin SR, Manoharan V, et al. Microfluidic Bioprinting of Heterogeneous 3d Tissue Constructs Using Low-Viscosity Bioink. *Advanced materials* 2016;28:677-84.
377. O'Brien J, Pognan F. Investigation of the Alamar Blue (Resazurin) Fluorescent Dye for the Assessment of Mammalian Cell Cytotoxicity. In: *Toxicology*. ELSEVIER SCI IRELAND LTD CUSTOMER RELATIONS MANAGER, BAY 15, SHANNON ...; 2001:132-.
378. Page B, PAGE M, NOEL C. A New Fluorometric Assay for Cytotoxicity Measurements in-Vitro. *International journal of oncology* 1993;3:473-6.
379. Zhou S, Cui Z, Urban J. Dead Cell Counts During Serum Cultivation Are Underestimated by the Fluorescent Live/Dead Assay. In: *Wiley Online Library*; 2011.
380. Scientific TF. Live/Dead™ Viability/Cytotoxicity Kit for Mammalian Cells. Thermo Fisher Scientific 2015.
381. Augustine R, Hasan A, Dalvi YB, et al. Growth Factor Loaded in Situ Photocrosslinkable Poly (3-Hydroxybutyrate-Co-3-Hydroxyvalerate)/Gelatin Methacryloyl Hybrid Patch for Diabetic Wound Healing. *Materials Science and Engineering: C* 2021;118:111519.
382. Fathi A, Lee S, Breen A, et al. Enhancing the Mechanical Properties and Physical Stability of Biomimetic Polymer Hydrogels for Micro-Patterning and Tissue Engineering Applications. *European polymer journal* 2014;59:161-70.
383. Liu B, Wang Y, Miao Y, et al. Hydrogen Bonds Autonomously Powered Gelatin Methacrylate Hydrogels with Super-Elasticity, Self-Heal and Underwater Self-Adhesion for Sutureless Skin and Stomach Surgery and E-Skin. *Biomaterials* 2018;171:83-96.
384. Sun Y, Deng R, Ren X, et al. 2d Gelatin Methacrylate Hydrogels with Tunable Stiffness for Investigating Cell Behaviors. *ACS Applied Bio Materials* 2018;2:570-6.
385. Aslantürk ÖS. In Vitro Cytotoxicity and Cell Viability Assays: Principles, Advantages, and Disadvantages. *Genotoxicity-A predictable risk to our actual world* 2018;2:64-80.
386. Al-Nasiry S, Geusens N, Hanssens M, et al. The Use of Alamar Blue Assay for Quantitative Analysis of Viability, Migration and Invasion of Choriocarcinoma Cells. *Human reproduction* 2007;22:1304-9.
387. Camci-Unal G, Cuttica D, Annabi N, et al. Synthesis and Characterization of Hybrid Hyaluronic Acid-Gelatin Hydrogels. *Biomacromolecules* 2013;14:1085-92.
388. Wu Y, Xiang Y, Fang J, et al. The Influence of the Stiffness of Gelma Substrate on the Outgrowth of Pc12 Cells. *Bioscience reports* 2019;39.
389. Molladavoodi S, Kwon H-J, Medley J, Gorbet M. Human Corneal Epithelial Cell Response to Substrate Stiffness. *Acta biomaterialia* 2015;11:324-32.
390. Masterton S, Ahearne M. Influence of Polydimethylsiloxane Substrate Stiffness on Corneal Epithelial Cells. *Royal Society open science* 2019;6:191796.
391. Chen CS. Mechanotransduction—a Field Pulling Together? *Journal of cell science* 2008;121:3285-92.
392. Shiu Y-T, Li S, Marganski WA, et al. Rho Mediates the Shear-Enhancement of Endothelial Cell Migration and Traction Force Generation. *Biophysical journal* 2004;86:2558-65.
393. Pelham Jr RJ, Wang Y-l. Cell Locomotion and Focal Adhesions Are Regulated by Substrate Flexibility. *Proceedings of the national academy of sciences* 1997;94:13661-5.

394. Lo C-M, Wang H-B, Dembo M, Wang Y-l. Cell Movement Is Guided by the Rigidity of the Substrate. *Biophysical journal* 2000;79:144-52.
395. Cameron AR, Frith JE, Cooper-White JJ. The Influence of Substrate Creep on Mesenchymal Stem Cell Behaviour and Phenotype. *Biomaterials* 2011;32:5979-93.
396. Weiser JR, Saltzman WM. Controlled Release for Local Delivery of Drugs: Barriers and Models. *Journal of controlled release : official journal of the Controlled Release Society* 2014;190:664-73.
397. Siegel RA, Rathbone MJ. Overview of Controlled Release Mechanisms. In. *Fundamentals and Applications of Controlled Release Drug Delivery*: Springer; 2012:19-43.
398. Pitt C. The Controlled Parenteral Delivery of Polypeptides and Proteins. *International Journal of Pharmaceutics* 1990;59:173-96.
399. Uhrich KE, Cannizzaro SM, Langer RS, Shakesheff KM. Polymeric Systems for Controlled Drug Release. *Chemical Reviews-Columbus* 1999;99:3181-98.
400. During MJ, Freese A, Sabel BA, et al. Controlled Release of Dopamine from a Polymeric Brain Implant: In Vivo Characterization. *Annals of Neurology: Official Journal of the American Neurological Association and the Child Neurology Society* 1989;25:351-6.
401. Ludwig A. The Use of Mucoadhesive Polymers in Ocular Drug Delivery. *Advanced drug delivery reviews* 2005;57:1595-639.
402. Orloff LA, Domb AJ, Teomim D, et al. Biodegradable Implant Strategies for Inhibition of Restenosis. *Advanced drug delivery reviews* 1997;24:3-9.
403. Boateng JS, Matthews KH, Stevens HN, Eccleston GM. Wound Healing Dressings and Drug Delivery Systems: A Review. *Journal of pharmaceutical sciences* 2008;97:2892-923.
404. Cheng R, Yan Y, Liu H, et al. Mechanically Enhanced Lipo-Hydrogel with Controlled Release of Multi-Type Drugs for Bone Regeneration. *Applied Materials Today* 2018;12:294-308.
405. Shao Y, You D, Lou Y, et al. Controlled Release of Naringin in Gelma-Incorporated Rutile Nanorod Films to Regulate Osteogenic Differentiation of Mesenchymal Stem Cells. *ACS omega* 2019;4:19350-7.
406. Yi M-H, Lee J-E, Kim C-B, et al. Locally Controlled Diffusive Release of Bone Morphogenetic Protein-2 Using Micropatterned Gelatin Methacrylate Hydrogel Carriers. *BioChip Journal* 2020;14:405-20.
407. Serafim A, Tucureanu C, Petre D-G, et al. One-Pot Synthesis of Superabsorbent Hybrid Hydrogels Based on Methacrylamide Gelatin and Polyacrylamide. Effortless Control of Hydrogel Properties through Composition Design. *New Journal of Chemistry* 2014;38:3112-26.
408. Vigata M, O'Connell CD, Cometta S, et al. Gelatin Methacryloyl Hydrogels for the Localized Delivery of Cefazolin. *Polymers* 2021;13:3960.
409. Paul A, Hasan A, Kindi HA, et al. Injectable Graphene Oxide/Hydrogel-Based Angiogenic Gene Delivery System for Vasculogenesis and Cardiac Repair. *ACS nano* 2014;8:8050-62.
410. Qu M, Kim H-J, Zhou X, et al. Biodegradable Microneedle Patch for Transdermal Gene Delivery. *Nanoscale* 2020;12:16724-9.
411. Eichler W, Bechtel JM, Schumacher J, et al. A Rise of Mmp-2 and Mmp-9 in Bronchoalveolar Lavage Fluid Is Associated with Acute Lung Injury after Cardiopulmonary Bypass in a Swine Model. *Perfusion* 2003;18:107-13.
412. Acera A, Vecino E, Duran JA. Tear Mmp-9 Levels as a Marker of Ocular Surface Inflammation in Conjunctivochalasis. *Investigative Ophthalmology & Visual Science* 2013;54:8285-91.

413. Singh A, Maurya O, Jagannadhan M, Patel A. Matrix Metalloproteinases (Mmp-2 and Mmp-9) Activity in Corneal Ulcer and Ocular Surface Disorders Determined by Gelatin Zymography. *Journal of ocular biology, diseases, and informatics* 2012;5:31-5.
414. Efron N, Young G, Brennan NA. Ocular Surface Temperature. *Curr Eye Res* 1989;8:901-6.
415. Tang L, Wu J, Ma Q, et al. Human Lactoferrin Stimulates Skin Keratinocyte Function and Wound Re-Epithelialization. *British Journal of Dermatology* 2010;163:38-47.
416. Groves ML. The Isolation of a Red Protein from Milk<sup>2</sup>. *Journal of the American Chemical Society* 1960;82:3345-50.
417. Raphael GD, Jeney EV, Baraniuk JN, et al. Pathophysiology of Rhinitis. Lactoferrin and Lysozyme in Nasal Secretions. *The Journal of clinical investigation* 1989;84:1528-35.
418. Gruden Š, Poklar Ulrih N. Diverse Mechanisms of Antimicrobial Activities of Lactoferrins, Lactoferricins, and Other Lactoferrin-Derived Peptides. *International journal of molecular sciences* 2021;22:11264.
419. Masson P, Heremans J, Dive C. An Iron-Binding Protein Common to Many External Secretions. *Clinica Chimica Acta* 1966;14:735-9.
420. Haridas M, Anderson B, Baker E. Structure of Human Diferric Lactoferrin Refined at 2.2 Å Resolution. *Acta Crystallographica Section D: Biological Crystallography* 1995;51:629-46.
421. Baker HM, Baker EN. Lactoferrin and Iron: Structural and Dynamic Aspects of Binding and Release. *Biometals* 2004;17:209-16.
422. Janssen H, Hancock RE. Antimicrobial Properties of Lactoferrin. *Biochimie* 2009;91:19-29.
423. Zarzosa-Moreno D, Avalos-Gómez C, Ramírez-Texcalco LS, et al. Lactoferrin and Its Derived Peptides: An Alternative for Combating Virulence Mechanisms Developed by Pathogens. *Molecules* 2020;25:5763.
424. Actor JK, Hwang S-A, Kruzel ML. Lactoferrin as a Natural Immune Modulator. *Current pharmaceutical design* 2009;15:1956-73.
425. Lepanto MS, Rosa L, Paesano R, et al. Lactoferrin in Aseptic and Septic Inflammation. *Molecules* 2019;24:1323.
426. Rosa L, Cutone A, Lepanto MS, et al. Lactoferrin: A Natural Glycoprotein Involved in Iron and Inflammatory Homeostasis. *International journal of molecular sciences* 2017;18:1985.
427. Siqueiros-Cendón T, Arévalo-Gallegos S, Iglesias-Figueroa BF, et al. Immunomodulatory Effects of Lactoferrin. *Acta Pharmacologica Sinica* 2014;35:557-66.
428. Duellman T, Burnett J, Yang J. Functional Roles of N-Linked Glycosylation of Human Matrix Metalloproteinase 9. *Traffic* 2015;16:1108-26.
429. Li D-Q, Pflugfelder SC. Matrix Metalloproteinases in Corneal Inflammation. *The ocular surface* 2005;3:S-198-S-202.
430. Behzadian MA, Wang X-L, Windsor LJ, et al. Tgf-B Increases Retinal Endothelial Cell Permeability by Increasing Mmp-9: Possible Role of Glial Cells in Endothelial Barrier Function. *Investigative ophthalmology & visual science* 2001;42:853-9.
431. Sternlicht MD, Werb Z. How Matrix Metalloproteinases Regulate Cell Behavior. *Annual review of cell and developmental biology* 2001;17:463-516.
432. Pflugfelder SC. Antiinflammatory Therapy for Dry Eye. *American journal of ophthalmology* 2004;137:337-42.

433. Afonso AA, Sobrin L, Monroy DC, et al. Tear Fluid Gelatinase B Activity Correlates with IL-1 $\alpha$  Concentration and Fluorescein Clearance in Ocular Rosacea. *Investigative ophthalmology & visual science* 1999;40:2506-12.
434. Chotikavanich S, de Paiva CS, Chen JJ, et al. Production and Activity of Matrix Metalloproteinase-9 on the Ocular Surface Increase in Dysfunctional Tear Syndrome. *Investigative ophthalmology & visual science* 2009;50:3203-9.
435. Acera A, Rocha G, Vecino E, et al. Inflammatory Markers in the Tears of Patients with Ocular Surface Disease. *Ophthalmic research* 2008;40:315-21.
436. Lam-Franco L, Perfecto-Avalos Y, Patiño-Ramírez BE, García AR. IL-1 $\alpha$  and Mmp-9 Tear Levels of Patients with Active Ocular Rosacea before and after Treatment with Systemic Azithromycin or Doxycycline. *Ophthalmic Research* 2018;60:109-14.
437. Lema I, Durán JA. Inflammatory Molecules in the Tears of Patients with Keratoconus. *Ophthalmology* 2005;112:654-9.
438. Lema I, Sobrino T, Duran JA, et al. Subclinical Keratoconus and Inflammatory Molecules from Tears. *British Journal of Ophthalmology* 2009;93:820-4.
439. Langer R. Drugs on Target. *Science* 2001;293:58-9.
440. Ulijn RV. Enzyme-Responsive Materials: A New Class of Smart Biomaterials. *Journal of Materials Chemistry* 2006;16:2217-25.
441. Aparecida Da Silva A, Leal-Junior ECP, Alves ACA, et al. Wound-Healing Effects of Low-Level Laser Therapy in Diabetic Rats Involve the Modulation of Mmp-2 and Mmp-9 and the Redistribution of Collagen Types I and III. *Journal of Cosmetic and Laser Therapy* 2013;15:210-6.
442. Tankam P, Won J, Canavesi C, et al. Optical Assessment of Soft Contact Lens Edge-Thickness. *Optometry and vision science: official publication of the American Academy of Optometry* 2016;93:987.
443. Krachmer JH, Mannis MJ, Holland EJ. *Cornea E-Book: Elsevier Health Sciences*; 2010.
444. Kowtharapu BS, Stahnke T, Wree A, et al. Corneal Epithelial and Neuronal Interactions: Role in Wound Healing. *Experimental eye research* 2014;125:53-61.
445. Vaidyanathan U, Hopping GC, Liu HY, et al. Persistent Corneal Epithelial Defects: A Review Article. *Medical Hypothesis, Discovery and Innovation in Ophthalmology* 2019;8:163.
446. Segal KL, Fleischut PM, Kim C, et al. Evaluation and Treatment of Perioperative Corneal Abrasions. *Journal of Ophthalmology* 2014;2014.
447. Morris A, Bonanno L, Bennett M. Effectiveness of Corneal Abrasion Prevention Interventions for Adults Undergoing General Anesthesia for More Than One Hour: A Systematic Review Protocol. *JBIC Evidence Synthesis* 2018;16:1785-90.
448. Shields T, Sloane PD. A Comparison of Eye Problems in Primary Care and Ophthalmology Practices. *Family medicine* 1991;23:544-6.
449. Domingo E, Moshirfar M, Zabbo CP. Corneal Abrasion. In: *Statpearls [Internet]: StatPearls Publishing*; 2021.
450. Britigan BE, Serody JS, Cohen MS. The Role of Lactoferrin as an Anti-Inflammatory Molecule. *Lactoferrin* 1994:143-56.
451. Ward PP, Paz E, Conneely OM. Multifunctional Roles of Lactoferrin: A Critical Overview. *Cellular and molecular life sciences : CMLS* 2005;62:2540-8.
452. Andersen JH. Technology Evaluation: Rh Lactoferrin, Agennix. *Current opinion in molecular therapeutics* 2004;6:344-9.

453. Hagiwara T, Shinoda I, Fukuwatari Y, Shimamura S. Effects of Lactoferrin and Its Peptides on Proliferation of Rat Intestinal Epithelial Cell Line, Iec-18, in the Presence of Epidermal Growth Factor. *Bioscience, biotechnology, and biochemistry* 1995;59:1875-81.
454. Todaro GJ, Lazar GK, Green H. The Initiation of Cell Division in a Contact-Inhibited Mammalian Cell Line. *Journal of Cellular and Comparative Physiology* 1965;66:325-33.
455. Willmann D, Fu L, Melanson SW. Corneal Injury. In. *Statpearls* [Internet]: StatPearls Publishing; 2021.
456. Brewitt H. Sliding of Epithelium in Experimental Corneal Wounds. A Scanning Electron Microscopic Study. *Acta Ophthalmol (Copenh)* 1979;57:945-58.
457. Danjo Y, Gipson IK. Specific Transduction of the Leading Edge Cells of Migrating Epithelia Demonstrates That They Are Replaced During Healing. *Exp Eye Res* 2002;74:199-204.
458. Channa R, Zafar SN, Canner JK, et al. Epidemiology of Eye-Related Emergency Department Visits. *JAMA ophthalmology* 2016;134:312-9.
459. Gekka M, Miyata K, Nagai Y, et al. Corneal Epithelial Barrier Function in Diabetic Patients. *Cornea* 2004;23:35-7.
460. Levin MH, Verkman AS. Aquaporin-3-Dependent Cell Migration and Proliferation During Corneal Re-Epithelialization. *Invest Ophthalmol Vis Sci* 2006;47:4365-72.
461. Son YJ, John WT, Zhou Y, et al. Biomaterials and Controlled Release Strategy for Epithelial Wound Healing. *Biomaterials science* 2019;7:4444-71.
462. Stamm A, Reimers K, Strauß S, et al. In Vitro Wound Healing Assays—State of the Art. *BioNanoMaterials* 2016;17:79-87.
463. Poujade M, Grasland-Mongrain E, Hertzog A, et al. Collective Migration of an Epithelial Monolayer in Response to a Model Wound. *Proceedings of the National Academy of Sciences* 2007;104:15988-93.
464. Jacinto A, Martinez-Arias A, Martin P. Mechanisms of Epithelial Fusion and Repair. *Nature cell biology* 2001;3:E117-E23.
465. Kiehart DP. Wound Healing: The Power of the Purse String. *Current biology* 1999;9:R602-R5.
466. Tamada M, Perez TD, Nelson WJ, Sheetz MP. Two Distinct Modes of Myosin Assembly and Dynamics During Epithelial Wound Closure. *The Journal of cell biology* 2007;176:27-33.
467. Fenteany G, Janmey PA, Stossel TP. Signaling Pathways and Cell Mechanics Involved in Wound Closure by Epithelial Cell Sheets. *Current biology* 2000;10:831-8.
468. Bement WM, Forscher P, Mooseker MS. A Novel Cytoskeletal Structure Involved in Purse String Wound Closure and Cell Polarity Maintenance. *The Journal of cell biology* 1993;121:565-78.
469. Block ER, Matela AR, SundarRaj N, et al. Wounding Induces Motility in Sheets of Corneal Epithelial Cells through Loss of Spatial Constraints: Role of Heparin-Binding Epidermal Growth Factor-Like Growth Factor Signaling. *Journal of Biological Chemistry* 2004;279:24307-12.
470. van Horssen R, Galjart N, Rens JA, et al. Differential Effects of Matrix and Growth Factors on Endothelial and Fibroblast Motility: Application of a Modified Cell Migration Assay. *Journal of cellular biochemistry* 2006;99:1536-52.
471. Kim MJ, Jun RM, Kim WK, et al. Optimal Concentration of Human Epidermal Growth Factor (Hegf) for Epithelial Healing in Experimental Corneal Alkali Wounds. *Curr Eye Res* 2001;22:272-9.
472. Sotozono C, Inatomi T, Nakamura M, Kinoshita S. Keratinocyte Growth Factor Accelerates Corneal Epithelial Wound Healing in Vivo. *Invest Ophthalmol Vis Sci* 1995;36:1524-9.

473. Kamiyama K, Iguchi I, Wang X, Imanishi J. Effects of Pdgf on the Migration of Rabbit Corneal Fibroblasts and Epithelial Cells. *Cornea* 1998;17:315-25.
474. Nishida T, Nakamura M, Mishima H, Otori T. Interleukin 6 Promotes Epithelial Migration by a Fibronectin-Dependent Mechanism. *Journal of cellular physiology* 1992;153:1-5.
475. Nishida T, Nakamura M, Mishima H, et al. Interleukin 6 Facilitates Corneal Epithelial Wound Closure in Vivo. *Archives of ophthalmology (Chicago, Ill : 1960)* 1992;110:1292-4.
476. Lu L, Reinach PS, Kao WW. Corneal Epithelial Wound Healing. *Experimental biology and medicine (Maywood, NJ)* 2001;226:653-64.
477. Nakajima M, Shinoda I, Samejima Y, et al. Lactoferrin as a Suppressor of Cell Migration of Gastrointestinal Cell Lines. *Journal of cellular physiology* 1997;170:101-5.
478. Cumberbatch M, Dearman RJ, Uribe-Luna S, et al. Regulation of Epidermal Langerhans Cell Migration by Lactoferrin. *Immunology* 2000;100:21-8.
479. Takayama Y, Takezawa T. Lactoferrin Promotes Collagen Gel Contractile Activity of Fibroblasts Mediated by Lipoprotein Receptors. *Biochemistry and cell biology = Biochimie et biologie cellulaire* 2006;84:268-74.
480. Na YJ, Han SB, Kang JS, et al. Lactoferrin Works as a New Lps-Binding Protein in Inflammatory Activation of Macrophages. *International immunopharmacology* 2004;4:1187-99.
481. Sorimachi K, Akimoto K, Hattori Y, et al. Activation of Macrophages by Lactoferrin: Secretion of Tnf-Alpha, Il-8 and No. *Biochemistry and molecular biology international* 1997;43:79-87.
482. Artym J, Zimecki M, Kruzel ML. Effect of Lactoferrin on the Methotrexate-Induced Suppression of the Cellular and Humoral Immune Response in Mice. *Anticancer research* 2004;24:3831-6.
483. Kruzel ML, Harari Y, Mailman D, et al. Differential Effects of Prophylactic, Concurrent and Therapeutic Lactoferrin Treatment on Lps-Induced Inflammatory Responses in Mice. *Clinical and experimental immunology* 2002;130:25-31.
484. Krueger J, Ray A, Tamm I, Sehgal PB. Expression and Function of Interleukin-6 in Epithelial Cells. *Journal of cellular biochemistry* 1991;45:327-34.
485. Imanishi J, Kamiyama K, Iguchi I, et al. Growth Factors: Importance in Wound Healing and Maintenance of Transparency of the Cornea. *Prog Retin Eye Res* 2000;19:113-29.
486. Nishida T, Nakagawa S, Awata T, et al. Fibronectin Promotes Epithelial Migration of Cultured Rabbit Cornea in Situ. *The Journal of cell biology* 1983;97:1653-7.
487. Murakami J, Nishida T, Otori T. Coordinated Appearance of Beta 1 Integrins and Fibronectin During Corneal Wound Healing. *The Journal of laboratory and clinical medicine* 1992;120:86-93.
488. Phan TM, Foster CS, Zagachin LM, Colvin RB. Role of Fibronectin in the Healing of Superficial Keratectomies in Vitro. *Invest Ophthalmol Vis Sci* 1989;30:386-91.
489. Tervo K, van Setten GB, Beuerman RW, et al. Expression of Tenascin and Cellular Fibronectin in the Rabbit Cornea after Anterior Keratectomy. *Immunohistochemical Study of Wound Healing Dynamics. Invest Ophthalmol Vis Sci* 1991;32:2912-8.
490. Rohini G, Murugeswari P, Prajna NV, et al. Matrix Metalloproteinases (Mmp-8, Mmp-9) and the Tissue Inhibitors of Metalloproteinases (Timp-1, Timp-2) in Patients with Fungal Keratitis. *Cornea* 2007;26:207-11.
491. Yang X, Sun X, Liu J, et al. Photo-Crosslinked Gelma/Collagen Membrane Loaded with Lysozyme as an Antibacterial Corneal Implant. *International Journal of Biological Macromolecules* 2021;191:1006-16.

492. Mahdavi SS, Abdekhodaie MJ, Kumar H, et al. Stereolithography 3d Bioprinting Method for Fabrication of Human Corneal Stroma Equivalent. *Annals of Biomedical Engineering* 2020;48:1955-70.
493. Prina E. Recreating 3d Limbal Architectures by Two-Photon Polymerization for Cornea Regeneration. University of Nottingham; 2018.
494. Nichols JJ. Deposition on Silicone Hydrogel Lenses. *Eye & contact lens* 2013;39:20-3.
495. Luensmann D, Jones L. Protein Deposition on Contact Lenses: The Past, the Present, and the Future. *Contact Lens and Anterior Eye* 2012;35:53-64.
496. Phan C-M, Bajgrowicz-Cieslak M, Subbaraman LN, Jones L. Release of Moxifloxacin from Contact Lenses Using an in Vitro Eye Model: Impact of Artificial Tear Fluid Composition and Mechanical Rubbing. *Translational vision science & technology* 2016;5:3-.
497. Kompella UB, Hartman RR, Patil MA. Extraocular, Periocular, and Intraocular Routes for Sustained Drug Delivery for Glaucoma. *Progress in retinal and eye research* 2021;82:100901.
498. Kuno N, Fujii S. Recent Advances in Ocular Drug Delivery Systems. *Polymers* 2011;3:193-221.
499. O'Rourke MJ, Wilson CG. The Development and Commercialization of Sustained-Release Ocular Drug Delivery Technologies. In. *Ophthalmic Product Development: Springer*; 2021:591-612.



## Appendix A- Copyright permission

### National Eye Institute Image copyright

**Figure 1-1: Anatomy of the eye**



[Learn About Eye Health](#) ⌵

[Grants and Training](#) ⌵

[Research at NEI](#) ⌵

[Home](#) » [Web Policies](#) » [Copyright Policy](#)

## Copyright Policy

Unless otherwise noted, information on the [National Eye Institute website](#) is in the public domain. Public domain information may be freely distributed and copied, but, as a courtesy, we request that the National Eye Institute be given an appropriate acknowledgement: "Courtesy: National Eye Institute, National Institutes of Health (NEI/NIH)."

When using [the NEI website](#), you may encounter documents, illustrations, photographs or other information that has been licensed by private individuals, companies or organizations that may be protected by United States and foreign copyright laws. Transmission or reproduction of these protected items requires the written permission of the copyright owners. For information about the copyright owners of a given graphic, photo or illustration on [the NEI website](#); how they can be contacted; and what, if any, use those owners allow of their material; please provide the URL and file name to the [NEI Website Manager](#).

## Figure1-2: Structure of the cornea



### The role of lipids in corneal diseases and dystrophies: a systematic review

**Author:** Dimitrios Karamichos, Tyler G. Rowsey

**Publication:** Clinical and Translational Medicine

**Publisher:** John Wiley and Sons

**Date:** Sep 1, 2017

© This is an open access article under the terms of the [Creative Commons Attribution License](#), which permits use, distribution and reproduction in any medium, provided the original work is properly cited

#### Open Access Article

This is an open access article distributed under the terms of the [Creative Commons CC BY](#) license, which permits unrestricted use, distribution, and reproduction in any medium, provided the original work is properly cited.

You are not required to obtain permission to reuse this article.

For an understanding of what is meant by the terms of the Creative Commons License, please refer to [Wiley's Open Access Terms and Conditions](#).

Permission is not required for this type of reuse.

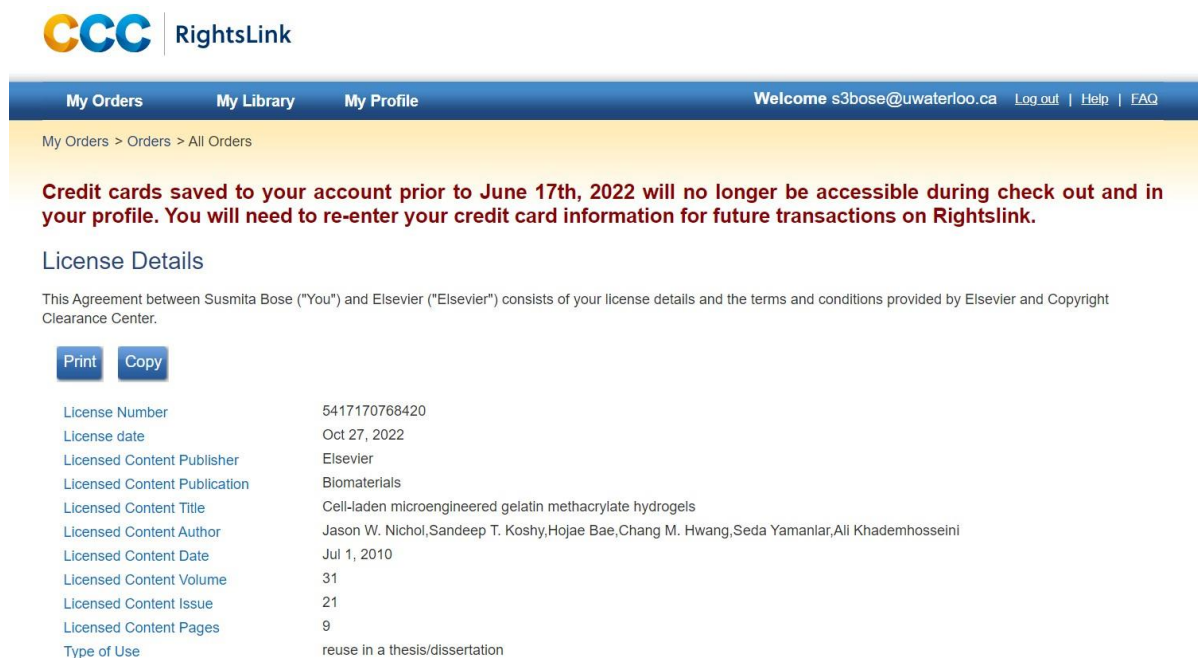
Wiley offers a professional reprint service for high quality reproduction of articles from over 1400 scientific and medical journals. Wiley's reprint service offers:

**Figure 1-3: Cross-sectional view of corneal epithelial layer**

The screenshot displays the CCC RightsLink website interface. At the top left is the CCC RightsLink logo. A navigation bar includes links for 'My Orders', 'My Library', and 'My Profile', along with a welcome message for user 's3bose@uwaterloo.ca' and links for 'Log out', 'Help', and 'FAQ'. Below the navigation bar, a breadcrumb trail reads 'My Orders > Orders > All Orders'. A prominent red warning message states: 'Credit cards saved to your account prior to June 17th, 2022 will no longer be accessible during check out and in your profile. You will need to re-enter your credit card information for future transactions on Rightslink.' The main section is titled 'License Details' and contains a paragraph explaining the agreement between Susmita Bose and Wolters Kluwer Health, Inc. Below this text are 'Print' and 'Copy' buttons. A table lists the license details:

License Number	5422310302499
License date	Nov 05, 2022
Licensed Content Publisher	Wolters Kluwer Health, Inc.
Licensed Content Publication	Journal of Cataract and Refractive Surgery
Licensed Content Title	Anatomy and physiology of the cornea
Licensed Content Author	Derek DelMonte and Terry Kim
Licensed Content Date	Mar 1, 2011
Licensed Content Volume	37
Licensed Content Issue	3
Type of Use	Dissertation/Thesis
Requestor type	University/College

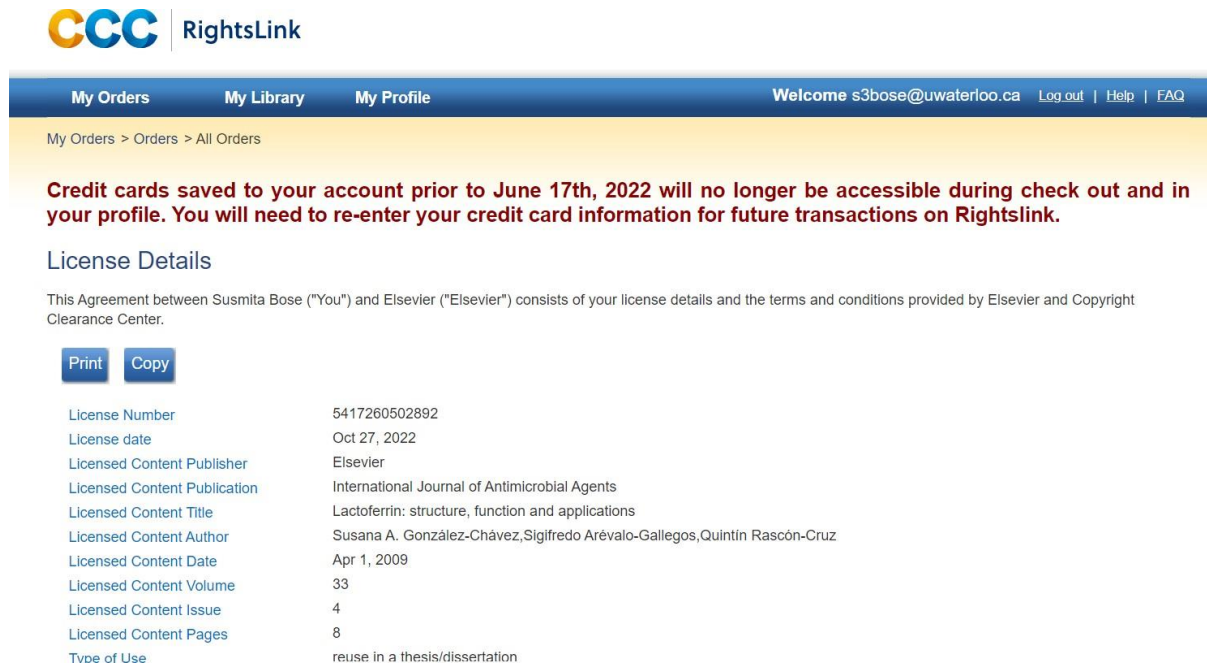
## Figure 1-5: Synthesis of GelMA



The screenshot shows the RightsLink interface. At the top left is the CCC RightsLink logo. A navigation bar contains links for 'My Orders', 'My Library', and 'My Profile'. On the right of the navigation bar, it says 'Welcome s3bose@uwaterloo.ca' with links for 'Log out', 'Help', and 'FAQ'. Below the navigation bar, a breadcrumb trail reads 'My Orders > Orders > All Orders'. A prominent red message states: 'Credit cards saved to your account prior to June 17th, 2022 will no longer be accessible during check out and in your profile. You will need to re-enter your credit card information for future transactions on Rightslink.' Below this is the 'License Details' section, which includes a paragraph explaining the agreement between Susmita Bose and Elsevier. There are 'Print' and 'Copy' buttons. A table lists the following license details:

License Number	5417170768420
License date	Oct 27, 2022
Licensed Content Publisher	Elsevier
Licensed Content Publication	Biomaterials
Licensed Content Title	Cell-laden microengineered gelatin methacrylate hydrogels
Licensed Content Author	Jason W. Nichol, Sandeep T. Koshy, Hojae Bae, Chang M. Hwang, Seda Yamanlar, Ali Khademhosseini
Licensed Content Date	Jul 1, 2010
Licensed Content Volume	31
Licensed Content Issue	21
Licensed Content Pages	9
Type of Use	reuse in a thesis/dissertation

## Figure 1-6: Structure of biferric BLF



The screenshot shows the RightsLink interface. At the top left is the CCC RightsLink logo. A navigation bar contains links for 'My Orders', 'My Library', and 'My Profile'. On the right of the navigation bar, it says 'Welcome s3bose@uwaterloo.ca' with links for 'Log out', 'Help', and 'FAQ'. Below the navigation bar is a breadcrumb trail: 'My Orders > Orders > All Orders'. A red warning message states: 'Credit cards saved to your account prior to June 17th, 2022 will no longer be accessible during check out and in your profile. You will need to re-enter your credit card information for future transactions on Rightslink.' Below this is the 'License Details' section. It includes a paragraph: 'This Agreement between Susmita Bose ("You") and Elsevier ("Elsevier") consists of your license details and the terms and conditions provided by Elsevier and Copyright Clearance Center.' There are 'Print' and 'Copy' buttons. A table lists the license details:

License Number	5417260502892
License date	Oct 27, 2022
Licensed Content Publisher	Elsevier
Licensed Content Publication	International Journal of Antimicrobial Agents
Licensed Content Title	Lactoferrin: structure, function and applications
Licensed Content Author	Susana A. González-Chávez, Sigifredo Arévalo-Gallegos, Quintín Rascón-Cruz
Licensed Content Date	Apr 1, 2009
Licensed Content Volume	33
Licensed Content Issue	4
Licensed Content Pages	8
Type of Use	reuse in a thesis/dissertation